Karlsruhe Institute of Technology

The Strong CP Problem and Non-Supersymmetric Grand Unification

Zur Erlangung des akademischen Grades eines

DOKTORS DER NATURWISSENSCHAFTEN

von der KIT-Fakultät für Physik des
Karlsruher Instituts für Technologie (KIT)
genehmigte

DISSERTATION

von

Jakob Hermann Schwichtenberg

aus Mannheim

Tag der mündlichen Prüfung:	26. Juli 2019
Referent:	Prof. Dr. Ulrich Nierste
Korreferent:	Prof. Dr. Thomas Schwetz-Mangold

"The universe is full
of magical things
patiently waiting
for our wits
to grow sharper."

- Eden Phillpotts

Contents

List of Figures

List of Tables

1 Introduction

Although the Standard Model is undoubtedly the most successful theory of fundamental physics ever formulated, there are many reasons to believe that it is incomplete.

On the one hand, there are several "hard" facts which cannot be described in the context of the Standard Model like, for example, nonzero neutrino masses, and the existence of dark matter and gravitational interactions. On the other hand, there is an even longer list of "softer" arguments why the Standard Model is theoretically unsatisfying. For example, the Standard Model offers no explanation for why the gauge couplings have the values they have, for the quantization of electric charge $Q_{\text{proton}} + Q_{\text{electron}} < \mathcal{O}(10^{-20})$, or for the pattern of mixing angles and masses of the fermions. In addition, the Standard Model does not explain why CP violating effects in strong interactions are tiny — if they exist at all. This is puzzling because there is nothing in the Standard Model that forbids CP violation in the strong sector and therefore, according to Gell-Mann's totalitarian principle (*"Everything not forbidden is compulsory"* [1]), it should be measurable.

While most physicist agree that the Standard Model needs to be modified, there is no consensus on how this should be done. This is unsurprising since there are, in principle, infinitely many models that yield the Standard Model at low energies. For this reason, it is impossible to deduce *the* correct model which replaces the Standard Model at high energies from low energy data alone. Technically this follows from the fact that the process of integrating out fields is not invertible. (We can "zoom out" but cannot "zoom in".) For this reason, work on beyond the Standard Model physics always depends, to some extent, on personal preferences. In other words, in the quest for theories beyond the Standard Model, the available low energy data always needs to be supplemented by guiding principles. One type of guiding principle which has proven to be highly successful in the past are symmetries [2]. Therefore, it may seem reasonable, to quote Paul Dirac, that *"further progress lies in the direction of making our equations invariant under wider and still wider transformations."* [3]

One intriguing way to realize this idea in concrete terms is to embed the Standard Model gauge group

$$G_{\text{SM}} = SU(3)_C \times SU(2)_L \times U(1) \tag{1.1}$$

in a simple group $G_{\text{GUT}} \supset G_{\text{SM}}$. This is known as grand unification.

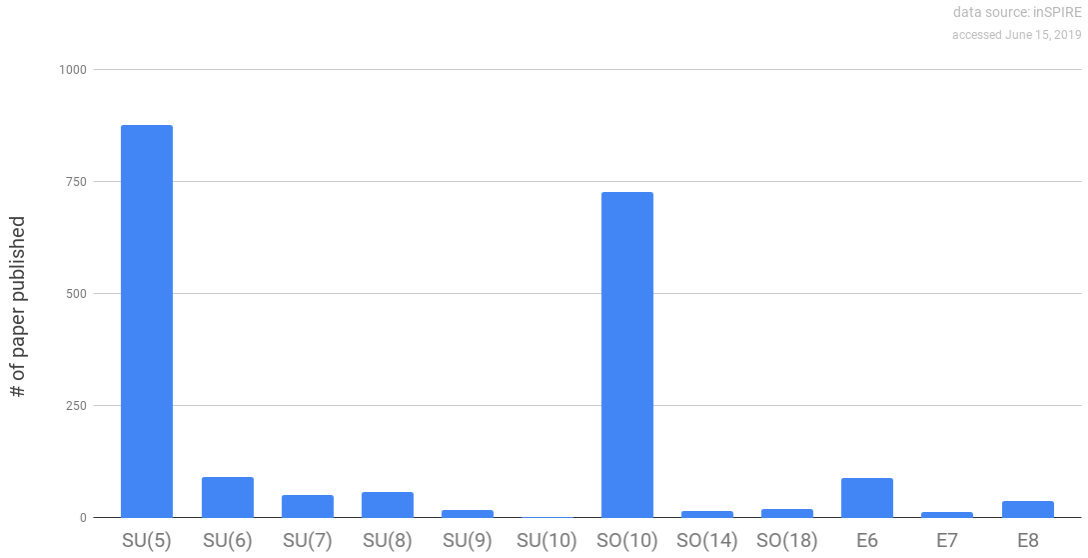

Figure 1.1.: *The total number of papers published that mention a given group plus unification in the title or abstract.*

As shown in Figure 1.1, the most popular simple groups that are commonly used in the context of Grand Unified Theories (GUTs) are:

- $SU(5)$ — the smallest viable simple group and was used in the original GUT, which was proposed by Georgi and Glashow [4].
- $SO(10)$ — popular since its spinorial 16-dimensional representation contains a complete generation of Standard Model fermions plus a right-handed neutrino [5].
- E_6 — the only exceptional group that can be used in conventional GUTs [6].

A generic consequence of the embedding of G_{SM} in a larger group is that there are additional gauge bosons which have not been observed so far. Therefore, G_{GUT} must be broken

$$G_{\mathrm{GUT}} \overset{M_{\mathrm{GUT}}}{\to} \ldots \overset{M_I}{\to} G_{\mathrm{SM}} \overset{M_Z}{\to} SU(3)_C \times U(1)_Q \tag{1.2}$$

at a sufficiently high scale M_{GUT}.

In the following sections, we will discuss why the embedding of G_{SM} in a simple group G_{GUT} is an attractive idea and how specific unified models can, in principle, be tested.

1.1. Postdictions

Coupling Strengths

First of all, unified models are intriguing because they allow us to understand the relative strengths of the Standard Model gauge couplings. This is possible since at scales above M_{GUT} there is only one unified gauge coupling g_{GUT} and therefore, the Standard Model gauge couplings have a common origin:[1]

$$g_{1Y}(M_{\mathrm{GUT}}) = g_{2L}(M_{\mathrm{GUT}}) = g_{3C}(m_{\mathrm{GUT}}) \equiv g_G(M_{\mathrm{GUT}})\,. \tag{1.3}$$

After the breaking of G_{GUT}, the gauge couplings corresponding to the various remnant groups run differently such that at the electroweak scale, we find

$$g_{1Y}(M_Z) < g_{2L}(M_Z) < g_{3C}(M_Z)\,. \tag{1.4}$$

This difference is a result of the fact that fermions screen charges if we look at them from a distance, while gauge bosons have the opposite effect [7].

Since $SU(3)$ has dimension 8, we have 8 corresponding gauge bosons and their effect outweighs the effect of the color-charged fermions. In contrast, for the rank-3 group $SU(2)$, the effect of the gauge bosons and fermions almost cancel each other, while for $U(1)$ the effect of the fermions dominates since there is only one associated gauge boson with no self-coupling. This implies that g_{3C} becomes stronger as we zoom out from M_{GUT} to M_Z, while g_{1Y} becomes weaker and g_{2L} stays approximately the same. This is shown schematically in Figure 1.2.

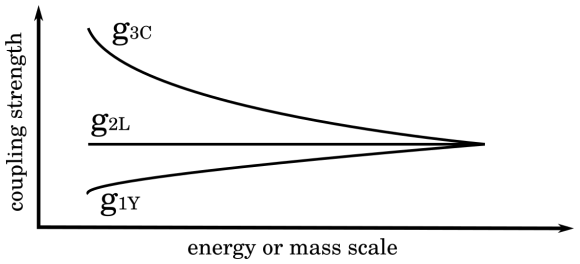

Figure 1.2.: *Schematic running of the gauge couplings in the Standard Model. The couplings become approximately equal at a sufficiently high energy scale. This supports the GUT idea.*

From a bottom-up perspective, we can argue that the running of the Standard Model couplings supports the idea that they unify at a high energy scale. If the particle content of the Standard Model were different, the differences between the couplings could become larger at higher scales as shown in Figure 1.3. This, in turn, would be a strong argument against the GUT framework.

Interestingly, the Standard Model couplings do not only approximately unify but they also do this at a scale that is sufficiently high to be in agreement with bounds from proton decay experiments.[2] Again, the situation could be very different if the particle content of the Standard Model and the measured values of the gauge couplings were different.

[1] At two-loop order and beyond this naive unification conditions must be modified. This is discussed in Chapter 2.

[2] This is discussed in more detail in Section 1.2.

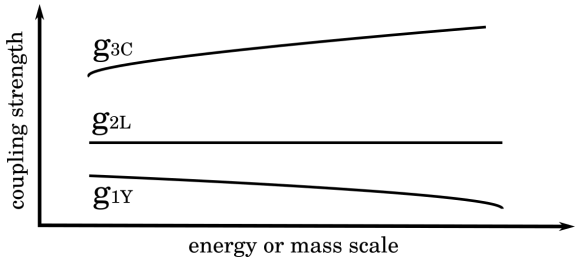

Figure 1.3.: *Alternative scenario with different values for the gauge couplings at low energies and a different particle content. This would be a strong argument against the GUT idea.*

To summarize, in grand unified models we can understand the relative strengths of the gauge couplings solely using group theoretical properties of the corresponding gauge groups. Moreover, the particle content and the gauge couplings of the Standard Model might, optimistically, be interpreted as hints for the correctness of the general unification hypothesis.

Quantization of Electric Charge

Another beautiful aspect of grand unification is that it allows us to understand why the electric charges of leptons and quarks are related. In the Standard Model, electric charges are free parameters since there is no group theoretical restriction on the values of $U(1)$ charges.

In GUTs, however, the Standard Model gauge group is a remnant of the GUT group. In particular, each Standard Model generator corresponds to a generator of the GUT group and quarks and leptons live in common representations. This makes it possible to derive relations between the $U(1)$ charges of different particles. For example, in $SU(5)$ models the down quark and lepton doublet live in a single representation

$$\bar{5} = \begin{pmatrix} \nu_L \\ e_L \\ (d_R^c)_{\text{red}} \\ (d_R^c)_{\text{blue}} \\ (d_R^c)_{\text{green}} \end{pmatrix} . \tag{1.5}$$

Moreover, all $SU(5)$ Cartan generators can be written as (5×5) diagonal matrices with trace zero. For the electric charge generator Q this implies

$$\begin{aligned} 0 &\stackrel{!}{=} \text{Tr}(Q) \\ 0 &\stackrel{!}{=} \text{Tr} \begin{pmatrix} Q(\nu_L) & 0 & 0 & 0 & 0 \\ 0 & Q(e_L) & 0 & 0 & 0 \\ 0 & 0 & Q((d_R^c)_{\text{red}}) & 0 & 0 \\ 0 & 0 & 0 & Q((d_R^c)_{\text{blue}}) & 0 \\ 0 & 0 & 0 & 0 & Q((d_R^c)_{\text{green}}) \end{pmatrix} \\ 0 &\stackrel{!}{=} Q(\nu_L) + Q(e_L) + 3Q(d_R^c) \\ Q(d_R^c) &\stackrel{!}{=} -\frac{1}{3} Q(e_L) \,. \end{aligned} \tag{1.6}$$

Analogous relations can be derived for all other fermions. Thus, once more from an optimistic bottom-up perspective, one might argue that the experimental fact

$Q_{\text{proton}} + Q_{\text{electron}} = \mathcal{O}(10^{-20})$ is another strong hint that the Standard Model gauge group should be embedded in a simple group.

Neutrino Masses

In many GUT models the existence of right-handed neutrinos is an automatic consequence of the group theoretical structure of G_{GUT}. For example, in $SO(10)$ and E_6 models, the smallest representation which contains all Standard Model fermions of one generation, automatically contains a right-handed neutrino. Since right-handed neutrinos are Standard Model singlets, they can develop a nonzero mass at scales far above the electroweak scale. In GUTs, they usually get their mass from a Higgs vacuum expectation value that is also responsible for one specific step in the breaking chain (Eq. (1.2)). After the breaking of the electroweak symmetry, one finds, quite generically, a type-I seesaw structure in the neutrino sector [8–11]. Therefore, unified models do not only provide a mechanism that yields nonzero mass terms for the left-handed neutrinos, but can also help to understand why they are so light.

Matter-Antimatter Asymmetry

Grand unified models contain generically all ingredients that are necessary to provide an explanation for the observed matter-antimatter asymmetry [12]. In particular, baryon number violating processes are permitted in unified models since quarks and leptons live in common representations of the GUT group. One the one hand, this leads to the prediction that the proton is not stable.[3] On the other hand, baryon number violation is one of the Sakharov conditions [13]. Therefore, to quote Nanopoulos "*if the proton was stable it would not exist*" [14].

Next, after this short discussion of generic *post*dictions of grand unified models, we discuss actual *pre*dictions in the following section.

[3] This is discussed in more detail in the next section.

1.2. Predictions

Proton Decay

The most famous consequence of the GUT paradigm is that the proton is unstable.[4] As mentioned above, this follows since quarks and leptons live together in one or multiple representations of the GUT group. Thus, there are gauge bosons that carry color *and* weak isospin which, in turn, implies that they are capable of mixing quarks and leptons. In particular, such X-bosons can transform a quark into a positron and therefore mediate the process $p \to e^+ + \pi^0$ (Figure 1.4).

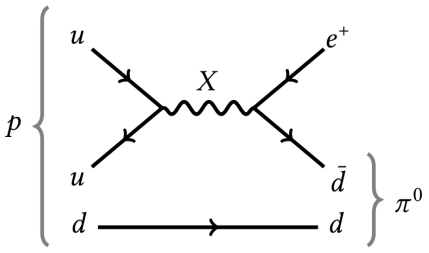

Figure 1.4.: *Proton decay process $p \to e^+ + \pi^0$ mediated by a superheavy X-boson, which is the dominant process in most non-supersymmetric GUTs [16].*

The resulting proton lifetime can be estimated using the formula [16]

$$\tau_p = \frac{M_X^4}{g_{\mathrm{GUT}}^4 m_p^5}\,, \tag{1.7}$$

where m_p denotes the proton mass, g_{GUT} is the unified gauge coupling and M_X is the mass of the relevant GUT gauge bosons.

The detection of proton decay is commonly regarded as the "*smoking gun signature of Grand Unified Theories*" [17]. Unfortunately, proton decay, so far, has never been observed and as a result, many models like the original GUT model by Georgi and Glashow [4] are already ruled out. Minimal $SU(5)$ models like the Georgi-Glashow model predict a proton lifetime of around $10^{28.5} \sim 10^{31.5}$ yrs [18], which is far below the current experimental limit [19]

$$\tau_P \gtrsim 1.6 \cdot 10^{34}\ \mathrm{yrs}\,. \tag{1.8}$$

However, as we will discuss in detail in Chapter 2, there are still several simple scenarios which are not yet ruled out by proton decay experiments.

Magnetic Monopoles

The second most famous generic prediction of grand unified models is the existence of magnetic monopoles [20]. In fact, magnetic monopoles appear in the spectrum of any gauge theory in which a semi-simple group is broken to a subgroup that contains a $U(1)$ factor [21, 22]. Therefore, all realistic GUT models contain monopole solutions.

[4] It is, of course, possible to construct GUT models in which the proton is stable or quasi-stable. But, as Nanopoulos puts it: *"OK, you can do it, but ... you cannot show it to your mother with a straight face."* [15]

In simple GUT models, there is only one type of monopole solution and its mass can be approximated using the formula [18]

$$m_M \approx \frac{4\pi M_{\mathrm{GUT}}}{g^2_{\mathrm{GUT}}}\,. \tag{1.9}$$

Using this approximation and the fact that magnetic monopoles are absolutely stable, it can be shown that they are produced in large numbers in the early universe [23] and therefore would *"dominate the mass density of the universe by many orders of magnitude"* [24]. But this is clearly in conflict with experimental bounds since, so far, no magnetic monopole has ever been observed [25] and a large number of magnetic monopoles would have a significant effect on nucleosynthesis and the expansion of the universe [26].

Therefore, some suppression mechanism like cosmological inflation [27], inverse symmetry breaking [28], a strong first order phase transition [29] or Planck scale corrections [24] must be invoked.

New Particles

Although the detection of proton decay and magnetic monopoles would be strong hints for the correctness of the GUT paradigm, the ultimate test is whether new particles predicted by a specific unified model can be detected. At a minimum, models with an enlarged gauge symmetry contain additional gauge bosons. In addition, conventional GUT models often contain additional scalars and fermions. The scalars are necessary for the breaking of the enlarged symmetry and for a realistic pattern of fermion masses and mixing angles. Additional fermions are necessary, as mentioned above, to explain the smallness of neutrino masses using a type-I seesaw and can arise as an automatic consequence of the GUT group structure.

Unfortunately, the GUT scale is likely to be above 10^{15} GeV, as can be concluded from the slow running of the gauge couplings and the limits from proton decay experiments (Eq. (1.8)). To probe such high energies using present day technologies, a collider with a diameter comparable to the size of our solar system would be necessary. Therefore, it will probably not be possible to detect all particles predicted by GUT models in the near future. However, in specific scenarios there can be remnants of the broken GUT symmetry at much lower scales [30, 31]. While the discovery of such low energy remnants would not be a definite proof of the GUT hypothesis, it could lend further support to the general "larger symmetry" guiding principle and help us to figure out the correct GUT group and breaking chain.

1.3. Intrinsic vs. External Solutions

In the preceding sections, we have discussed which Standard Model puzzles can, quite generically, be solved in unified models and how such models can, in principle, be tested. One can certainly argue that these features are reason enough to study grand unified theories in detail. At the same time, there are several problems, like, for example, the strong CP problem, the flavor puzzle and the dark matter problem, unified models seemingly cannot help us with. Moreover, GUT models introduce new problems. One issue is that the Standard Model gauge couplings almost unify but not exactly. In the following, we call this the gauge unification problem. A second GUT puzzle is why proton decay has never been observed so far.

One way to deal with these issues is to extend grand unified models with additional ingredients. For example, it is possible to construct unified models which contain viable dark matter candidates by introducing supersymmetry [32] or additional fermion representations plus discrete symmetries [33]. Alternatively, one can solve the strong CP and dark matter problem simultaneously by introducing an additional Peccei-Quinn symmetry [17, 34, 35]. The flavor puzzle can possibly be solved by enlarging the symmetry group using family symmetries [36]. Moreover, the proton decay and gauge coupling unification problems can also be solved by supersymmetry [37].

A second possibility is to try to construct specific GUT models which solve additional Standard Model problems intrinsically. For example, there have been several (not entirely satisfactory) attempts to construct GUT models that contain a Peccei-Quinn symmetry accidentally [38–41].[5] This is an attractive idea because in such models "*the whole PQ machinery serves not simply for one purpose — solving the strong CP problem.*" [43] Using the terminology introduced in this section, we can say that models with an accidental Peccei-Quinn symmetry solve the strong CP problem intrinsically, while models in which it must be added by hand solve it externally. A key difference is that a Peccei-Quinn symmetry can, in principle, be added by hand to any GUT model but only appears accidentally in very specific models. Other examples for intrinsic solutions are specific E_6 models which contain automatically a viable dark matter candidate [44] and models in which intrinsic flavor symmetries can possibly help to solve the flavor puzzle [45, 46]. Again, the main difference between these intrinsic solutions and the external solutions mentioned above is that intrinsic solutions only work in a small subclass of models. In contrast, it is possible to add suitable new representations plus a discrete symmetry and a family symmetry to any model to get a viable dark matter candidate and to solve the flavor puzzle. Therefore, intrinsic solutions have the advantage that they potentially yield concrete guidelines for GUT model builders. This is helpful because one of the biggest problem of the GUT framework is that there, in principle, infinitely many grand unified models since there is an infinite number of viable groups G_{GUT}. Moreover, even if G_{GUT} is fixed, there are usually several viable breaking chains which lead to very different scenarios. By focusing on intrinsic solutions, however, the number of compatible GUT groups and breaking chains can be narrowed down significantly.

From an optimistic perspective, we can therefore argue that by searching for intrinsic

[5] Most models with accidental Peccei-Quinn symmetry are phenomenologically unacceptable [42] (e.g., Ref. [38] predicts a massless fermion generation) .

solutions, we try to reinterpret problems of the Standard Model as hints for specific GUT models.

In this thesis, we focus on intrinsic solutions of GUT and Standard Model problems. In Chapter 2, we discuss how the gauge unification and proton decay problem can be intrinsically solved in non-supersymmetric GUT models. In addition, after a short review of the strong CP problem in Chapter 3, we discuss in Chapter 4 an intrinsic GUT solution to the strong CP problem. This is summarized by the following diagram.

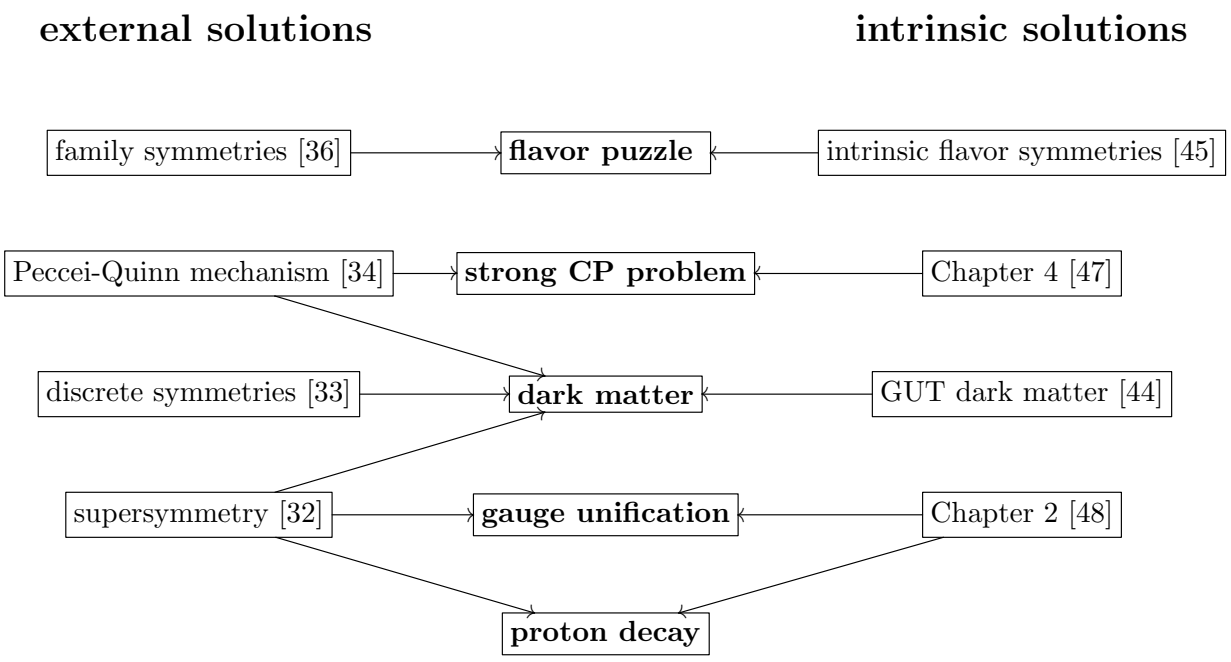

Gauge Coupling Unification without Supersymmetry 2

This chapter is based on Ref. [48].

The first model with a unified gauge symmetry was proposed by Georgi and Glashow in 1974 [4]. At this time, α_s and $\sin^2\theta_W$ were not well known experimentally and it therefore seemed reasonable that the three Standard Model gauge couplings indeed meet at a single point at a sufficiently high energy scale. In particular, the gauge couplings are running towards each other and become approximately of the same order of magnitude at around $M_X > 10^{14}$ [18].

However, when the CERN SPS experiment measured for the Weinberg angle $\sin^2\theta_W = 0.24 \pm 0.02$ [49], it was quickly pointed out by Buras, Ellis, Gaillard and Nanopoulos that the value predicted by the Georgi-Glashow model ($\sin^2\theta_W(10\text{ GeV}) \approx 0.20$) is *"somewhat low"* and therefore, that there is *"a possible problem with the value of* $\sin^2\theta_W$*"* [50]. Moreover, when α_s was measured more precisely by the DELPHI experiment [51], Amaldi, de Boer and Fürstenau concluded that *"in the minimal non-supersymmetric Standard Model with one Higgs doublet a single unification point is excluded by more than 7 standard deviations"* [37]. The running of the gauge couplings in the Standard Model using present-day data is shown in Figure 2.1.

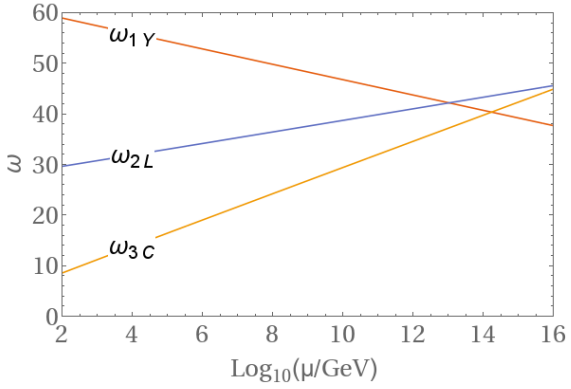

Figure 2.1.: *Running of the Standard Model couplings* ($\omega_i = \alpha_i^{-1} = \frac{4\pi}{g_i^2}$) *at two-loop order.*

The fact that the Standard Model gauge couplings do not meet at a single point can be interpreted in two ways:

1. The grand unification framework is wrong.

2. There is no "grand desert" between the electroweak and the unification scale.

Since, as discussed in the previous chapters, unified models have many attractive features, the second option was and still is preferred by many physicists.

One possibility to achieve unification of the gauge couplings is by introducing low-energy supersymmetry (SUSY). Famously, the authors of Ref. [37] noted in 1991 that *"the minimal supersymmetric extension of the Standard Model leads to unification"*. In particular, they discovered that for a SUSY scale of around 1 TeV, the gauge couplings almost perfectly unify. In the years after this discovery, supersymmetry and grand unified models were thought to be in a symbiotic relationship. On the one hand, supersymmetry was regularly invoked to achieve unification of the gauge couplings. On the other hand, the fact that the gauge couplings meet almost perfectly at a point in supersymmetric models was interpreted as a further hint for low-energy supersymmetry. As shown in Figure 2.2, this is visible in the fraction of GUT papers which explicitly invoke supersymmetry.

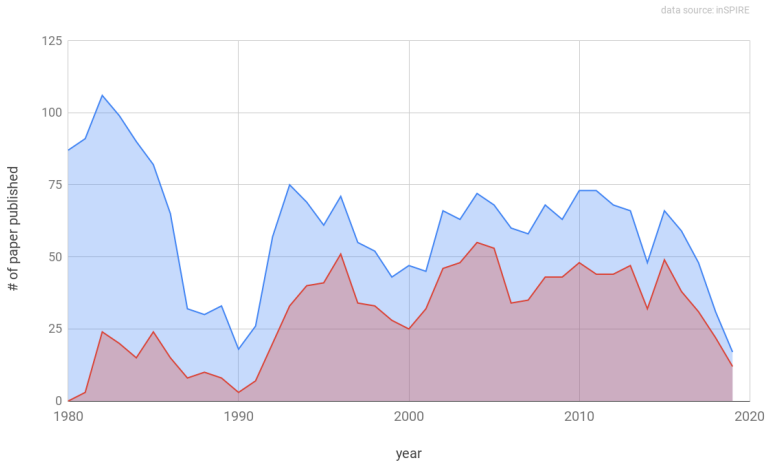

Figure 2.2.: *The blue area indicates the total number of paper published with either $SU(5)$, $SO(10)$ or E_6 in the title. The red area indicates the fraction of these papers with additionally "susy", "supersymmetry" or "supersymmetric" in the title or abstract. The dip in the years from 1987 to 1990 resulted when early GUT models were ruled out by proton decay experiments [52]. In 1991 it was discovered that the proton lifetime can be much longer in supersymmetric unified models [37].*

However, so far, no supersymmetric partner of a Standard Model particle has ever been experimentally observed. For this reason, there has been recently a revival of unified models without low-energy supersymmetry [34, 35, 53–57]. In these kind of models, the mismatch of gauge couplings requires a different explanation.

In the following sections, we will discuss the various possibilities to achieve unification of the gauge couplings without low-energy supersymmetry in general and systematic terms. For concreteness, we will focus on the three most popular GUT groups $SU(5)$, $SO(10)$ and E_6. Moreover, we will restrict ourselves to a class of models ("conservative models") that mimic the structure of the Standard Model as much as possible. As a guideline, we can observe that the structure of the Standard Model follows the rules:

- Only scalar representations that couple to fermions are permitted.
- Only fermions that live in the fundamental or trivial representation of the gauge group are permitted.
- And, of course, only gauge bosons that live in the adjoint of the gauge group are permitted.

Unfortunately, the models that we find by applying these rules to $SU(5)$ and $SO(10)$ models are non-viable and we are forced to bend the rules outlined above. But in these scenarios, we try to bend the rules as little as possible and therefore only add representations that are necessary to make them realistic.

In particular, in $SU(5)$ models we are forced to add a fermionic 10-dimensional representation since the fundamental 5 is too small to contain all Standard Model fermions. Moreover, in $SO(10)$ and $SU(5)$ models at least one additional scalar representation that does not couple to fermions is necessary to accomplish the symmetry breaking down to G_{SM}.

These additions can also be understood from a top-down perspective by noting that all representations that are necessary to make $SO(10)$ and $SU(5)$ models viable automatically exist in conservative E_6 models and that $SU(5) \subset SO(10) \subset E_6$.

After a short discussion of the renormalization group equations for the gauge couplings, we discuss in Section 2.2 if threshold corrections are sufficient to explain the mismatch in conservative grand desert scenarios. In Section 2.3, we then analyze the running of the gauge couplings in conservative scenarios with particles at intermediate scales.

2.1. The Standard Model RGEs and Hypercharge Normalization

In general, the renormalization group equations for the gauge couplings g_i up to two-loop order read [58]

$$\frac{d\omega_i(\mu)}{d\ln\mu} = -\frac{a_i}{2\pi} - \sum_j \frac{b_{ij}}{8\pi^2\omega_j}. \tag{2.1}$$

Here,

$$\omega_i = \alpha_i^{-1} = \frac{4\pi}{g_i^2} \tag{2.2}$$

and a_i and b_{ij} are the one-loop and two-loop coefficients respectively. The RGE coefficients depend on the particle content of the model and can be calculated using the general formulas in Ref. [58] or more conveniently, using PyR@TE 2 [59].

For the Standard Model, the one-loop and two-loop coefficients read

$$a_{\text{SM}} = \left(\tfrac{41}{6}, -\tfrac{19}{6}, -7 \right), \qquad b_{\text{SM}} = \begin{pmatrix} \frac{199}{18} & \frac{9}{2} & \frac{44}{3} \\ \frac{9}{10} & \frac{35}{6} & 12 \\ \frac{11}{10} & \frac{9}{2} & -26 \end{pmatrix}. \tag{2.3}$$

The Standard Model RGE's can then, in principle, be solved using the experimental boundary conditions [60]

$$\begin{aligned} \omega_{1Y}(M_Z) &= 98.3686 \\ \omega_{2L}(M_Z) &= 29.5752 \\ \omega_{3C}(M_Z) &= 8.54482 \\ M_Z &= 91.1876 \ \text{GeV}. \end{aligned} \tag{2.4}$$

However, there is an ambiguity in the running of ω_{1Y} since the hypercharge normalization is not fixed in the Standard Model. The Standard Model Lagrangian only involves the product of the gauge coupling constant g_{1Y} and the hypercharge operator Y. Therefore, the Lagrangian remains unchanged under rescalings of the hypercharge $(g_{1Y}, Y) \to \left(n_Y^{-1} g_{1Y}, n_Y Y\right)$ for any $n_Y \in \mathbb{R}$. It is conventional to define n_g as the normalization constant relative to the "Standard Model normalization" in which the left-handed lepton doublets carry hypercharge -1 and the left-handed quark doublets carry hypercharge $1/3$. Moreover, it is conventional to normalize the generators of non-abelian gauge groups T^i such that

$$\text{Tr}(T^i T^j) = \frac{1}{2}\delta^{ij}. \tag{2.5}$$

The values in Eq. (2.4) and the coefficients in Eq. (2.3) are only valid as long as these particular normalizations are used.

In particular, this implies that we can achieve that the gauge couplings meet at a common point solely by modifying the hypercharge normalization appropriately. The solutions of the Standard Model RGEs for different hypercharge normalizations are shown in Figure 2.3. We can see here that for $n_Y \approx \sqrt{3/4}$, the three gauge couplings indeed meet approximately at around $\mu \approx 10^{16.5}$ GeV.

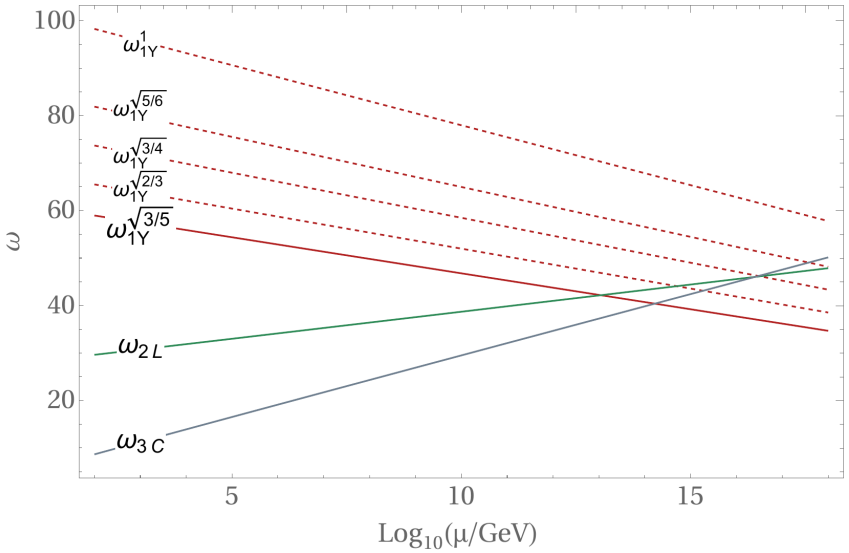

Figure 2.3.: *Solutions of the 2-loop RGEs for the Standard Model gauge couplings with different normalizations of the hypercharge, as indicated by the superscripts. The solid line corresponds to the canonical normalization that we get, for example, in $SU(5)$, $SO(10)$ and E_6 models.*

However, in models with a unified gauge symmetry it is no longer possible to rescale the hypercharge arbitrarily. In such models, the hypercharge group $U(1)_Y$ is a remnant of the simple unification group G_{GUT} and therefore its normalization is fixed by the normalization of the G_{GUT} charges. In particular, the hypercharge generator Y corresponds to a generator of the unified gauge group and therefore, it must be consistently normalized like all other generators of G_{GUT}, as specified in Eq. (2.5).

For example, in $SU(5)$ models the G_{SM} representations $d^c = \left(\overline{\mathbf{3}}, \mathbf{1}, \frac{1}{3}n_Y\right)$ and $L = \left(\mathbf{1}, \mathbf{2}, -\frac{1}{2}n_Y\right)$ are usually embedded in the fundamental $\overline{5}$. The hypercharge generator therefore reads $Y = n_Y \times \text{diag}\left(\frac{1}{3}, \frac{1}{3}, \frac{1}{3}, -\frac{1}{2}, -\frac{1}{2}\right)$. Using this, we can calculate

$$\text{Tr}\left(Y^2\right) = \frac{5}{6}n_Y^2 \overset{(2.5)}{=} \frac{1}{2} \tag{2.6}$$

and therefore, we find $|n_Y| = \sqrt{3/5}$.

The value $n_Y = \sqrt{3/5}$ is known as the canonical normalization since it automatically follows in models based on the most popular unification groups like $SU(5)$, $SO(10)$ and E_6. We can see in Figure 2.3 that for $n_Y = \sqrt{3/5}$, the gauge couplings do not meet at a common point.

For alternative unification groups or non-standard embeddings of G_{SM}, different values of n_Y are possible [61]. Therefore, one could argue that this is a hint that $SU(5)$, $SO(10)$ and E_6 are the wrong choices for G_{GUT}. In particular, we could search for a group G_{GUT} which yields $n_Y \approx \sqrt{3/4}$. But unfortunately, the value $n_Y = \sqrt{3/5}$ is quite generic in realistic models since it follows whenever the Standard Model is embedded in a way that allows us to assume an intermediate $SU(5)$ symmetry, i.e. $G_{GUT} \to SU(5) \to G_{SM}$ [62].

In the following sections, we will consider models involving the groups $SU(5)$, $SO(10)$ and E_6 and therefore always use the canonical normalization $n_Y = \sqrt{3/5}$. Nevertheless, in particular for proposals that go beyond the standard GUT paradigm [63–65], it is

important to keep in mind that from a bottom up perspective, the gauge couplings can meet perfectly at a point since the hypercharge normalization is not fixed in the Standard Model.

Before we can discuss unification scenarios in more concrete terms, we need to define a criterion that tells us when exactly the merging of the gauge couplings is successful. In general, the nonzero vacuum expectation value that breaks G_{GUT} yields masses m_X for some of the gauge bosons associated with G_{GUT}. But in processes involving only energies much larger than m_X, the breaking of G_{GUT} can be neglected and the gauge couplings are approximately equal [66]. Therefore, a naive unification condition reads

$$\omega_{1Y}(m_X) = \omega_{2L}(m_X) = \omega_{3C}(m_X) \equiv \omega_G(m_X)\,, \tag{2.7}$$

where ω_G denotes the unified gauge coupling.

However, if we use two-loop RGEs this condition must be refined and in particular, threshold corrections can alter Eq. (2.7) significantly [67].

2.2. Thresholds Corrections

Threshold corrections are necessary if the masses of the particles which become massive through the breaking of G_{GUT} are not exactly degenerate. While the corrections are small for individual particles, they can become significant in unified models since they typically predict a large number of superheavy particles [67, 68]. In principle, threshold corrections can be so large that they alone are sufficient to explain the observed mismatch of the gauge couplings in Figure. 2.1 [69].

Threshold corrections can be taken into account by modifying the matching conditions (Eq. (2.7)) as follows [70]:

$$\omega_i(\mu) = \omega_G(\mu) - \frac{\lambda_i(\mu)}{12\pi}, \tag{2.8}$$

where

$$\begin{aligned} \lambda_i(\mu) \;=\; & \overbrace{(C_G - C_i)}^{\lambda_i^G} - 21 \overbrace{Tr\left(t_{iV}^2 \ln \frac{M_V}{\mu}\right)}^{\lambda_i^V} \\ & + \underbrace{Tr\left(t_{iS}^2 P_{GB} \ln \frac{M_S}{\mu}\right)}_{\lambda_i^S} + 8 \underbrace{Tr\left(t_{iF}^2 \ln \frac{M_F}{\mu}\right)}_{\lambda_i^F}. \end{aligned} \tag{2.9}$$

Here, S, F, and V denote the scalars, fermions and vector bosons which are integrated out at the matching scale μ, t_{iS},t_{iF}, t_{iV} are the generators of G_i for the various representations, and C_G and C_i are the quadratic Casimir operators for the groups G and G_i. P_{GB} is an operator that projects out the Goldstone bosons. The traces of the quadratic generators are known as the Dynkin indices and can be found in Ref. [71]. It is convenient to define

$$\eta_j = \ln\left(\frac{M_j}{\mu}\right), \tag{2.10}$$

where j labels a given multiplet.

Of course, no experimental data on the masses of superheavy particles is available and therefore the exact magnitude of the threshold corrections is unknown. We can, however, estimate the impact of threshold corrections systematically by generating random spectra for the superheavy particles. Specifically, we generate the masses of all superheavy particles M_i randomly within a reasonable given range around the GUT scale

$$M_i = R M_{GUT}, \tag{2.11}$$

where R is a random number within a fixed range. It is usually argued that a spread of $R \in [\frac{1}{10}, 10]$ [68, 72] or $R \in [\frac{1}{10}, 2]$ [35] is, "*from a theoretical point of view, quite reasonable*" [69].[1] For each random spectrum that is generated this way, we can calculate the corresponding threshold corrections explicitly by using Eq. (2.9).

For the further analysis, it is convenient to define the following quantities, which are independent of the unified gauge coupling $\omega_G(\mu)$ [75]

$$\Delta\lambda_{ij}(\mu) \equiv 12\pi\left(\omega_i(\mu) - \omega_j(\mu)\right) = \lambda_j(\mu) - \lambda_i(\mu), \tag{2.12}$$

[1] In particular, specific scalar masses can be significantly below the GUT if there are spontaneously broken accidental global symmetries in the scalar potential and therefore pseudo-Goldstone modes [73, 74].

for $i, j = 1, 2, 3$, $i \neq j$. It is conventional to use $\Delta\lambda_{12}$ and $\Delta\lambda_{23}$. These quantities can be evaluated in two ways.

- Firstly, the $\Delta\lambda_{ij}(\mu)$ can be evaluated from an IR perspective by evolving the measured values of the couplings up to some scale μ. The value of $\Delta\lambda_{ij}(\mu)$ at a specific scale μ indicates the distance between the values of the gauge couplings ω_i and ω_j. Formulated differently, $\Delta\lambda_{ij}(\mu)$ is a measure of how much ω_i and ω_j fail to unify.

- Secondly, the $\Delta\lambda_{ij}(\mu)$ can be calculated from an UV perspective by using a specific mass spectrum of the superheavy particles. For a given mass spectrum, the corresponding $\Delta\lambda_{ij}(\mu)$ can be calculated using Eq. (2.9). Therefore, the $\Delta\lambda_{ij}(\mu)$ can be used as a measure for the size of the threshold corrections in a specific model.

By combining these two perspectives, we reach the conclusion that if a specific unified model yields large enough $\Delta\lambda_{ij}(\mu)$ as required from the IR input, the threshold corrections can successfully explain the mismatch in the gauge couplings.

An important point that we need to take into account before we can discuss concrete models is that some gauge bosons mediate proton decay. Therefore, in realistic scenarios the gauge couplings unify at a sufficiently high scale such that the corresponding proton lifetime is in agreement with the experimental bound from Super-Kamiokande [19]

$$\tau_P(p \to e^+\pi^0) > 1.6 \times 10^{34} \text{ yrs}\,. \tag{2.13}$$

If proton decay is mediated primarily by superheavy gauge bosons, we can use Eq. (1.7) and Eq. (2.13) to derive

$$\left(\frac{\omega_G}{45}\right) 10^{2(k_{\rm GUT}-15)} > 16.6\ , \tag{2.14}$$

where $M_{\rm GUT} \equiv 10^{k_{\rm GUT}}$ GeV. For a typical value like $\omega_G = 45$, Eq. (2.14) yields $k_{\rm GUT} > 15.6$.

Moreover, since the masses of the various superheavy gauge bosons can be non-degenerate, it is conventional to define the unification scale M_{GUT} as the mass scale of the lightest proton decay mediating gauge boson. Figure 2.4 shows $\Delta\lambda_{23}(\mu)$ over $\Delta\lambda_{12}(\mu)$ as evaluated from an IR perspective using the experimental values given in Eq. (2.4). Here we assume that there is a "grand desert", i.e. no new physics between the electroweak and the GUT scale

---

In the following sections, we discuss if sufficiently large values of $\Delta\lambda_{12}(\mu)$ and $\Delta\lambda_{23}(\mu)$, as shown in Figure 2.4, can be explained by threshold corrections in specific GUT models.

In conservative $SU(5)$ models, threshold corrections only arise from additional scalar representations, while in conservative $SO(10)$ scenarios there can be additional contributions from gauge bosons and in E_6 scenarios from gauge bosons and exotic fermions.[2]

[2] There are, of course, additional gauge bosons in $SU(5)$ models, too. However, these gauge bosons mediate proton decay and therefore cannot live below the GUT scale.

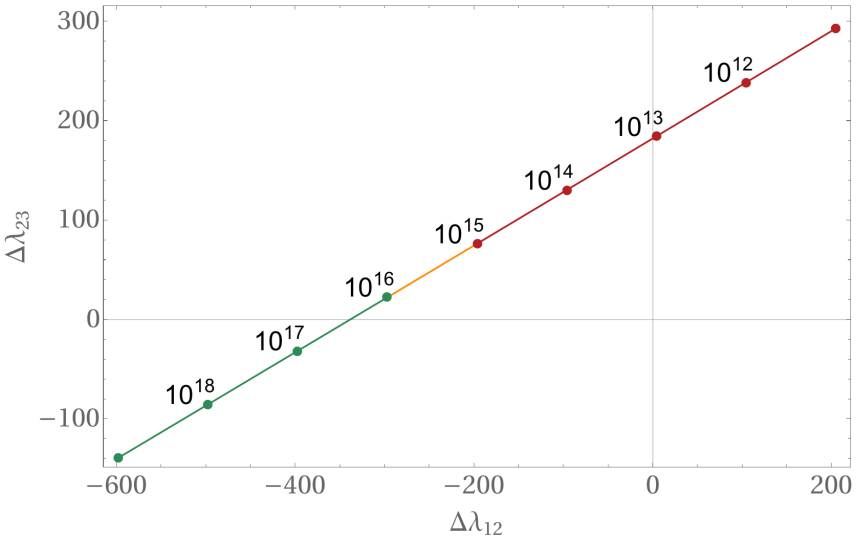

Figure 2.4.: $\Delta\lambda_{23}(\mu)$ *over* $\Delta\lambda_{12}(\mu)$ *evaluated from the IR input in Eq.* (2.4) *for a grand desert scenario. The numbers above the line denote the scale* μ *in GeV. The red section of the line indicates scales which are in conflict with proton lifetime bounds (Eq.* (2.14)*). The orange section implies a proton lifetime close to and the green section a proton lifetime above the current bound.*

2.2.1. $SU(5)$

One of the most important tasks in GUT model building is to find a suitable representation of $G_{\rm GUT}$ for the fermions. In particular, the $G_{\rm SM}$ representations given in Table 2.1 must be embedded in a $G_{\rm GUT}$ representation.

Name	Symbol	$SU(3)_C \times SU(2)_L \times U(1)_Y$
Left-handed Leptons	$\begin{pmatrix}\nu_L\\ e_L^-\end{pmatrix}$	$(1,2,-1/2)$
Left-handed Quarks	$\begin{pmatrix}u_L^r, u_L^g, u_L^b\\ d_L^r, d_L^g, d_L^b\end{pmatrix}$	$(3,2,1/6)$
Right-handed Electron	e_R^-	$(1,1,-1)$
Right-handed Up Quark	$\left(u_R^r, u_R^g, u_R^b\right)$	$(3,1,2/3)$
Right-handed Down Quark	$\left(d_R^r, d_R^g, d_R^b\right)$	$(3,1,-1/3)$

Table 2.1.: *$G_{\rm SM}$ representations of one generation of Standard Model fermions.*

In $SU(5)$ models, each generation of the Standard Model fermions lives in the composite $\overline{5} \oplus 10$ representation. Using the products [71]

$$\begin{aligned} 5 \times 5 &= 10 \oplus 15\,, \\ 5 \times \overline{10} &= \overline{5} \oplus \overline{45}\,, \\ \overline{10} \times \overline{10} &= 5 \oplus 45 \oplus 50\,, \end{aligned} \tag{2.15}$$

we can conclude that scalars with renormalizable Yukawa couplings to the Standard Model fermions live in the

$$\overline{5} \oplus 5 \oplus 10 \oplus 15 \oplus 45 \oplus \overline{45} \oplus 50 \tag{2.16}$$

representation.

The smallest representation which can accomplish the breaking of $SU(5)$ to G_{SM} is the adjoint 24. However, additional scalar representations are necessary to get realistic fermion masses and mixing angles. For completeness, we estimate the threshold correction for scenarios in which all the representations in Eq. (2.16) are present. The detailed decomposition of these representations with respect to G_{SM} is given in Appendix A.1.

Using these decompositions and Eq. (2.9), we find

$$\begin{aligned} \lambda_{3C} = 2 &+ \eta_{\varphi_2} + \eta_{\varphi_3} + \eta_{\varphi_5} + 2\eta_{\varphi_6} + 2\eta_{\varphi_8} + 5\eta_{\varphi_9} + 3\eta_{\varphi_{11}} + \eta_{\varphi_{13}} + 3\eta_{\varphi_{14}} \\ &+ \eta_{\varphi_{15}} + 2\eta_{\varphi_{16}} + 5\eta_{\varphi_{17}} + 12\eta_{\varphi_{18}} + \eta_{\varphi_{20}} + 3\eta_{\varphi_{21}} + \eta_{\varphi_{22}} + 2\eta_{\varphi_{23}} \\ &+ 5\eta_{\varphi_{24}} + 12\eta_{\varphi_{25}} + \eta_{\varphi_{27}} + 2\eta_{\varphi_{28}} + 15\eta_{\varphi_{29}} + 5\eta_{\varphi_{30}} + 12\eta_{\varphi_{31}}\,, \end{aligned}$$

$$\begin{aligned} \lambda_{2L} = 3 &+ \eta_{\varphi_1} + 3\eta_{\varphi_6} + 4\eta_{\varphi_7} + 3\eta_{\varphi_8} + 2\eta_{\varphi_{10}} + \eta_{\varphi_{12}} + 12\eta_{\varphi_{14}} + 3\eta_{\varphi_{16}} \\ &+ 8\eta_{\varphi_{18}} + \eta_{\varphi_{19}} + 12\eta_{\varphi_{21}} + 3\eta_{\varphi_{23}} + 8\eta_{\varphi_{25}} + 3\eta_{\varphi_{28}} + 24\eta_{\varphi_{29}} + 8\eta_{\varphi_{31}}\,, \end{aligned}$$

$$\lambda_{1Y} = 5 + \frac{3}{5}\eta_{\varphi_1} + \frac{2}{5}\eta_{\varphi_2} + \frac{2}{5}\eta_{\varphi_3} + \frac{6}{5}\eta_{\varphi_4} + \frac{8}{5}\eta_{\varphi_5} + \frac{1}{5}\eta_{\varphi_6} + \frac{18}{5}\eta_{\varphi_7} + \frac{1}{5}\eta_{\varphi_8} + \frac{16}{5}\eta_{\varphi_9} + \frac{3}{5}\eta_{\varphi_{12}} + \frac{2}{5}\eta_{\varphi_{13}} + \frac{6}{5}\eta_{\varphi_{14}} + \frac{32}{5}\eta_{\varphi_{15}} + \frac{49}{5}\eta_{\varphi_{16}} + \frac{4}{5}\eta_{\varphi_{17}} + \frac{24}{5}\eta_{\varphi_{18}} + \frac{3}{5}\eta_{\varphi_{19}} + \frac{2}{5}\eta_{\varphi_{20}} + \frac{6}{5}\eta_{\varphi_{21}} + \frac{32}{5}\eta_{\varphi_{22}} + \frac{49}{5}\eta_{\varphi_{23}} + \frac{4}{5}\eta_{\varphi_{24}} + \frac{24}{5}\eta_{\varphi_{25}} + \frac{24}{5}\eta_{\varphi_{26}} + \frac{2}{5}\eta_{\varphi_{27}} + \frac{49}{5}\eta_{\varphi_{28}} + \frac{12}{5}\eta_{\varphi_{29}} + \frac{64}{5}\eta_{\varphi_{30}} + \frac{24}{5}\eta_{\varphi_{31}} ,$$

with η_j defined in Eq. (2.10). These formulas can be used to calculate $\Delta\lambda_{23}$ and $\Delta\lambda_{23}$ for concrete mass spectra. As described above, we can generate these spectra by choosing the masses of all superheavy particles randomly within a fixed range. The result of such a scan for $R \in [\frac{1}{10}, 2]$ and $R \in [\frac{1}{20}, 2]$ is shown in Figure 2.5. We can see here that neither for $R \in [\frac{1}{10}, 2]$ nor for $R \in [\frac{1}{20}, 2]$, the threshold corrections are large enough to explain the mismatch in the gauge couplings.

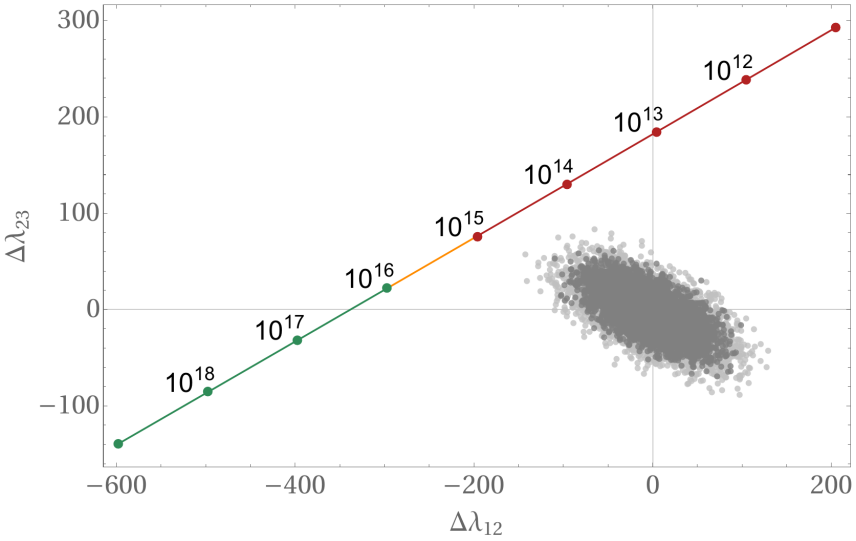

Figure 2.5.: *Threshold corrections in an $SU(5)$ GUT with scalars living in the $5 \oplus 10 \oplus 15 \oplus 23 \oplus 45 \oplus 50$ representation. The dark-gray points represent values of $\Delta\lambda_{23}(\mu)$ and $\Delta\lambda_{12}(\mu)$ for mass spectra with $R \in [\frac{1}{10}, 2]$. The light-gray points correspond to spectra with $R \in [\frac{1}{20}, 2]$.*

Next, we discuss the magnitude of threshold corrections in conservative $SO(10)$ models with a grand desert between the electroweak and the unification scale.

2.2.2. $SO(10)$

In $SO(10)$ models, each generation of the Standard Model fermions (Table 2.1) lives in a spinorial 16-dimensional representation. Therefore, scalar representations with renormalizable Yukawa couplings to the SM fermions live in the

$$\overline{16} \times \overline{16} = 10 \oplus 120 \oplus \overline{126} \tag{2.17}$$

representation. Moreover, the smallest representation which needs to be added to break $SO(10)$ down to the G_{SM} is the adjoint 45. As in the previous section, we consider the threshold effects for scenarios involving all representations listed in Eq. (2.17). The decomposition of these scalar representations with respect to G_{SM} and the corresponding formulas for the threshold corrections are given in Appendix A.2.

The main difference in $SO(10)$ models compared to $SU(5)$ models is that there are additional superheavy gauge bosons which do not mediate proton decay. This implies that there can be additional threshold corrections since the masses of these gauge bosons can be smaller or larger than M_{GUT}. Moreover, threshold correction from gauge bosons are potentially quite large compared to the corrections from scalars as can be seen in Eq. (2.9).

Using the formulas for the threshold corrections given in Appendix A.2, we can estimate the total size of the threshold correction through a scan with randomized masses. The result of such a scan, again with $R \in [\frac{1}{10}, 2]$ and $R \in [\frac{1}{20}, 2]$, is shown in Figure 2.6.

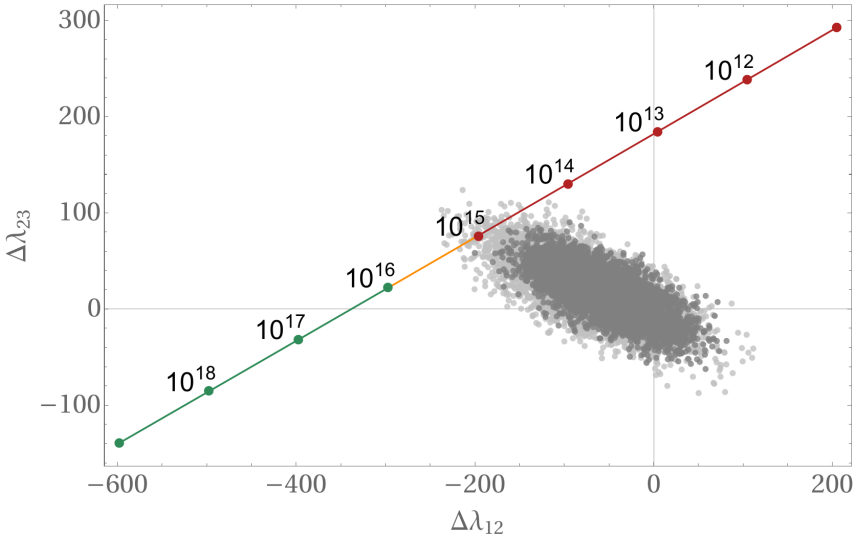

Figure 2.6.: *Threshold corrections in $SO(10)$ scenarios with scalars in the $10 \oplus 120 \oplus \overline{126} \oplus 45$ representation. The dark-gray points represent values of $\Delta\lambda_{23}(\mu)$ and $\Delta\lambda_{12}(\mu)$ for randomized mass spectra with $R \in [\frac{1}{10}, 2]$. The light-gray points correspond to scenarios with $R \in [\frac{1}{20}, 2]$.*

The main result of the scan is that there are scenario in which the threshold corrections are large enough to explain the mismatch of the gauge couplings. However, these scenarios imply a unification scale which is already ruled out by proton decay experiments (Eq. (2.14)).

Next, we discuss the magnitude of threshold corrections in conservative E_6 models with a grand desert between the electroweak and the unification scale.

2.2.3. E_6

In E_6 models, each generation of the Standard Model fermions (Table 2.1) lives in a fundamental 27-dimensional representation. Since there are only 15 fermions in each Standard Model generation, E_6 models always contain exotic fermions. To understand the particle content of the 27 it is instructive to decompose it with respect to the maximal subgroup $SO(10) \times U(1)$:

$$27 = 1_4 \oplus 10_{-2} \oplus 16_1 \,. \tag{2.18}$$

The 16_1 contains the usual Standard Model fermions plus a right-handed neutrino. The 1_4 is a sterile neutrino and the 10_{-2} contains a vector-like down quark and a vector-like lepton doublet. Since the Standard Model fermions and the exotic fermions live in the same E_6 representation, the existence of three Standard Model generations implies that there must be three generations of the exotic fermions, too.

Moreover, scalars with renormalizable Yuakwa couplings to the Standard Model fermions are contained in the

$$\overline{27} \times \overline{27} = 27 \oplus 351' \oplus 351 \tag{2.19}$$

representation. The decomposition of these scalar representations with respect to G_{SM} and the corresponding formulas for the threshold corrections are given in Appendix A.3. The main difference compared to the scenarios discussed in the previous sections is that in E_6 models, there are threshold corrections from the three generations of exotic fermions discussed above and from a much larger number of additional gauge bosons and scalars.

Using the threshold formulas given in Appendix A.3, we can estimate the magnitude of the threshold corrections using a scan over randomized mass spectra. The result of such a scan for $R \in [\frac{1}{10}, 2]$ and $R \in [\frac{1}{20}, 2]$ is shown in Figure 2.7.

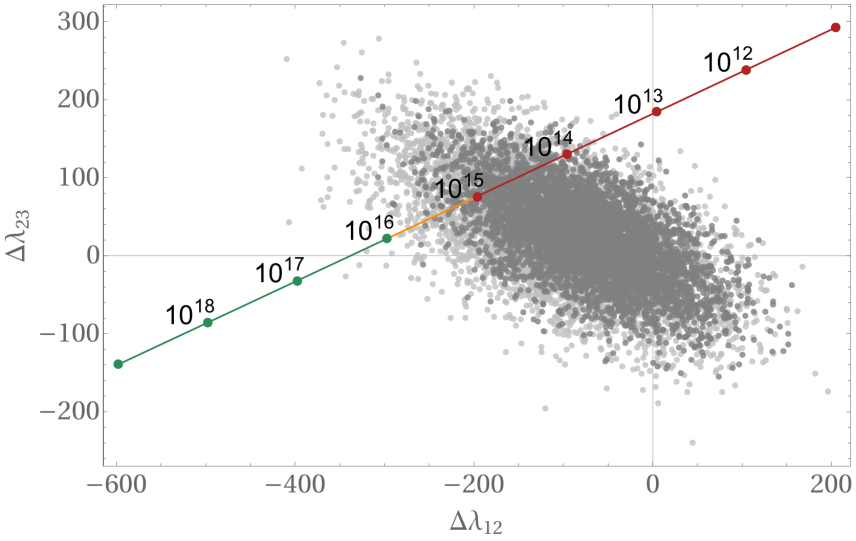

Figure 2.7.: *Threshold corrections in E_6 scenarios with scalars in the $27 \oplus 351' \oplus 351$ representation. The dark-gray points represent values of $\Delta\lambda_{23}(\mu)$ and $\Delta\lambda_{12}(\mu)$ for randomized mass spectra with $R \in [\frac{1}{10}, 2]$. The light-gray points correspond to scenarios with $R \in [\frac{1}{20}, 2]$.*

The main result of the scan is that there are scenarios in which the threshold corrections are sufficiently large to explain the mismatch of the gauge couplings and the unification scale is high enough to be in agreement with bounds from proton decay experiments (Eq. (2.14)).

In particular, the E_6 scale can be as high as $M_{E_6}^{\max} \simeq 10^{15.8}$ GeV for $R \in [\frac{1}{10}, 2]$ and $M_{E_6}^{\max} \simeq 10^{16.3}$ GeV for $R \in [\frac{1}{20}, 2]$.

In the previous sections, we have learned that in conservative $SU(5)$ and $SO(10)$ models, threshold corrects cannot explain the mismatch of the gauge couplings. However, this does not rule out conservative $SU(5)$ and $SO(10)$ models since we can also interpret the non-unification of the gauge couplings in the Standard Model as a hint for scenarios *without* a great desert.

In the following sections, we discuss this possibility in detail.

2.3. Additional Light Particles

In scenarios without a grand desert, there are particles at an intermediate scale between the electroweak and the GUT scale. The presence of these particles modifies the RGEs at all scales above the intermediate scale and it is possible that this is the reason for the mismatch in the gauge couplings if we extrapolate the Standard Model RGEs all the way up to the Planck scale. Formulated differently, the fact that the three Standard Model gauge couplings do not merge at any scale can be interpreted as a hint that there must be *something* in between the electroweak and the GUT scale. *"An oasis or two in the desert is always welcome"*, as Goran Senjanović puts it [76]. Therefore, we now discuss which particles at intermediate scales help to bring the gauge couplings sufficiently close together at scales that are in agreement with bounds from proton decay experiments.

In principle, specific scalars, fermions or gauge bosons can improve the running of the gauge couplings. However, as discussed above, which kinds of particles and which representations are present, depends crucially on the group G_{GUT}. In particular:

- In conservative $SU(5)$ models, the only possibility are scalars at intermediate scales.
- In conservative $SO(10)$ models, there can be scalars and gauge bosons at intermediate scales.
- In conservative E_6 models, there can be scalars, gauge bosons and fermions at intermediate scales.

Moreover, we have

$$SU(5) \subset SO(10) \subset E_6\,. \tag{2.20}$$

For these reasons, we discuss the impact of scalars in the context of $SU(5)$ models, the impact of gauge bosons in the context of $SO(10)$ models, and the impact of fermions in the context of E_6 models.

The idea to interpret the mismatch of the Standard Model gauge couplings as a hint for new particles at intermediate scales is, of course, not new [77, 78]. For example, to quote Ernest Ma [79]: "*If split supersymmetry can be advocated as a means to have gauge-coupling unification as well as dark matter, another plausible scenario is to enlarge judiciously the particle content of the Standard Model to achieve the same goals without supersymmetry.*" This idea was studied extensively in Refs. [33, 80].

Our goal in the following sections, however, is a different one. Instead of adding particles to achieve gauge-couplings unification and to have dark matter candidates, we study the impact of particles that are automatically present in conservative models. In other words, our focus here are *intrinsic* solutions to the gauge-coupling unification problem. In particular, we calculate the impact of all representations which are present in conservative models and discuss for each of the three possibilities (scalars, gauge bosons, fermions), all minimum viable scenarios. A minimum viable scenario in this context is a model with particles at exactly *one* intermediate scale in which the gauge couplings successfully merge.

There is, of course, a multitude of more elaborate scenarios which we do not discuss here. But using the tools and tables discussed below these scenarios can be straightforwardly

identified and studied.

We start by discussing the impact of additional light scalars in the context of $SU(5)$ models.

2.3.1. Additional Light Scalars

As mentioned above, each non-singlet particle modifies the RGEs at all scales above the scale at which it gets integrated out. However, not every representation improves the running of the gauge couplings and, in fact, most representations make the situation worse.

A useful method to check which representations help to achieve gauge-coupling unification was developed in Ref. [78]. The main idea is to define the quantities

$$A_{ij} = A_i - A_j \,, \tag{2.21}$$

where

$$A_i = a_i + \sum_I a_{iI} r_I, \qquad r_I = \frac{\ln M_{GUT}/M_I}{\ln M_{GUT}/M_Z}. \tag{2.22}$$

As usual, a_i are the one-loop RGE coefficients which were defined in Eq. (2.1). Using these quantities, it is possible to find the following (one-loop) conditions for a succesful merging of the gauge couplings [78]

$$\begin{aligned} \frac{A_{23}}{A_{12}} &= \frac{5}{8}\frac{\sin^2\theta_w - \alpha_{em}/\alpha_s}{3/8 - \sin^2\theta_w}, \\ \ln\frac{M_{GUT}}{M_Z} &= \frac{16\pi}{5\alpha_{EM}}\frac{3/8 - \sin^2\theta_w}{A_{12}}. \end{aligned} \tag{2.23}$$

The quantities A_{23} and A_{12} depend on the particle content, while all quantities on the right-hand side of the first line can be calculated using experimental input. The experimental values [60]

$$\begin{aligned} \alpha_{EM}^{-1}(M_Z) &= 127.950 \pm 0.017 \\ \alpha_s(M_Z) &= 0.1182 \pm 0.0012 \\ \sin^2\theta_w(M_Z) &= 0.23129 \pm 0.00050 \end{aligned} \tag{2.24}$$

yield

$$\frac{A_{23}}{A_{12}} \simeq 0.719, \quad \ln\frac{M_{GUT}}{M_Z} \simeq \frac{184.9}{A_{12}}. \tag{2.25}$$

For the grand desert scenarios that we discussed in the previous sections, we find $\frac{A_{23}}{A_{12}} \simeq 0.51$. As a consistency check, we can compare this value with the condition given in Eq. (2.25) and thus conclude once more that the gauge couplings do not successfully unify in such scenarios. In addition, this result for grand desert scenarios tells us that all representations which lower A_{12} and increase A_{23} or increase A_{23} more than they increase A_{12}, improve the situation. In addition, the second relation in Eq. (2.25) tells us that representations that lower A_{12} raise the GUT scale M_{GUT}.

The contributions to A_{12} and A_{23} for all scalar $SU(5)$ representations listed in Eq. (2.16) are given in Table A.1. These results tells us, for example, that $SU(2)_L$ doublets with the same quantum numbers as the Standard Model Higgs improve the running of the gauge couplings. However, the impact is extremely small and at least eight doublets are necessary to bring the ratio $\frac{A_{23}}{A_{12}}$ sufficiently close to the value given in Eq. (2.25). Similarly, while contributions from $(1, 3, 6)$ and $(3, 2, 1)$ scalars are helpful, their total impact is too

small to play a dominant role in minimum viable scenarios. The only representations with significant impact on the ratio A_{23}/A_{12} are $(1,3,0)$, $(3,3,-2)$ and $(\overline{6},3,-2)$.

The RGE coefficients for three models in which the Standard Model is supplemented by these scalar representations are

$$
\begin{aligned}
a_{(1,3,0)} &= \left(\tfrac{41}{10}, -\tfrac{5}{2}, -7 \right), \quad b_{(1,3,0)} = \begin{pmatrix} \frac{199}{50} & \frac{27}{10} & \frac{44}{5} \\ \frac{9}{10} & \frac{49}{2} & 12 \\ \frac{11}{10} & \frac{9}{2} & -26 \end{pmatrix}, \\
a_{(3,3,-2)} &= \left(\tfrac{43}{10}, -\tfrac{7}{6}, -\tfrac{13}{2} \right), b_{(3,3,-2)} = \begin{pmatrix} \frac{207}{50} & \frac{15}{2} & 12 \\ \frac{5}{2} & \frac{371}{6} & 44 \\ \frac{3}{2} & \frac{33}{2} & -15 \end{pmatrix}, \\
a_{(\overline{6},3,-2)} &= \left(\tfrac{9}{2}, \tfrac{5}{6}, -\tfrac{9}{2} \right), \quad b_{(\overline{6},3,-2)} = \begin{pmatrix} \frac{43}{10} & \frac{123}{10} & \frac{124}{5} \\ \frac{369}{10} & \frac{707}{6} & 172 \\ \frac{131}{10} & \frac{129}{2} & 89 \end{pmatrix}.
\end{aligned} \tag{2.26}
$$

Using these coefficients and Eq. (2.12), we can calculate $\Delta\lambda_{12}$ and $\Delta\lambda_{23}$ to check if the improvements are sufficiently large. The results are shown in Figures 2.8-2.10.

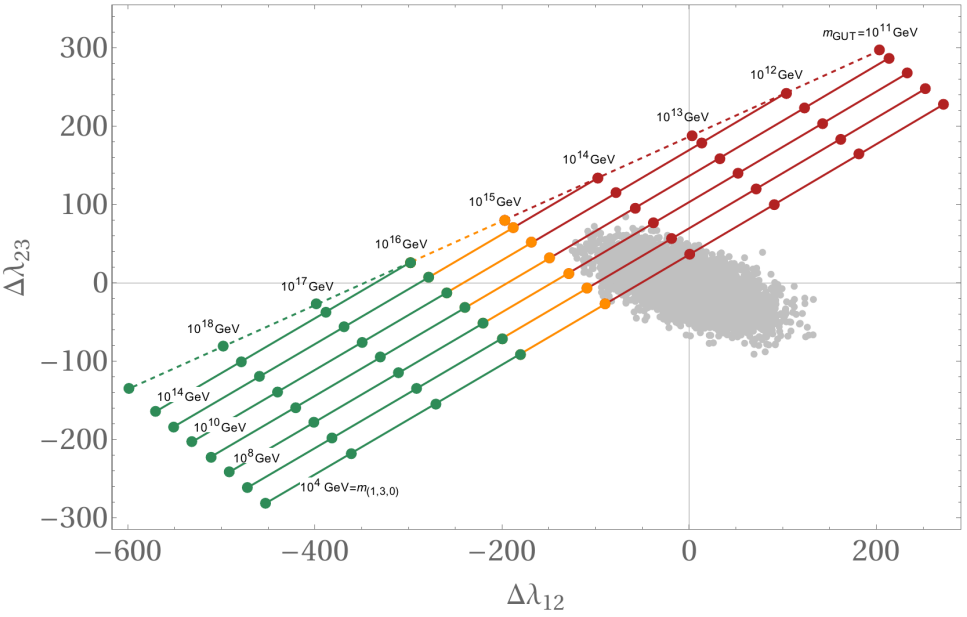

Figure 2.8.: *Running of the gauge couplings for the Standard Model supplemented by a scalar* $(1,3,0)$ *representation at an intermediate scale* $m_{(1,3,0)}$. *The light-gray points indicate, as before, possible threshold corrections with* $R \in [\frac{1}{20}, 2]$ *and the dashed line indicates the running in a grand desert scenario.*

The main result is that unification at a sufficiently high scale is impossible solely with $(1,3,0)$ scalars or $(3,3,-2)$ scalars at an intermediate scale. An important point that we need to take into account in these scenarios is that scalars in the $(3,3,-2)$ mediate proton decay and therefore they need to be heavier than 10^{10} GeV [81].

The representation with the largest positive impact is the $(\overline{6},3,-2)$. In scenarios with $(\overline{6},3,-2)$ at $m_{(\overline{6},3,-2)} \simeq 10^{12}$ GeV, the unification scale can be as high as $M_{GUT}^{\max} \simeq 10^{15.9}$ GeV. This scenario is therefore on the verge of being excluded by proton decay experiments.

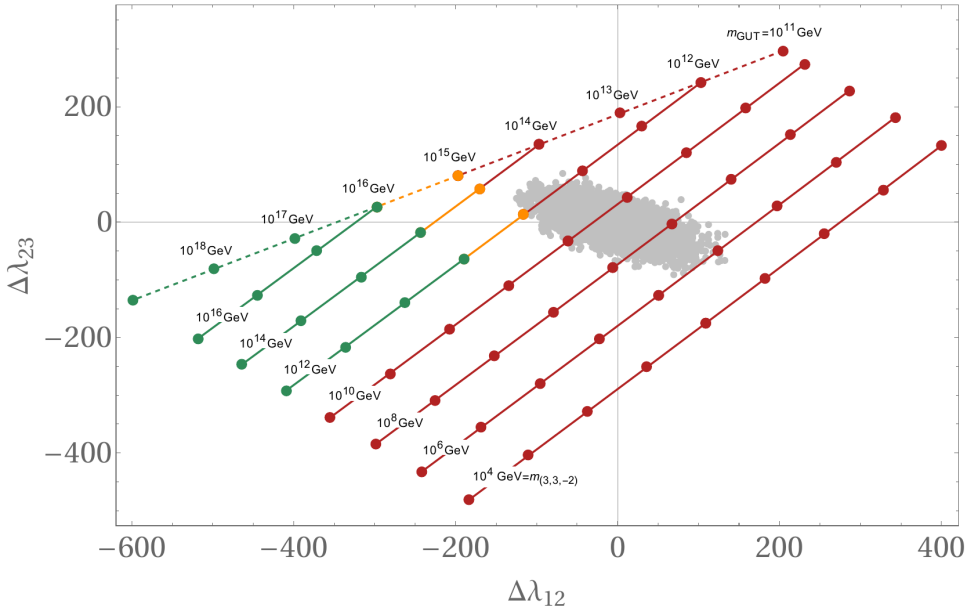

Figure 2.9.: *Running of the gauge couplings for the Standard Model supplemented by a scalar* $(3, 3, -2)$ *representation at an intermediate scale* $m_{(3,3,-2)}$. *The light-gray points indicate, as before, possible threshold corrections with* $R \in [\frac{1}{20}, 2]$. *Scenarios with* $m_{(3,3,-2)} < 10^{10}$ *GeV are already ruled out by proton decay experiments [81].*

As mentioned above, it is also possible to consider scenarios with multiple scalar repesentations at intermediate scales. However, each additional scalar representation with a mass far below the GUT scale requires additional fine-tuning [66, 82] and since at least one scenario with just one additional light scalar representation is still viable, we do not discuss more complicated scenarios any further here.

Next, we discuss the impact of additional light gauge bosons on the running of the gauge couplings.

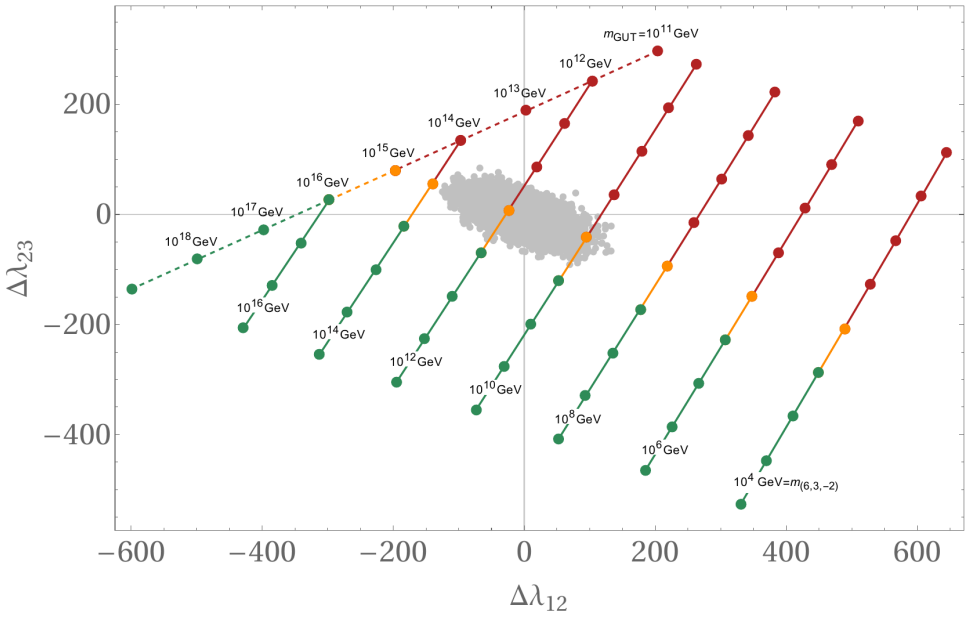

Figure 2.10.: *Running of the gauge couplings for the Standard Model supplemented by a scalar* $(\overline{6}, 3, -2)$ *representation at an intermediate scale* $m_{(\overline{6},3,-2)}$. *The light-gray points indicate, as before, possible threshold corrections with* $R \in [\frac{1}{20}, 2]$.

2.3.2. Additional Light Gauge Bosons

Since in conservative $SU(5)$ models, there are no additional gauge bosons which do not mediate proton decay ("harmless gauge bosons"), we discuss the impact of gauge bosons in the context of $SO(10)$ models. This is further motivated by the observation that the scalar representations appearing in conservative E_6 models (Eq. (2.19)) contain no singlet with respect to any maximal subgroup other than $SO(10)$. Therefore, breaking chains of the form

$$E_6 \to SO(10) \to \dots \tag{2.27}$$

are the only viable possibilities in agreement with Michel's conjecture [83, 84].[3] This implies that even though there are additional harmless gauge bosons in E_6 scenarios, we can neglect them in conservative models without a grand desert. For this reason, we will focus in the following on the impact of harmless gauge bosons that appear in the adjoint of $SO(10)$.

In physical terms, gauge bosons living at an intermediate scale correspond to an intermediate gauge symmetry

$$G_{GUT} \to G_I \to G_{SM}\,. \tag{2.28}$$

As mentioned above, we restrict ourselves to minimum viable scenarios which means that we allow at most one intermediate scale between the electroweak and the unification scale. A detailed recent discussion of scenarios with two intermediate symmetries was published in Ref. [86]. Earlier studies of scenarios with intermediate symmetries can be found in Refs. [30, 87–89]

Unification of the gauge couplings is, of course, also possible if there is an intermediate symmetry which gets broken at G_I *and* there are, additionally, scalars living somewhere in-between G_I and G_{GUT}.[4] The breaking of $SO(10)$ to G_{SM} is achieved by G_{SM} singlets living in one of the conservative scalar representations

$$10 \oplus 120 \oplus \overline{126} \oplus 45\,. \tag{2.29}$$

There are no G_{SM} singlets in the 10 and 120 and therefore, all breaking steps must be accomplished by singlets living in the $\overline{126} \oplus 45$. Moreover, if the singlet in the $\overline{126}$ is responsible for the breaking of $SO(10)$, we necessarily end up with an intermediate $SU(5)$ symmetry. But in such a scenario, the gauge couplings need to unify already at the $SU(5)$ scale and we therefore effectively end up with the class of scenarios that we already discussed in the previous section.

The only remaining possibility is that the breaking from $SO(10)$ to G_I is accomplished by scalars in the adjoint 45. There are exactly two G_{SM} singlets in the adjoint 45 and the

[3] According to Michel's conjecture, the minima of Higgs potentials correspond to VEVs which imply the breaking of a given gauge group to a *maximal* subgroup. While there are well known counterexamples [85], it provides a helpful guideline since "*it expresses the maximizing tendency very well. Even the counter-examples are only slightly less than maximal*" [84]. Moreover, note that in E_6 models with an intermediate $SO(10)$ symmetry, the gauge couplings already unify at $M_{SO(10)}$ and therefore, the E_6 scale cannot be computed using low-energy data.

[4] One interesting example is a partial unification through the merging of ω_{1Y} and ω_{2L} at around $M_I \simeq 10^{13}$ GeV. This is motivated by the observation that ω_{1Y} and ω_{2L} meet at around 10^{13} GeV in the Standard Model. The final merging with ω_{3C} can then be achieved at a sufficiently high scale through scalars living between M_I and M_{GUT} [90].

resulting intermediate symmetry depends on the relative values of their VEVs. In general, the following breaking chains are possible [74, 91]

$$\begin{aligned}
&SO(10) \to SU(4)_C \times SU(2)_L \times U(1)_R \\
&SO(10) \to SU(3)_C \times SU(2)_L \times SU(2)_R \times U(1)_X \\
&SO(10) \to SU(3)_C \times SU(2)_L \times U(1)_R \times U(1)_X \\
&SO(10) \to SU(5)' \times U(1)_Z \\
&SO(10) \to SU(5) \times U(1)_Z \,,
\end{aligned} \tag{2.30}$$

where $SU(5)'$ denotes the flipped $SU(5)$ embedding [92, 93].

The further breaking of the intermediate symmetry needs to be accomplished by the G_{SM} singlet in the $\overline{126}$. However, this singlet only breaks $SU(5) \times U(1)_Z$ to $SU(5)$ and therefore this chain is not viable. Moreover, it is well known that an intermediate $SU(5)' \times U(1)_Z$ or $SU(3)_C \times SU(2)_L \times U(1)_R \times U(1)_X$ symmetry yields no improvement for the running of the gauge couplings [33, 89].[5]

Therefore, the only relevant breaking chains in conservative $SO(10)$ models with just one intermediate symmetry are the first and second one listed in Eq. (2.30).

In general, before we can discuss the impact of these intermediate symmetries on the running of the gauge couplings, we need to specify suitable scalar spectra. It is conventional in this context to invoke the extended survival hypothesis which states that "*Higgses acquire the maximum mass compatible with the pattern of symmetry breaking*" [98]. This is a hypothesis of minimal fine tuning since only scalars that are necessary for the breaking chain get a mass significantly below M_{GUT} [82]. In addition, at least one $SU(2)_L$ doublet at M_I or below is necessary because otherwise, the structure of the Yukawa sector is too simple to permit a succesful fit of all low-energy observables [99].

With this in mind, we will now discuss the breaking chains listed in the first and second line of Eq. (2.30).

$SO(10) \to SU(4)_C \times SU(2)_L \times U(1)_R \to G_{SM}$

The breaking of $SU(4)_C \times SU(2)_L \times U(1)_R$ to G_{SM} is accomplished by a VEV in the $(\overline{10}, 1, -1) \subset \overline{126}$ representation of the intermediate group. This implies that all scalars in the $(\overline{10}, 1, -1)$ have a mass of order M_{421}. Since, as mentioned above, one additional $SU(2)_L$ doublet is necessary, we assume that all scalars in the $(15, 2, \frac{1}{2}) \subset \overline{126}$ have a mass of order M_{421}, too.

While below M_{421} the Standard Model RGEs are valid, above M_{421} the RGE coefficients

[5] Take note that there are further possibilities if we consider conservative E_6 models with an intermediate $SO(10)$ symmetry. In particular, alternative intermediate symmetries can be realized through the G_{SM} singlets contained in the $54 \subset 351'$ and $144 \subset 351$. The singlet in the 144 is able to break $SO(10)$ directly to G_{SM} and therefore, the problem of gauge unification persists [94]. The singlet in the 54 breaks $SO(10)$ to the famous Pati-Salam group $SU(4)_C \times SU(2)_L \times SU(2)_R \times D$, where D denotes D-parity which exchanges $SU(2)_L \leftrightarrow SU(2)_R$ [95, 96]. For detailed recent discussions of this breaking chain, see Refs. [35, 97].

read

$$a_{124} = \left(\ 10, -\tfrac{2}{3}, -7 \ \right) , \qquad b_{124} = \begin{pmatrix} 51 & 24 & \frac{645}{2} \\ 8 & \frac{115}{3} & \frac{285}{2} \\ \frac{43}{2} & \frac{57}{2} & \frac{265}{2} \end{pmatrix} . \tag{2.31}$$

In addition, we need the matching condition [89]

$$\omega_{1Y} = \frac{3}{5}\omega_{1R} + \frac{2}{5}\left(\omega_{4C} - \frac{C_4}{12\pi}\right) . \tag{2.32}$$

Using Eq. (2.31) and Eq. (2.32), we find

$$M_{421} \simeq 10^{11.4} \text{ GeV} , \quad M_{SO(10)} \simeq 10^{14.5} \text{ GeV} . \tag{2.33}$$

This result seems to imply that the breaking chain $SO(10) \to SU(4)_C \times SU(2)_L \times U(1)_R \to G_{SM}$ is "*is definitely ruled out*" [89] since the value for $M_{SO(10)}$ in Eq. (2.37) implies a proton lifetime far below the current experimental bound (Eq. (2.13)). However, to be certain, we have to check whether the $SO(10)$ scale can be sufficiently raised through threshold corrections.

As discussed already in Section 2.2, threshold corrections depend on the detailed mass spectrum of all superheavy particles and can be estimated by generating randomized mass spectra. The decomposition of all relevant scalar representations and the resulting threshold formulas are given in Appendix A.4. The result of a scan using randomized mass spectra is shown in Figure 2.11.

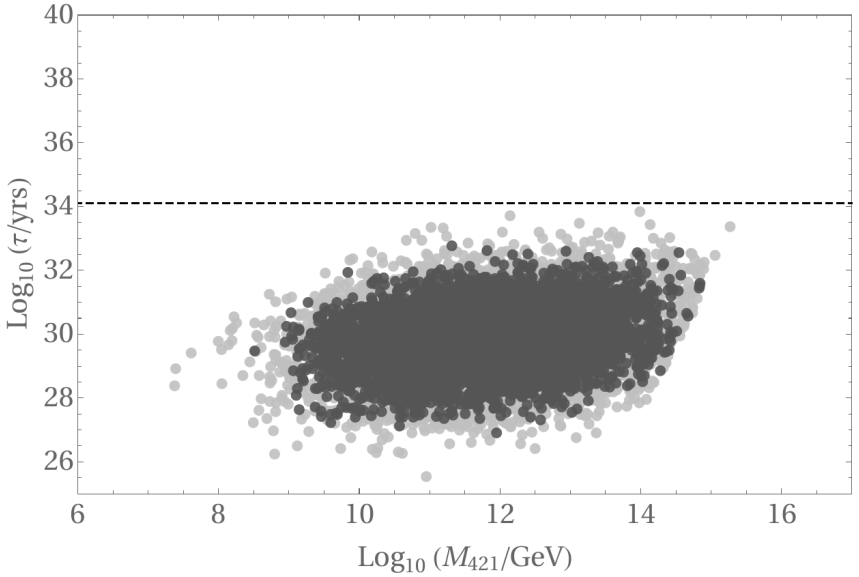

Figure 2.11.: *Impact of threshold corrections on the proton lifetime τ in $SO(10)$ scenarios with an intermediate $SU(4)_C \times SU(2)_L \times U(1)_R$ symmetry. The dark-gray dots indicate mass spectra with $R \in [\frac{1}{10}, 2]$ and the light-gray dots indicate spectra with $R \in [\frac{1}{20}, 2]$. The dashed line indicates the proton lifetime bound from Super-Kamiokande [19].*

The main result is that even if we take threshold corrections into account, the proton lifetime can be at most:

$$\begin{aligned} \tau_{max} &= 6.15 \times 10^{32} \text{ yrs.} \quad \text{for} \quad R \in [1/10, 2] , \\ \tau_{max} &= 7.33 \times 10^{33} \text{ yrs.} \quad \text{for} \quad R \in [1/20, 2] . \end{aligned} \tag{2.34}$$

This is still below the current experimental bound $\tau > 1.6 \times 10^{34}$ yrs (Eq. (2.13)).

We can therefore conclude that conservative scenarios involving the breaking chain

$$SO(10) \to SU(4)_C \times SU(2)_L \times U(1)_R \to G_{SM}$$

are in conflict with bounds from proton decay experiments, even if we take threshold corrections into account.

$\boldsymbol{SO(10) \to SU(3)_C \times SU(2)_L \times SU(2)_R \times U(1)_X \to G_{SM}}$

In scenarios in which $SO(10)$ gets broken to $SU(3)_C \times SU(2)_L \times SU(2)_R \times U(1)_X$, the breaking to G_{SM} is accomplished by a VEV in the $(1,1,3,-2) \subset \overline{126}$ representation of the intermediate group.[6] Moreover, the Standard Model Higgs lives in a $(1,2,1,0) \subset 10$ and the additional doublet, which is indispensable for a realistic flavour structure, lives in a $(1,2,1,0) \subset \overline{126}$ representation of $SU(3)_C \times SU(2)_L \times SU(2)_R \times U(1)_X$.

This implies that all scalars have a mass of order M_{GUT} except for $(1,2,1,0) \subset 10$, which lives at the electroweak scale, and the $(1,1,3,1) \subset \overline{126}$ and $(1,2,1,0) \subset \overline{126}$, which live at the M_{3221} scale.

Therefore, the Standard Model RGEs remain valid below M_{3221}, but need to be modified accordingly above M_{3221}. The one-loop and two-loop coefficients read

$$a_{3221} = \left(\tfrac{11}{2}, -\tfrac{8}{3}, -2, -7 \right), \qquad b_{3221} = \begin{pmatrix} \frac{61}{2} & \frac{9}{2} & \frac{81}{2} & 4 \\ \frac{3}{2} & \frac{37}{3} & 6 & 12 \\ \frac{27}{2} & 6 & 31 & 12 \\ \frac{1}{2} & \frac{9}{2} & \frac{9}{2} & -26 \end{pmatrix}. \tag{2.35}$$

Additionally, we need the matching condition [89]

$$\omega_{1Y} = \frac{3}{5}\left(\omega_{2R} - \frac{C_2}{12\pi}\right) + \frac{2}{5}\omega_{1X}\,. \tag{2.36}$$

Using Eq. (2.35) and Eq. (2.36), we find

$$M_{3221} \simeq 10^{10.2}\ \text{GeV}\,, \quad M_{SO(10)} \simeq 10^{15.9}\ \text{GeV}\,. \tag{2.37}$$

Therefore, this breaking chain is not in conflict with proton decay bounds. For completeness, we estimate once more the magnitude of possible threshold corrections.

The decomposition of the relevant scalar representations and the resulting threshold formulas are given in Appendix A.5. The result of a scan with randomized masses of the superheavy particles is shown in Figure 2.12.

Using this result, we find that the proton lifetime can be as high as

$$\begin{aligned} \tau_{max} &= 7.16 \times 10^{41}\ \text{yrs.} \quad \text{for} \quad R \in [1/10, 2]\,, \\ \tau_{max} &= 5.24 \times 10^{44}\ \text{yrs.} \quad \text{for} \quad R \in [1/20, 2]\,. \end{aligned} \tag{2.38}$$

[6] Note that here $X = B - L$.

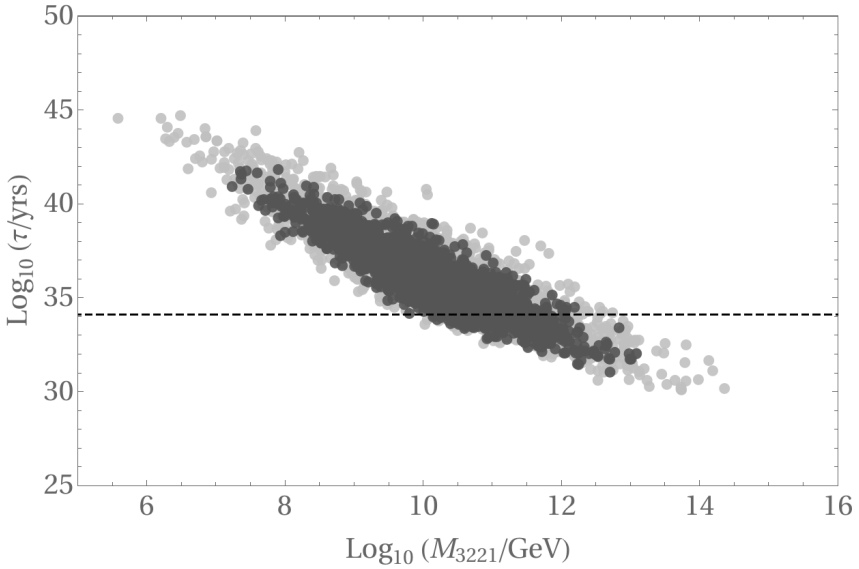

Figure 2.12.: *Impact of threshold corrections on the proton lifetime τ in $SO(10)$ scenarios with an intermediate $SU(3)_C \times SU(2)_L \times SU(2)_R \times U(1)_X$ symmetry. The dark-gray dots indicate mass spectra with $R \in [\frac{1}{10}, 2]$ and the light-gray dots indicate spectra with $R \in [\frac{1}{20}, 2]$. The dashed line indicates the proton lifetime bound from Super-Kamiokande [19].*

Therefore, it will not be possible to rule out conservative scenarios involving the breaking chain

$$SO(10) \to SU(3)_C \times SU(2)_L \times SU(2)_R \times U(1)_X \to G_{SM}\,,$$

even with the next generation of proton decay experiments [100, 101].

In the following final section of this chapter, we will discuss the impact of additional light fermions on the running of the gauge couplings.

2.3.3. Additional Light Fermions

E_6 models always contain exotic fermions since the fundamental representation of E_6 is 27-dimensional. The decomposition of the 27, shown in Eq. (2.18), tells us that these exotic fermions live in the

$$(1,2,3) \oplus (1,2,-3) \oplus (3,1,-2) \oplus (\overline{3},1,2) \oplus (1,1,0) \tag{2.39}$$

of G_{SM}. Moreover, since we have three generations of Standard Model fermions, E_6 models automatically predict three generations of exotic fermions.

The singlet $(1,1,0)$ has, of course, no influence on the running of the gauge couplings. For the remaining exotic fermions, we can check their impact on the running by using the method introduced in Section 2.3.1. In particular, their contributions to the ratio A_{23}/A_{12} are listed in Table A.7 in Appendix A.3. The main result here is that the vector-like lepton doublets improve the running, while the vector-like quarks make the situation worse. Moreover, the contributions of the exotic leptons and exotic quarks cancel at the one-loop level.

Therefore, we need a scenario with a huge mass splitting between the vector like quarks and leptons. This is possible since the $45 \subset 351$ contains one singlet that yields a mass term solely for the vector-like quarks, while a second one solely yields a mass term for the vector-like leptons. This is known as the Dimopoulos-Wilzeck structure and historically it was invoked to explain the mass splitting between scalar $SU(2)_L$ doublets and scalar $SU(2)_L$ triplets in the context of the infamous doublet-triplet problem [102, 103]. In the following, we assume that this or a similar structure leads to a sufficiently large mass splitting between the vector-like quarks and leptons. In particular, we assume that all vector-like quarks have a mass of order M_{E_6}.

Secondly, take note that the Yukawa couplings of the exotic fermions and the Yukawa couplings of the Standard Model fermions have a common origin. This follows since above the E_6 scale, we have a unified Yukawa sector:

$$\mathcal{L}_{\mathrm{Y}} = \Psi^T i\sigma_2 \Psi (Y_{27}\varphi + Y_{351'}\phi + Y_{351}\xi) + h.c.\,. \tag{2.40}$$

It is therefore reasonable to expect that the mass splitting between the three exotic generations is of the same order as the splitting between the Standard Model generations, i.e.

$$m_{2L}/m_{3L} \simeq 10^{-2} \quad m_{1L}/m_{3L} \simeq 10^{-4}\,. \tag{2.41}$$

The RGE coefficients for models consisting of the Standard Model plus one, two and three

vector-like lepton doublets read:

$$a_{\text{SM+1L}} = \left(\tfrac{9}{2}, -\tfrac{5}{2}, -7 \right), \qquad b_{\text{SM+1L}} = \begin{pmatrix} \frac{104}{25} & \frac{18}{5} & \frac{44}{5} \\ \frac{6}{5} & 14 & 12 \\ \frac{11}{10} & \frac{9}{2} & -26 \end{pmatrix},$$

$$a_{\text{SM+2L}} = \left(\tfrac{49}{10}, -\tfrac{11}{6}, -7 \right), \qquad b_{\text{SM+2L}} = \begin{pmatrix} \frac{217}{50} & \frac{9}{2} & \frac{44}{5} \\ \frac{3}{2} & \frac{133}{6} & 12 \\ \frac{11}{10} & \frac{9}{2} & -26 \end{pmatrix},$$

$$a_{\text{SM+3L}} = \left(\tfrac{53}{10}, -\tfrac{7}{6}, -7 \right), \qquad b_{\text{SM+3L}} = \begin{pmatrix} \frac{113}{25} & \frac{27}{5} & \frac{44}{5} \\ \frac{9}{5} & \frac{91}{3} & 12 \\ \frac{11}{10} & \frac{9}{2} & -26 \end{pmatrix}. \tag{2.42}$$

The impact of these exotic leptons on the running is illustrated in Figure. 2.13. An important constraint on this class of scenarios is that vector-like lepton doublets with a mass below 450 GeV are ruled out by collider searches [104].

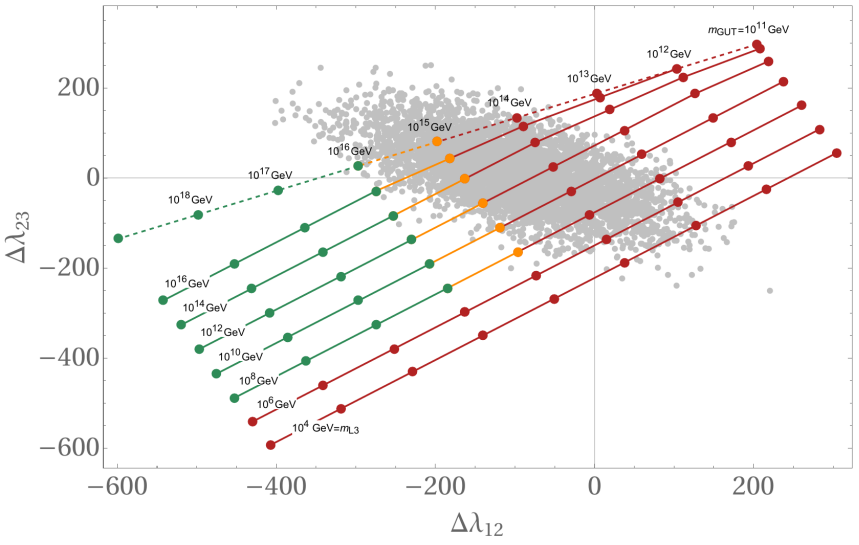

Figure 2.13.: *Impact on the RGE running of three generations of exotic E_6 lepton doublets ($(1,2,3)$) with a "Standard Model-like" mass splitting $m_{2L}/m_{3L} \simeq 10^{-2}$, $m_{1L}/m_{3L} \simeq 10^{-4}$. The numbers in the lower-left corner indicate the mass scale of the heaviest vector-like lepton doublet for each corresponding scenario. The dashed line represents the grand desert scenario without any exotic leptons. The light-gray points indicate threshold corrections with $R \in [1/20, 2]$.*

The main result here is that the gauge couplings successfully unify if $m_{3L} \simeq 10^{10}$ GeV, $m_{2L} \simeq 10^{8}$ GeV and $m_{1L} \simeq 10^{6}$ GeV. However, an obvious problem in this scenario is that the unification scale is quite low ($M_{E_6} \approx 10^{15.5}$ GeV) and therefore already in conflict with proton decay bounds (Eq. (2.14)).

If we take threshold corrections into account, however, we find that if the heaviest lepton generation has a mass of around $m_{3L} \simeq 10^{14}$ GeV, the E_6 scale can be as high as $M_{E_6}^{\max} \simeq 10^{16}$ GeV. Therefore, this scenario is still viable.

The Strong CP Problem 3

The goal of this chapter is to motivate several of the main notions that are commonly used in the context of the strong CP problem in order to set the stage for the discussion in the following chapter. More comprehensive discussions can be found, for example, in Refs. [43, 105–107].

One of the unsolved puzzles in the Standard Model is why CP violating effects, so far, have never been observed in strong interactions. The violation of CP symmetry in the strong sector is encoded in the theta parameter

$$\bar{\theta} = \theta_{QCD} - \theta_{\mathrm{F}}\,, \tag{3.1}$$

where $\theta_{\mathrm{F}} = \arg\det M_u M_d$, M_u and M_d denote the quark mass matrices, and θ_{QCD} is the coefficient of the CP violating Lagrangian term $\alpha_s/8\pi\, G\tilde{G}$. Since CP is already broken in the Yukawa interactions, there is no reason why $\bar{\theta}$ should be zero or especially small.

However, from the 95% CL experimental bound on the electric dipole moment of the neutron [108]

$$|d_n| \leq 3.6 \times 10^{-26} e\, cm \tag{3.2}$$

it is possible to derive the upper bound [109]

$$\bar{\theta} < 10^{-10}\,. \tag{3.3}$$

This is known as the strong CP problem.

The experimental result in Eq. (3.3) is especially puzzling since, as indicated in Eq. (3.1), there are two contributions to $\bar{\theta}$ from completely different sectors of the theory. In particular, the parameter θ_{QCD} describes a property of the ground state in pure QCD, while θ_{F} depends on the flavor structure of the model.

In the following sections, we discuss the origin and interpretation of these contributions. But before we discuss the QCD vacuum itself, it is instructive to introduce the most important concepts in the context of two much simpler models.

The basic properties of a topological parameter like θ_{QCD} and of a topological term can be understood nicely by considering a particle on a ring. Moreover, the nature of tunneling processes in the presence of a topological term can be studied in a simplified setup by considering a quantum pendulum.

3.1. Helpful Analogies

The following discussion is mainly inspired by Refs. [110–112].

3.1.1. Particle on a Ring

The location of the particle can be described by an angle $\phi(t)$ and the action

$$S[\phi] = \int dt\, L(\phi, \dot{\phi}), \qquad L = \frac{\tilde{M}}{2}\dot{\phi}^2 r^2\,, \tag{3.4}$$

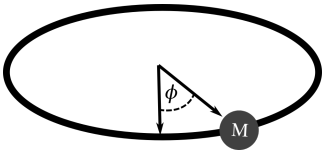

where $\tilde{M}$ is the mass of the particle and r the radius of the ring. To unclutter the notation, we define $M \equiv \tilde{M} r^2$.

It is well known that classically, we can always add a total time derivative to the Lagrangian without changing anything:

$$L = \frac{M}{2}\dot{\phi}^2 + A\dot{\phi}\,, \tag{3.5}$$

where A is a constant. This topological term[1] can be rewritten as

$$S_{top} = \int_{t_1}^{t_2} dt\, A\dot{\phi} = A\Big(\phi(t_2) - \phi(t_1)\Big) = \theta\frac{\Delta\phi}{2\pi}\,, \tag{3.6}$$

where we defined $\theta \equiv A2\pi$. We can see that the topological term changes by θ each time the particle moves a full circle on the ring, i.e. $\phi \to \phi + 2\pi$.

The equation of motion can be derived by using the Euler-Lagrange equation ($\frac{d}{dt}\frac{\partial L}{\partial \dot{\phi}} - \frac{\partial L}{\partial \phi} = 0$) and reads

$$M\ddot{\phi} = 0. \tag{3.7}$$

Therefore, the additional term $A\dot{\phi}$ has, as expected, no influence on the equation of motion.

We will see below, however, that it plays an extremely important role if we consider the same system in a quantum context. Moreover, already at this point we note that there are infinitely many paths which connect each initial position at $t = t_1$ with a specific final position at t_2.

The conjugated momentum reads

$$p = \frac{\partial L}{\partial \dot{\phi}} = M\dot{\phi} + A, \tag{3.8}$$

and therefore, the Hamiltonian reads

$$H = p\dot{\phi} - L = \frac{1}{2M}(p - A)^2. \tag{3.9}$$

[1] The defining property of a topological term in the Lagrangian is its metric independence. This can be verified by checking if a given term contributes nothing to the stress-energy tensor, which arises in the variation of the action with respect to the metric [112].

The resulting Hamilton equations

$$\dot{\phi} = \frac{1}{M}(p - A), \tag{3.10}$$

$$\dot{p} = 0, \tag{3.11}$$

are physically equivalent to Eq. (3.7) since we always have the freedom to perform a canonical transformation $p \to p + A$.

Quantum Particle on a Ring

In a quantum context, the particle can be described by a wave function $\psi(\phi)$. To unclutter the notation, we use $\hbar = 1$. The Hamiltonian operator reads

$$H = \frac{1}{2M}\left(-i\partial_\phi - A\right)^2 \tag{3.12}$$

and it is convenient to demand that the wave function is a single-valued function, i.e. to impose periodic boundary conditions $\psi(\phi + 2\pi) = \psi(\phi)$. The solutions of the eigenvalue equation

$$H\psi_m = E_m\psi_m \tag{3.13}$$

read

$$\psi_m = e^{im\phi}, \tag{3.14}$$

$$E_m = \frac{1}{2M}(m - A)^2, \tag{3.15}$$

where m is an integer number.

We can see that A directly modifies the quantized energy spectrum (c.f. Figure 3.1).

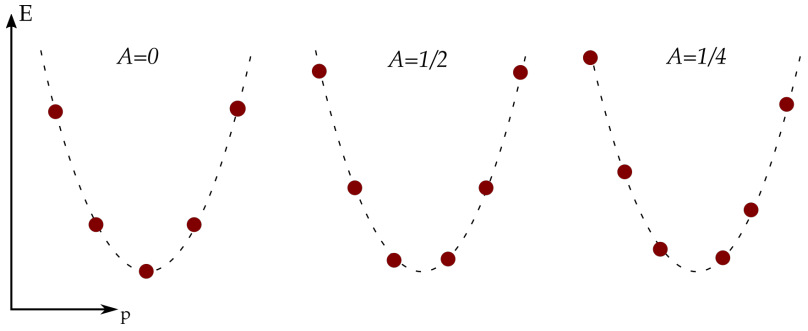

Figure 3.1.: *Quantized energy spectrum of a particle on a ring as given in Eq.* (3.15) *for* $A = \frac{\theta}{2\pi} = 0, \frac{1}{2}, \frac{1}{4}$. *The dashed line shows the classical continuous spectrum, while the dots indicate allowed energy values for a quantum particle which are labelled by the eigenvalues* m *of the momentum operator* $-i\frac{\partial}{\partial\phi}$.

While A, of course, also appears in the classical Hamiltonian (Eq. (3.9)), it has no measurable effect in a classical context since the classical spectrum is continuous. Moreover, as mentioned above, for a classical particle on a ring, all contributions from A can be removed through a canonical transformation $p \to p + A$.

To see that this is no longer possible in a quantum context, take note that while we can use a gauge transformation $\psi \to e^{iA\phi}\psi$ to bring the Hamiltonian (Eq. (3.12)) into the form

$$H = \frac{1}{2M}\left(-i\partial_\phi\right)^2, \tag{3.16}$$

this does not remove A from the model because it now shows up in the boundary conditions. In particular, after the gauge transformation the periodic boundary condition $\psi(\phi + 2\pi) = \psi(\phi)$ become twisted $\psi(\phi + 2\pi) = e^{-i2\pi A}\psi(\phi)$.

The spectrum of the modified Hamiltonian (Eq. (3.16)) with twisted boundary conditions is exactly equal to the spectrum (Eq. (3.15)) of the original Hamiltonian (Eq. (3.12)) with periodic boundary conditions.

Therefore, there are two ways of how we can understand the impact of the topological term for a quantum particle on a ring.

- On the one hand, we can include an additional term $A\dot{\phi}$ in the Hamiltonian and use periodic boundary conditions.
- On the other hand, we can use a Hamiltonian without this additional term are then forced to use twisted boundary conditions.

The second perspective allows for an interesting interpretation of the topological term.

In words, the twisted boundary condition imply that the particle picks up a phase $\theta = 2\pi A$, each time it moves a full circle on the ring. This is exactly what happens, for example, when there is a nonzero magnetic flux penetrating the ring. While the magnetic potential has no impact in a classical context, it can shift the phase of the wave function. This is analogous to what happens in the famous Aharonov-Bohm experiment.

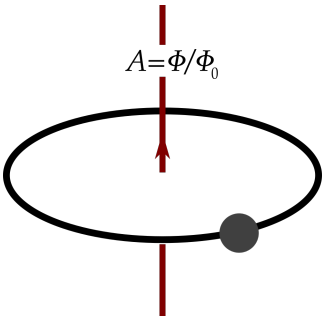

In particular, we can make the identification

$$A = \frac{\Phi}{\Phi_0}\,, \tag{3.17}$$

where Φ denotes the magnetic flux and $\Phi_0 = 2\pi\frac{\hbar c}{e}$ is the flux quantum.

An important point is that different values of A (and equivalently θ) define different systems. If A is zero, we are dealing with a particle on a ring without any magnetic flux present. But if $A \neq 0$, the particle's phase is directly influenced by the magnetic flux and this leads to measurable effects. Moreover, the value of A can not be changed dynamically from within the system but must be changed externally.

Winding Number

To study the properties of the system further, it is instructive to focus on a specific initial and final configuration of the particle. The situation becomes especially transparent when we investigate a situation for which $\mathrm{e}^{i\phi(0)} = \mathrm{e}^{i\phi(\beta)}$. In words this means, that the system returns after β seconds to its initial configuration. This is known as periodic temporal boundary conditions and is satisfied provided that

$$\phi(\beta) - \phi(0) = 2\pi Q\,, \tag{3.18}$$

where $Q \in \mathbb{Z}$ is known as the winding number.

The winding number quantifies how many times the particle's path winds around the ring before it returns to the initial position and can be calculated using the formula

$$Q = \int_0^\beta \frac{dt}{2\pi}\,\dot{\phi}\,. \tag{3.19}$$

Using this definition, we can rewrite the topological term in Eq. (3.6) as

$$S_{top} = \theta Q\,, \tag{3.20}$$

To calculate the total amplitude that the particle returns after β seconds back to its initial configuration, we need to take all possible paths into account.

Since we only considered paths for which the particle returns to its initial configuration, we have effectively compactified time to a circle $S^1_t = t \in [0, \beta]$. This is illustrated in Figure 3.2.

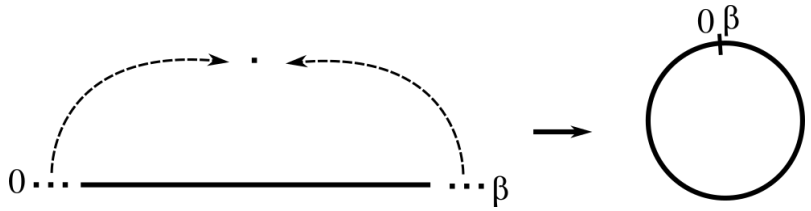

Figure 3.2.: *By imposing* $e^{i\phi(0)} = e^{i\phi(\beta)}$*, we effectively compactify the time axis to a circle.*

Moreover, the movement of the particle is restricted to a circle $S^1_\phi = \phi \in [0, 2\pi]$ too. We are therefore dealing with maps

$$\phi(t): \quad S^1_t \to S^1_\phi\,. \tag{3.21}$$

These maps fall into topologically distinct classes. Each such class is labelled by a winding number Q and consists of all paths which involve Q revolutions around the ring.

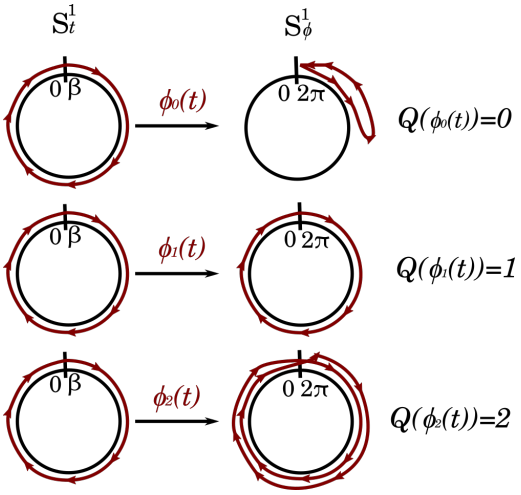

The key observation is that paths within one specific topological class cannot be *smoothly* transformed into paths within another class. This can be understood by considering a simple example.

A winding number zero path is

$$\phi_0(t) = 0\,, \tag{3.22}$$

whereas an example of a winding number one path is

$$\phi_1(t) = \frac{2\pi}{\beta} t\,. \tag{3.23}$$

We say that paths can be smoothly transformed into each other if we can find a map $\phi^{(\lambda)}$, parameterized by a continuous variable λ, which yields ϕ_0 for $\lambda = 0$ and ϕ_1 for $\lambda = 1$. An

obvious first guess is

$$\phi^{(\lambda)} = \lambda\phi_1 \tag{3.24}$$

since $\phi^{(0)} = 0 = \phi_0(t)$ and $\phi^{(1)} = \phi_1(t)$. However, as λ runs from 0 to 1, we leave the set of permitted paths. For example, for $\lambda = \frac{1}{2}$, we have

$$\phi^{(\frac{1}{2})} = \frac{1}{2}\phi_1 = \frac{1}{2}\frac{2\pi}{\beta}t\,. \tag{3.25}$$

This path does not describe a particle which returns to $\phi = 0$ at $t = \beta$.

Graphically, this means that we need to detach the path from its start or end point in order to unwind it and generate a path with a lower winding number. For the transformation $\phi^{(\lambda)}$ this is shown in Figure 3.3.

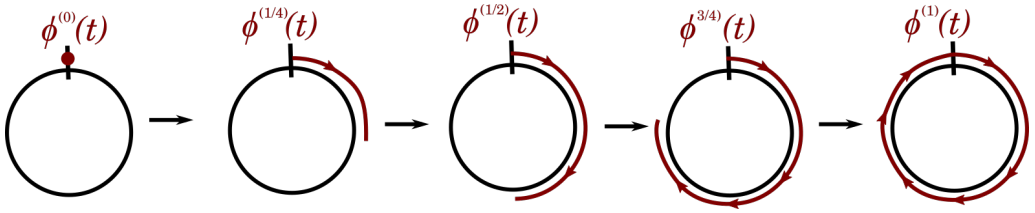

Figure 3.3.: *The transformation $\phi^{(\lambda)}$ yields ϕ_0 for $\lambda = 0$ and ϕ_1 for $\lambda = 1$. However, for all values of λ in-between we get paths that are not permitted since the starting and final position are different.*

But this is not a topologically permitted transformation and therefore paths with different winding numbers live in distinct classes.

The topological classes form a group if we introduce the product of two paths as

$$\phi_2 \cdot \phi_1(\tau) = \begin{cases} \phi_1(2\tau), & \text{for} \quad 0 < \tau < \beta/2\,, \\ \phi_1(\beta) + \phi_2(2\tau - \beta), & \text{for} \quad \beta/2 < \tau < \beta\,. \end{cases}$$

Using this definition, we can see that the product of a path ϕ_1 with winding number Q_1 and a path ϕ_2 with winding number Q_2 yields a path with winding number Q_3. Therefore, the group structure is equal to the structure of the integers $\mathbb{Z}$ equipped with operation addition "+" as the group product. This implies that maps from S^1 to S^1 can be classified using integers. In mathematical terms, this corresponds to the fact that the first homotopy group π_1 of the circle S^1 is the abelian group $\mathbb{Z}$:

$$\pi_1(S^1) = \mathbb{Z}\,. \tag{3.26}$$

The existence of distinct topological classes implies that the path integral for the particle on a ring

$$Z = \int D\phi\, e^{iS[\phi]}, \tag{3.27}$$

can be split into a sum over paths in distinct topological sectors [110]

$$Z = \sum_{Q=-\infty}^{+\infty} e^{i\theta Q} \int_{\phi(\beta)-\phi(0)=2\pi Q} \mathcal{D}\phi\, e^{i\int_0^\beta dt\, \frac{M}{2}\dot{\phi}^2}. \tag{3.28}$$

In words this means, as already mentioned above, that each path with a given winding number Q picks up an additional phase $Q\theta$. This leads to interference between different topological sectors.

Using this result, we can understand why the topological θ term (Eq. (3.6)) has a measurable effect although it does not appear in the equations of motion. The equation of motion is derived using infinitesimal variations of the action. Such infinitesimal variations cannot modify the winding number. However, $Q\theta$ plays an important role in the path integral where it acts as the phase of an additional weight factor for paths in different topological sectors.

Now that we have introduced the most important notions in a simplified setup, we will analyze one additional toy model which is an even closer analogue of the QCD vacuum [113].

3.1.2. Pendulum

A pendulum can be described by an angle ϕ and the action reads

$$S[\phi] = \int dt\, L(\phi, \dot{\phi}), \qquad L = \frac{M}{2}\dot{\phi}^2 - \frac{Mg}{l}\Big(1 - \cos(\phi)\Big)\,, \tag{3.29}$$

where $V = \frac{Mg}{l}\Big(1 - \cos(\phi)\Big)$ denotes the pendulum's potential in the earth's gravitational field, M is its mass and l its length.

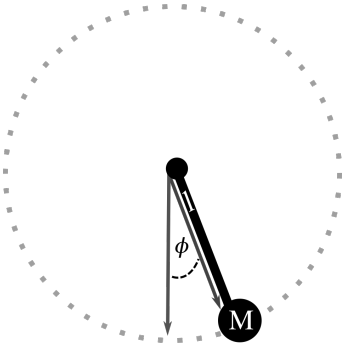

The movement of the pendulum is restricted to a circle $S^1_\phi = \phi \in [0, 2\pi]$ since after a full rotation by 2π it returns to its original position.

Again, we can introduce a total derivative term such that the Lagrangian reads

$$L = \frac{M}{2}\dot{\phi}^2 - \frac{Mg}{l}\Big(1 - \cos(\phi)\Big) + A\dot{\phi}\,, \tag{3.30}$$

where A is a constant. This additional term has no influence on the equations of motion

$$M\ddot{\phi} = -\frac{Mg}{l}\sin(\phi)\,, \tag{3.31}$$

which can be derived, as usual, by using the Euler-Lagrange equation.

The conjugated momentum

$$p = \frac{\partial L}{\partial \dot{\phi}} = M\dot{\phi} + A, \tag{3.32}$$

can be used to derive the Hamiltonian

$$H = p\dot{\phi} - L = \frac{1}{2M}(p - A)^2 + \frac{Mg}{l}\Big(1 - \cos(\phi)\Big). \tag{3.33}$$

The corresponding Schrödinger equation

$$-\left(\frac{d}{d\phi} - ieA\right)^2 \psi + q(1 - cos\phi)\psi = E\psi \tag{3.34}$$

for $A = 0$ is the famous Mathieu equation and its solutions are known as Mathieu functions.

Using the periodic boundary condition $\psi(\phi) = \psi(\phi + 2\pi)$, it is possible to derive the quantized energy spectrum of the pendulum [114].

As in the previous section, we can see that A plays no role in a classical description of the pendulum but directly influences the quantized quantum energy spectrum since it directly appears in the Schrödinger equation. In addition, we can again use a gauge transformation to generate a new wave function which obeys a Schrödinger equation without the A term. However, after such a transformation we are forced to use twisted boundary conditions.

Moreover, we can again interpret $A = \frac{\Phi}{\Phi_0}$ as the result of a magnetic Aharonov-Bohm-type potential. The fact that we end up with twisted boundary conditions if we try to get rid of the A term, tells us that the pendulum picks up a phase each time it undergoes a full rotation around its support.

While all these aspects are completely analogous to what we already discussed above for the particle on a ring, there are two additional aspects of a quantum pendulum which are worth discussing in more detail.

Tunneling

The main difference between a particle on a ring and a pendulum is the existence of a potential $V(\phi)$. As a result of this potential, there is an energy barrier which may prevent the pendulum from making a full rotation.

In a classical context, a pendulum with an energy less than the height of the potential barrier $V_{\max} = V(\pi) = \frac{2Mg}{l}$ will only oscillate back and forth. In addition, the ground state is simply $\phi = 0$.

But a quantum pendulum can always tunnel through the potential barrier. In particular, this implies that if we want to calculate the amplitude for ground state to ground state transitions, we need to take into account that there are infinitely many paths. As for the particle on a ring, these paths can be classified according to their winding number Q.

This implies that the general quantum ground state is a superposition of all possible configurations which have tunneled around the pendulum's support and then ended up back at $\phi = 0$:

$$|\theta\rangle = \sum_{Q=-\infty}^{\infty} e^{iQ\theta}|Q\rangle\,, \tag{3.35}$$

where $\theta \equiv \frac{A}{2\pi}$ is the phase the pendulum's state picks up as it moves in a full circle.

Moreover, it can be shown that the ground state energy depends directly on θ and is minimal for $\theta = 0$ [111].

Particle in a Periodic Potential vs. Pendulum

There is a slightly different way of how we can interpret the system described by the action in Eq. (3.29) if we don't impose $\phi \in [0, 2\pi]$.

In particular, the action

$$S[x] = \int dt\, L(x, \dot{x}), \qquad L = \frac{M}{2}\dot{x}^2 - \frac{Mg}{l}\Big(1 - \cos(x)\Big)\,, \tag{3.36}$$

where $x \in [-\infty, \infty]$, no longer describes a pendulum but a particle moving in a periodic potential which is shown in Figure 3.5.

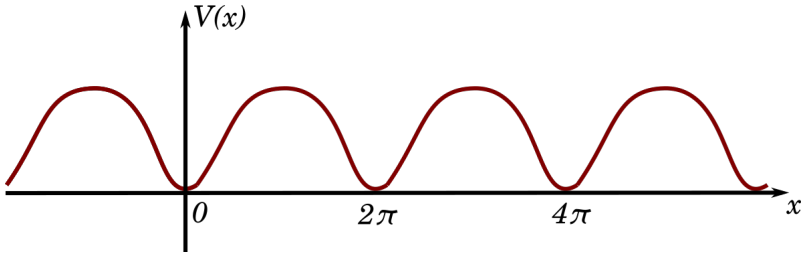

Figure 3.4.: *Periodic potential* $V(x) \propto 1 - \cos(x)$ *with* $x \in [-\infty, \infty]$.

For this system, there are infinitely many classical ground states which are separated by potential barriers. However, in a quantum context, a particle can tunnel trough these potential barriers.

Before we can write down the true quantum ground state, we need to take note that without tunneling effects there would be infinitely many degenerate ground states $|Q\rangle$ which are localized around the minima of the potential at $x = Q2\pi$. Moreover, according to Bloch's theorem, the wave functions are periodic up to a phase

$$|Q\rangle = e^{i\theta}|Q + 1\rangle\,. \tag{3.37}$$

The true quantum ground state can be understood as a superposition of these states [111]

$$|\theta\rangle = \sum_{Q=-\infty}^{\infty} e^{iQ\theta}|Q\rangle\,. \tag{3.38}$$

In condensed matter physics, a Lagrangian of the form given in Eq. (3.36) is used to describe an electron in an ideal crystal. The states of the form $|\theta\rangle$ are known as Bloch waves and θ is usually called the quasi-momentum.

An interesting aspect of this "dual" nature of the Lagrangian in Eq. (3.29) is "*that the interpretation of θ-states depends on the model; in the system with periodic potential [...] the θ-states are different states of the same system, while for the pendulum, these are states of different systems (pendula in the presence of different Aharonov-Bohm potentials).*" [111]

With these ideas in mind, we are ready to discuss the QCD vacuum.

3.2. The QCD Vacuum

First of all, there is nothing in the Standard Model which forbids an additional total derivative term of the form

$$L_{top} = \theta_{\mathrm{QCD}} \frac{\alpha_s}{8\pi} G\tilde{G}\,, \tag{3.39}$$

where G is the gluon field strength tensor and $\tilde{G}$ its dual. Therefore, according to Gell-Mann's totalitarian principle (*"Everything not forbidden is compulsory"* [1]), it should be included in the theory. This is analogous to how we are free to add a topological term to the Lagrangian of the particle on a ring (Eq. (3.6)) or of the pendulum (Eq. (3.30)).

To see that the term in Eq. (3.39) is indeed a total divergence, take note that [115]

$$\frac{1}{4} G_{\mu\nu}\tilde{G}^{\mu\nu} = \partial_\mu K^\mu\,, \tag{3.40}$$

where

$$K^\mu = \epsilon^{\mu\alpha\beta\gamma}\mathrm{Tr}\left(\frac{1}{2}A_\alpha\partial_\beta A_\gamma + \frac{i}{3}g_s A_\alpha A_\beta A_\gamma\right)$$

is known as the Chern-Simons current.

From the discussion in the previous sections, we know already that topological terms play no role for the equations of motion but can influence the quantum behavior of the system.

In addition, the topological term can again be rewritten in terms of a winding number Q [116]:[2]

$$S_{top} = \int d^4x\, L_{top} = \theta_{\mathrm{QCD}} \int d^4x\, \frac{\alpha_s}{8\pi} G\tilde{G} = \theta_{\mathrm{QCD}} Q\,. \tag{3.41}$$

However, in this case the interpretation of the topological term and winding number is more subtle since we are dealing with fields.

Interestingly, the interpretation of the topological QCD term depends crucially on the gauge used although, of course, all physical implications are independent of the chosen method of gauge fixing.

Temporal Gauge

Most commonly, the QCD vacuum is discussed in the temporal gauge [117–119]. However, the temporal gauge condition $A_0 = 0$ does not eliminate all gauge degrees of freedom. The residual gauge freedom consists of all time-independent gauge transformations. A discussion of the QCD ground state in the temporal gauge therefore requires a careful analysis of these residual gauge transformations. A key observation is that the classical QCD ground state ($G_{\mu\nu} = 0$) is "infinitely degenerate" since all gauge transformations of $A_\mu = 0$, i.e.

$$A_\mu = \frac{i}{g} U\partial_\mu U^\dagger \tag{3.42}$$

also correspond to configurations with a vanishing field strength tensor.

[2] This is analogous to what we discovered in Eq. (3.20).

A second key observation is that the set of gauge transformations that become equal to a specific but arbitrary constant matrix at spatial infinity[3]

$$U(\vec{x}) \to \text{const.} \quad \text{for} \quad |x| \to \infty\,, \tag{3.43}$$

fall into topologically distinct classes and therefore cannot be smoothly transformed into each other. This, in turn, implies that the pure gauge configuration in Eq. (3.42) fall into topologically distinct classes too.

Moreover, it can be shown that there is a potential barrier between topologically distinct ground states. This follows because a continuous transformation to a ground state configuration in a different topological class necessarily involves configurations which are not pure gauge [122]. In the temporal gauge, there are therefore infinitely many classical ground states which are separated by finite potential barriers. But since we are dealing

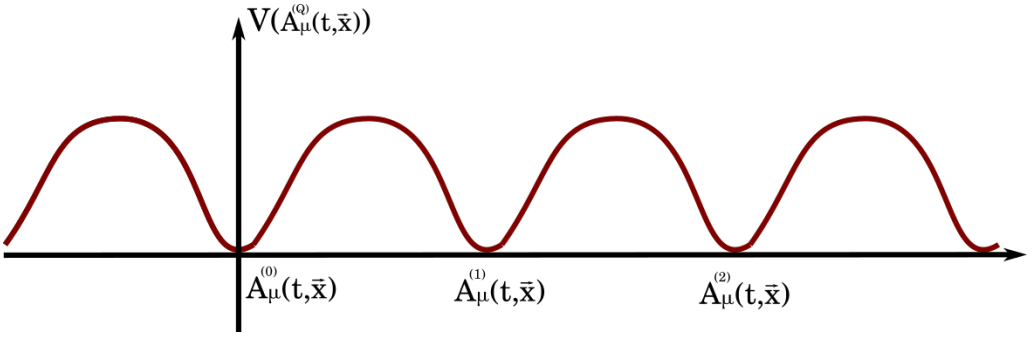

Figure 3.5.: *Schematic illustration of the QCD vacuum structure. Each minimum corresponds to a vacuum configuration, i.e. a gauge potential configuration with vanishing field strength tensor. These configurations can be understood as gauge transformations of* $A_\mu^{(0)} = 0$ *with a transformations that satisfies the boundary condition in Eq.* (3.43).

with quantum fields, a configuration corresponding to one classical ground state can tunnel through the potential barrier and turn into a different ground state configuration. This is known as an instanton process and can be described using a solution of the Yang-Mills equations [123].

The simplest non-trivial instanton solution contributes

$$(\Delta S_\theta)_{\text{in}} = \int d^4x\, (\Delta L_\theta)_{\text{in}} = \theta_{QCD} \tag{3.44}$$

to the total action [124]. In words, this means that such an instanton configuration carries a topological charge (winding number) of one.

[3] A proper discussion of the origin of this restriction is beyond the scope of this thesis. It should be noted, however, that the restriction to gauge transformations that become constant at infinity "*has always been recognized as weak but it had seemed necessary.*" [120] and "*while some plausible arguments can be given in support of this hypothesis [...] in the end we must recognize it as an assumption.*" [121]

In explicit terms, this instanton can be understood as a sequence of gauge potential configurations that starts at $t = -\infty$ with $A_\mu^{\text{inst.}}(-\infty, \vec{x}) = 0$ and ends at $t = \infty$ with another vacuum configuration that is given by $A_\mu^{\text{inst.}}(\infty, \vec{x}) = U^\dagger \partial_\mu U$, where U denotes the hedgehog gauge transformation

$$U(\vec{x}) = \exp\left(-\frac{i\pi\vec{x}\vec{\sigma}}{\sqrt{\vec{x}^2+\rho^2}}\right).$$

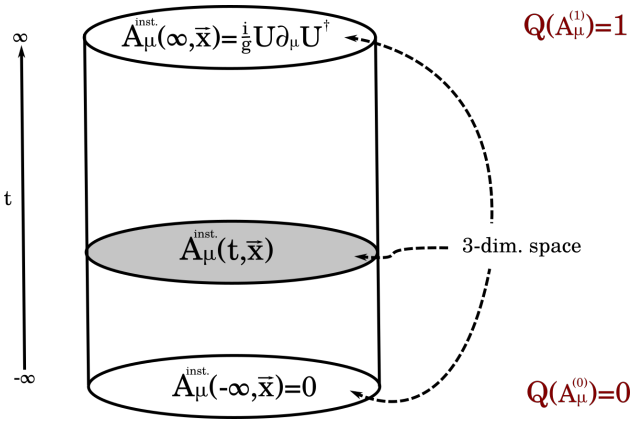

The initial and final gauge potential configuration both correspond to a vanishing field strength tensor and therefore, represent vacuum configurations. However, the final hedgehog configuration is topologically nontrivial and carries a winding number of one. This means that as we visit each location in space $\vec{x}$, we encounter each group element exactly once.[4]

The situation is therefore analogous to a particle moving in a periodic potential. This implies that the QCD ground state can then be understood as a superposition analogous to Eq. (3.38) and labeled by a parameter θ_{QCD}. However, in contrast to the particle example, the θ_{QCD}-state of the system cannot be changed by any gauge invariant operator and is therefore "frozen" in time [122].[5]

Axial Gauge

If we analyze the QCD vacuum in a gauge which removes all gauge freedom completely, there is no periodic structure. This is the case, for example, in the axial gauge. In such a "physical" gauge, the ground state is non-degenerate [125, 126].[6] Nevertheless, the structure of the ground state can be non-trivial.

In particular, gluon fields can still pick up a phase θ_{QCD} in vacuum to vacuum transitions. As already mentioned above, such transitions that result in a nontrivial phase are known as instanton processes. The situation is therefore analogous to the pendulum system discussed in Section 3.1.2. In particular, the minimum value of the ground state energy is realized for $\theta_{QCD} = 0$ [116].

But in the toy models we discussed in previous sections, the θ-term encodes the presence of an *external* magnetic flux.[7] Only if such a flux exists, the particle and pendulum pick up a phase θ each time they move in a full circle. Thus one may wonder which "surplus

[4] An explicit construction of this instanton process can be found, for example, in Ref. [115].

[5] For the particle in a periodic potential, there are different energy bands labelled by θ_{QCD}. Therefore, there can be transitions between states labeled by different values of θ_{QCD}. Another difference is that for the particle, the various ground states are *spatially* separated, while there is no such spatial separation in QCD.

[6] In a "physical" gauge, the potentials A_μ are uniquely determined by $F_{\mu\nu}$.

[7] External here means that it is not generated by the particle on a ring or pendulum itself but is something additional the experimenter adds to the system.

structure" provides further justification for the presence of the θ_{QCD}-term in the Standard Model. Formulated differently, so far we have only learned that the gluon fields *can* pick up a phase in vacuum to vacuum transitions. But why should they?

This is what we will discuss in the next section.[8]

[8] A speculative possibility to understand the θ_{QCD}-term as a result of an additional field (analogous to the magnetic flux in the toy models) is realized in axion models. This is discussed in more detail in the following chapter.

3.3. Axial Rotations

As mentioned at the end of the previous section, the θ_{QCD}-term might be interpreted as some kind of "surplus structure" from the perspective of pure QCD.

Analogous to the topological term for a pendulum, it should certainly be taken into account if we want to write down the most general quantum description. But the topological term plays no role for the pendulum if there is no external Aharonov-Bohm-type potential. Thus one might argue that it seems reasonable to ignore the θ_{QCD}-term as long as there is no good additional reason why $\theta_{QCD} \neq 0$. This perspective gains further support if we recall the current experimental bound mentioned at the beginning of this chapter (Eq. (3.3)).

Moreover, strong interactions violate CP symmetry if $\theta_{QCD} \neq 0$.[9] Therefore, if we introduce the θ_{QCD}-term for the QCD vacuum, we assume that CP symmetry was never a good symmetry of nature. But it is certainly an attractive idea that at some point in the early universe, the full Poincare group was a good symmetry of nature [129]. Formulated differently, if we assume that CP and T are only broken spontaneously, we have $\theta_{QCD} = 0$.

This, however, is by no means a solution of the strong CP puzzle since there is an interesting additional reason why the coefficient of the $G\tilde{G}$-term in the Lagrangian should be nonzero. To understand how this comes about, we need to understand the axial symmetry and how it is broken through quantum effects.

3.3.1. Vector and Axial Symmetry

In the absence of mass terms, the Standard Model Lagrangian is invariant under independent complex rotations of the left-chiral and right-chiral fermion fields

$$\begin{aligned} \Psi_L &\to e^{i\alpha}\Psi_L \\ \Psi_R &\to e^{i\beta}\Psi_R \end{aligned} \tag{3.45}$$

We can see this immediately because gauge and kinetic terms only couple fields of equal chirality:

$$L = -\frac{1}{4}G_a^{\mu\nu}G_{a\mu\nu} + \bar{\Psi}_L(i\partial_\mu\gamma^\mu - eA_\mu\gamma^\mu)\Psi_L + \bar{\Psi}_R(i\partial_\mu\gamma^\mu - eA_\mu\gamma^\mu)\Psi_R + \dots . \tag{3.46}$$

Noether's theorem therefore tells us that there are two corresponding conserved currents

$$\begin{aligned} J_L^\mu &= \Psi_L\gamma_\mu\Psi_L \\ J_R^\mu &= \Psi_R\gamma_\mu\Psi_R\,. \end{aligned} \tag{3.47}$$

This, however, is only true at the classical level. If we include quantum corrections, only the vector current

$$J_V^\mu = J_L^\mu + J_R^\mu = \bar{\Psi}\gamma_\mu\Psi \tag{3.48}$$

[9] In fact, $\theta_{QCD} = \pi$ corresponds to a CP conserving ground state too but is in conflict with meson spectrum data [127, 128].

is conserved, while the axial current[10]

$$J_A^\mu = J_L^\mu - J_R^\mu = \bar{\Psi}\gamma_\mu\gamma_5\Psi \tag{3.49}$$

is not. This is known as the axial anomaly.

3.3.2. Axial Anomaly

The axial anomaly can be understood by observing that the fermion spectrum gets modified in the presence of gauge fields. In particular, certain modes get lifted up from the Dirac sea while holes get pushed down [130]. Since the spectrum of left-chiral and right-chiral fields get modified differently, there is a net axial charge production when particle-antiparticle pairs are produced this way [131].

Alternatively, the axial anomaly can be understood more precisely by an evaluation of the famous Adler-Bell-Jackiw triangle diagram[11], which yields [135, 136]

$$\partial_\mu J_5^\mu = \frac{\alpha_s}{8\pi} G^{\mu\nu a}\tilde{G}^a_{\mu\nu}\,. \tag{3.50}$$

In words, this result implies that the axial current is non-conserved whenever the gauge fields change in a way such that

$$\frac{\alpha_s}{8\pi}\int d^4x G^{\mu\nu a}\tilde{G}^a_{\mu\nu} \neq 0\,. \tag{3.51}$$

This is exactly the definition of the winding number (Eq. (3.41)) which, as discussed above, can be nonzero whenever instanton processes happen. Therefore, the axial anomaly can be intuitively understood as a result of the particle production through instanton processes [137, 138].

A consequence of the fact that the axial current is not conserved on a quantum level is that we effectively produce a new term in the Lagrangian each time we perform an axial rotation. In particular, if $\partial_\mu J_A^\mu \neq 0$ for the current that would be conserved if $\Psi \to e^{i\alpha\gamma_5}\Psi$ were a good symmetry, the Lagrangian changes by[12]

$$\delta L = \alpha\partial_\mu J_A^\mu = 2\alpha\frac{\alpha_s}{8\pi} G^{\mu\nu a}\tilde{G}^a_{\mu\nu}. \tag{3.53}$$

[10] Here $\gamma_5 = i\gamma^0\gamma^1\gamma^2\gamma^3$ is the usual chirality operator [2].

[11] Even more abstractly, the axial anomaly can be understood as a result of the celebrated Atiyah-Singer index theorem [132–134].

[12] This can be shown, for example, by using Fujikawa's observation that the path integral measure is not invariant under axial rotations [139, 140]. In particular one finds that the measure of the path integral

$$\int [d\Psi][d\overline{\Psi}][dA_\mu]\exp\left(\int d^4x\, iL\right)$$

is nontrivial since the Jacobian, which appears in the transformation

$$[d\Psi][d\overline{\Psi}] \to J[d\Psi'][d\overline{\Psi}']\,, \tag{3.52}$$

reads [116]

$$J = \exp\left(-i\int d^4x 2\alpha\frac{\alpha_s}{8\pi} G^{\mu\nu a}\tilde{G}^a_{\mu\nu}\right)\,.$$

This is interesting because in the real world, quarks are massive:

$$L_M = -\bar{\psi}_{Ri} M_{ij} \psi_{Lj} - \bar{\psi}_{Li} M^{\dagger}_{ij} \psi_{Rj} \,. \tag{3.54}$$

The mass matrix M_{ij} can be diagonalized through a bi-unitary transformation, which yields a real diagonal matrix times a common phase factor. This phase factor can be removed through an axial rotation $\psi_i \to \mathrm{e}^{i\frac{\delta}{2}\gamma_5}\psi_i$ with $\delta = \arg\det M$ [141].

Moreover, a transformation is necessary for each flavor and one finds that, in total, an axial rotation by

$$\alpha = \arg\det M_u M_d \tag{3.55}$$

is necessary to diagonalize the quark mass matrices. In the Standard Model, there is no reason why $\arg\det M_u M_d$ should be zero since CP violation has been observed in weak interactions and therefore, entries of the quark mass matrices are, in general, complex.

In summary, this implies that the CP violation in the Yukawa sector gets mediated into the strong sector through the axial anomaly. Therefore, even if we assume that CP is only broken spontaneously (i.e., $\theta_{\mathrm{QCD}} = 0$), we find that strong interactions, in general, should violate CP nevertheless.

It is conventional to describe all this by defining

$$\bar{\theta} = \theta_{QCD} - \theta_{\mathrm{F}} \,, \tag{3.56}$$

where $\theta_{\mathrm{F}} = \arg\det M_u M_d$. As mentioned at the beginning of this chapter, the current experimental bound reads $\bar{\theta} < 10^{-10}$ (Eq. (3.3)).

Solutions of the strong CP problem therefore need to explain why $\bar{\theta}$ is tiny (or zero) even though there are two viable reasons why this should, in general, not be the case. The most popular solutions are discussed in the following chapter.

A Unified Solution to the Strong CP Problem 4

This chapter is based on Ref. [47].

The most famous solutions to the strong CP problem can be classified as follows:

1. **Minimal solutions with a massless quark.** If one of the Standard Model quarks is massless, there is an additional chiral symmetry and this makes $\bar{\theta}$ unobservable. However, this possibility is strongly disfavored by experimental data [60].

2. **Models with dynamical $\bar{\theta}$.** In such models, one argues that the presence of the θ-term is due to interactions with a new, yet unobserved, axion field which plays a role similar to the role the magnetic flux plays in the examples discussed in the previous chapter [142–144]. However, a big difference to the magnetic flux in these toy models is that the axion field is not just a static external field but a dynamical part of the system. This implies that the system will relax into a $\theta = 0$ state since this is the value for which the potential is minimized [145, 146]. Therefore, models with a dynamical $\bar{\theta}$ provide an elegant and robust solution to the strong CP puzzle.

   The most famous mechanism which realizes this possibility is known as the Peccei-Quinn mechanism [147]. An attractive feature of the Peccei-Quinn mechanism is that it generically predicts a new light particle known as the axion. The axion is a viable cold dark matter candidate and can, possibly, be detected in the near future [148]. One aspect of models with a dynamical $\bar{\theta}$ that is sometimes critized is that "*enormous theoretical superstructures*" must be "*erected upon a very narrow foundation.*" [149]. In particular, an "*obvious question about the axion hypothesis is how natural it really is. Why introduce a global PQ 'symmetry' if it is not actually a symmetry? What is the sense in constraining a theory so that the classical Lagrangian possesses a certain symmetry if the symmetry is actually anomalous?*" [150]. Moreover, there are also more technical issues like the domain wall problem [151, 152].

3. **Scenarios with spontaneous CP violation.** The main idea in these scenarios is that as long as CP is a good fundamental symmetry of nature, we have $\bar{\theta} = 0$. However, CP can only be a good symmetry in the UV since CP violating effects have experimentally been observed in weak interactions. Therefore, CP must be broken spontaneously and the main task is to find a mechanism that makes sure that $\bar{\theta}$ stays small after CP has been broken spontaneously. The most famous possibility to achieve this is the Nelson-Barr mechanism, which was first proposed by Nelson [153,154] and later generalized by Barr [155,156]. An attractive feature of the Nelson-

Barr mechanism is that all necessary ingredients can be naturally present in Grand Unified Theories (GUTs) [156]. However, one fact that makes Nelson-Barr models quite unattractive is that they usually make no predictions that can be tested in the near future. In particular, below the CP breaking scale, Nelson-Barr models can be effectively described by the Standard Model. This is problematic since the CP breaking scale has to be far above the electroweak scale. Otherwise, there are generic problems with bounds on FCNCs and domain walls [43]. Formulated differently, *"one must introduce recondite physics to avoid these problems"* [148]. Moreover, proposed solutions of the strong CP problem that make use of spontaneous CP violation are commonly criticized because *"coincidences of scales are needed for the CKM angle to be large"* [157].[1]

In the following, we discuss one possibility to overcome these shortcomings of the Nelson-Barr mechanism.

The main idea is to implement the Nelson-Barr mechanism in the context of a unified model with gauge group E_6.[2] The group E_6 is an ideal choice since its fundamental representation automatically contains additional fermions with exactly the right quantum numbers that allow us to implement the Nelson-Barr mechanism. In addition, E_6 is an attractive gauge group [6, 161–163], since there is an automatic absence of anomalies [6], each generation of the Standard Model fermions fits into a single fundamental representation, and because of its "exceptional" mathematical status [164].

By imposing E_6 and CP symmetry at high scales, we end up with an extremely restricted Yukawa sector that allows us to make predictions that can be tested in the near future. In particular, the model makes a prediction for the Dirac CP phase in the PMNS matrix. This is possible since the CP violation at high scales enters low energy observables through the mixing between exotic and Standard Model fermions. This happens automatically in the quark and in the lepton sector and therefore, there is a correlation between the CKM phase and the phases in the neutrino sector.

Thus one reason for implementing the Nelson-Barr mechanism in a unified theory is that the GUT structure makes the mechanism predictive. Moreover, otherwise problematic "coincidences of scales" can be understood as a result of the breaking chain. But at the same time, the Nelson-Barr mechanism turns out to be an invaluable guide in GUT model building. A common problem in unified theories is that we can always ask "*why this group and not another?*" [164]. Moreover, for each given group there are usually dozens of viable breaking chains. But as we will discuss below, by using the Nelson-Barr mechanism, we can translate the experimental fact $\bar{\theta} < 10^{-10}$ (Eq. (3.3)) into a concrete GUT scenario.

The remainder of this chapter is organized as follows. In the following section, we start with a short discussion of the Nelson-Barr mechanism in general terms. Afterwards, we discuss how the Nelson-Barr mechanism can be implemented in a concrete unified model. In Section 4.2.1 and Section 4.2.2, we then analyze the quark and lepton sector of the model in analytical terms. Finally, in Section 4.2.3, we will discuss predictions of the

[1] A more detailed discussion of problems of the Nelson-Barr mechanism can be found in Ref. [158].
[2] The Nelson-Barr mechanism has been implemented in minimal non-unified models in Refs. [159, 160].

model and how these can be derived using a concrete fit of all relevant model parameters.

4.1. The Nelson-Barr Mechanism

The Nelson-Barr mechanism is motivated by the following two facts:

1. If CP is a good symmetry of nature, we have $\theta_{QCD} = 0$ since this value corresponds to the only experimentally viable CP conserving QCD ground state.[3] Moreover, θ_{QCD} cannot change dynamically and therefore θ_{QCD} stays zero if the CP symmetry is broken spontaneously.

2. If the determinants of the quark mass matrices M_u and M_d are real, we have

$$\theta_{\mathrm{F}} \equiv \arg\det M_u M_d = 0\,. \tag{4.1}$$

   However, there must be complex entries in the quark mass matrices since $\delta_{CKM} \neq 0$.

Therefore, if CP is broken spontaneously and we have a structure in the mass matrices such that $\theta_{\mathrm{F}} = \arg\det M_u M_d = 0$, it follows that $\bar{\theta} \equiv \theta_{QCD} + \theta_{\mathrm{F}} = 0$.

Nelson and Barr observed in Refs. [153–156] that we can make sure that we end up with complex matrices with a real determinant by using matrices of the form:

$$M \sim \begin{pmatrix} \mathbb{R} & 0 \\ \mathbb{C} & \mathbb{R} \end{pmatrix}\,. \tag{4.2}$$

Moreover, they observed that we can construct mass matrices of the desired form by introducing additional vector like quarks. In general, the Lagrangian including vector-like $SU(2)_L$-singlet quarks reads schematically

$$\begin{aligned}\mathcal{L}_{NB} &= d_L m_d d_R + d_L m_C D_R + D_L M_C d_R + D_L M_R D_R + \dots \\ &= \begin{pmatrix} d_L & D_L \end{pmatrix} \begin{pmatrix} m_d & m_C \\ M_C & M_R \end{pmatrix} \begin{pmatrix} d_R \\ D_R \end{pmatrix} + \dots\end{aligned}$$

Therefore, if complex numbers only appear in M_C, which describes the mixing between vector-like and chiral quarks, and there is no $SU(2)_L$ breaking mixing ($m_C = 0$), we end up with a matrix with real determinant.

These observations are summarized by the Barr criteria:

$$\boxed{m_c \overset{!}{=} 0, \quad M_C \overset{!}{\in} \mathbb{C}^{\mathrm{n}\times\mathrm{n}}, \quad m_d \overset{!}{\in} \mathbb{R}^{\mathrm{n}\times\mathrm{n}}, \quad M_R \overset{!}{\in} \mathbb{R}^{\mathrm{n}\times\mathrm{n}}} \tag{4.3}$$

In summary, if the Barr criteria are fulfilled and CP is only broken spontaneously, we have at tree-level $\bar{\theta} = 0$. At higher orders in perturbation theory, there can be nonzero corrections to θ_F which, however, are tiny since they are proportional to Yukawa couplings and suppressed by small mass ratios [153, 154, 156, 165].

An immediate consequence of this observation is that the CP breaking scale has to be far above the electroweak scale such that $v_{\mathrm{EW}}^2/V_{CP}^2 \ll 1$ [159,160]. Therefore, one may wonder how a sufficiently large enough CKM phase can be generated in Nelson-Barr models.

[3] As mentioned above, $\theta = \pi$ is also CP conserving but disfavored by meson spectrum data [127, 128].

This is possible since the effective mass matrix of the Standard Model down quarks reads schematically [159]

$$m_d^{eff} \approx m_d m_d^\dagger - m_d \frac{M_{CP}^2}{M_R^2} m_d^\dagger \,, \tag{4.4}$$

where m_d denotes the down quark mass matrix in the absence of vector like quarks, M_R the mass scale of the vector like quarks, and M_{CP} is the scale of CP breaking.[4] Therefore, the CKM phase θ_{CKM} can be sufficiently large if the ratio of the superheavy scales M_{CP} and M_R is not too small.

In the following section, we discuss how the Nelson-Barr mechanism can be implemented in the context of a unified model.

[4] The formula given here is only valid for one additional vector like quark. A generalized formula for N vector like quarks was derived in Ref. [166].

4.2. E_6 Unification with Spontaneous CP Breaking

As already mentioned in Chapter 2, we embed each Standard Model generation in a fundamental representation of E_6. We denote each such representation by 27_i. The particle content of the 27-dimensional representation of E_6 can be understood by decomposing it in terms of $SU(5)$ representations:

$$27 = (10 \oplus \bar{5} \oplus 1)_{16} \oplus (5 \oplus \bar{5})_{10} \oplus 1_1 \,. \tag{4.5}$$

The subscripts here denote the corresponding $SO(10)$ representations (c.f. Eq. (2.18)). As in $SU(5)$ models, the Standard Model fermions live in the $10_{16} \oplus \bar{5}_{16}$. Additionally, each 27_i contains exotic particles that are contained in the $1_{16} \oplus (5 \oplus \bar{5})_{10} \oplus 1_1$. The $(5 \oplus \bar{5})_{10}$ contains a vector-like, $SU(2)_L$ singlet down-quark and a vector-like lepton doublet. The remaining two representations, 1_{16} and 1_1, describe Standard Model singlets. A more detailed decomposition of the 27 is given in Table B.1.

We assume that the breaking of the E_6 symmetry down to G_{SM} is accomplished by scalars contained in the

$$27_H \oplus 351'_H \,. \tag{4.6}$$

A detailed decomposition of the scalar representations is given in Table B.2. The Yukawa sector above the E_6 scale reads

$$\mathcal{L}_{yuk} = 27_i 27_j \left(Y_{27,ij} 27_H + Y_{351',ij} 351'_H \right) + \text{h.}c. \,. \tag{4.7}$$

Since we impose CP symmetry, all Yukawa couplings are assumed to be real [167]. Moreover, 27 and $351'$ are symmetric representations and therefore, the corresponding Yukawa couplings Y_{27} and $Y_{351'}$ are symmetric too [168]. The Yukawa sector can be simplified further by using the freedom to choose a suitable flavor basis. In the following, we use a basis in which $Y_{351'}$ is diagonal.

The combination of E_6 and CP symmetry therefore leads to an extremely restricted form of the Yukawa sector. In particular, excluding VEVs, the Yukawa sector contains in total only $3 + 6$ real parameters.

The VEV structure can be determined using the Barr criteria. For simplicity, we introduce the shorthand notations $t \equiv 10_{16}, \overline{f} \equiv \bar{5}_{16}, \overline{F} \equiv \bar{5}_{10}, F \equiv 5_{10}, N = 1_{16}, N' = 1_1$. The Barr criteria for our specific model then read:

- *i*) There are no $SU(2)_L$ breaking mass terms which generate $t - \overline{F}$ terms.
- *ii*) The only complex mass term is of the form $\overline{f} - F$.

These two conditions make sure that the effective low-energy down-quark mass contains complex entries but still has a real determinant. Therefore, the CKM phase can be nonzero and at tree level we have $\bar{\theta} = 0$.

The first Barr criterion tells us immediately that the VEVs of the scalar fields $h^c_{27,16,\bar{5}}, h^c_{351,144,\overline{45}}, h^c_{351,144,\bar{5}}$ have to be zero. The second Barr criterion implies that only the $s_{27,16,1}$ and $s_{351,144,24}$ VEVs can be complex.

For concreteness, we introduce the following notation for the VEVs:

$$\begin{aligned}
\langle h_{27,10,5}\rangle &= v_{u1}\,, & \langle h_{351,\overline{126},5}\rangle &= v_{u2}\,, & \langle h^c_{27,10,\overline{5}}\rangle &= v_{d1}\,, & \langle h^c_{351,\overline{126},\overline{45}}\rangle &= v_{d2}\,,\\
\langle s_{27,16,1}\rangle &\equiv V^c_{10}\,, & \langle s_{351,144,24}\rangle &\equiv V^c_5\,, & \langle s_{27,1,1}\rangle &\equiv V_6\,, & \langle s_{351,54,24}\rangle &\equiv V_5\,,\\
\langle s_{351,\overline{126},1}\rangle &\equiv V_{10}/2\,, & \langle s_{351,1,1}\rangle &\equiv \tilde{V}_6/2\,, & \langle s_{351,\overline{16},1}\rangle &\equiv V'_{10}\,, & \langle s_{78,45,24}\rangle &\equiv \tilde{V}_5\,. \qquad (4.8)
\end{aligned}$$

The subscripts denote which group is broken by the corresponding VEV (E_6, $SU(5)$ or $SO(10)$). As mentioned above, we assume that all VEVs except for V^c_{10}, V^c_5 are real. All $SU(2)_L$ doublet VEVs are assumed to be of order $v = 174\,\text{GeV}$ or below, while all G_{SM} singlet VEVs are assumed to be much larger.

The resulting fermion mass terms can be derived using the VEVs in Eq. (4.8) and a decomposition of Eq. (4.7) with respect to the relevant subgroups. We find

$$\begin{aligned}
\mathcal{L}_{mass} = {} & t_i t_j (m_{10})_{ij} + t_i \overline{f}_j (m_5)_{ij}\\
& + \overline{f}_i N_j (m_{10})_{ij} + \overline{F}_i N'_j (m_{10})_{ij} + F_i N'_j (m_5)_{ij}\\
& + \overline{f}_i F_j (M_{fF})_{ij} + \overline{F}_i F_j (M_{FF})_{ij}\\
& + \frac{1}{2} N_i N_j (M_{NN})_{ij} + \frac{1}{2} N'_i N'_j (M_{N'N'})_{ij} + \frac{1}{2} N_i N'_j (M_{NN'})_{ij} + \text{h.}c.. \qquad (4.9)
\end{aligned}$$

Here, we introduced the following notation for the mass matrices:

$$\begin{aligned}
(m_{10})_{ij} &= Y_{27,ij} v_{u1} + Y_{351',ij} v_{u2}\,, & (m_5)_{ij} &= Y_{27,ij} v_{d1} + Y_{351',ij} v_{d2}\,,\\
\left(M_{fF}\right)_{ij} &= Y_{27,ij} V^c_{10} + Y_{351',ij} V^c_5\,, & (M_{FF})_{ij} &= Y_{27,ij} V_6 + Y_{351',ij} V_5\,, \qquad (4.10)
\end{aligned}$$

and

$$(M_{NN})_{ij} = Y_{351',ij} V_{10}\,, \qquad \left(M_{N'N'}\right)_{ij} = Y_{351',ij} \tilde{V}_6 \qquad \left(M_{NN'}\right)_{ij} = Y_{351',ij} V'_{10}\,. \qquad (4.11)$$

All mass matrices are real except for M_{fF} since, as mentioned above, the only complex VEVs are V^c_{10} and V^c_5.

As discussed in the previous section, we need a breaking chain such that $M_{CP} \sim M_R$, where M_{CP} denotes the scale of CP breaking and M_R the mass scale of the vector-like quarks. Using the explicit VEVs in Eq. (4.8), we can conclude that one viable breaking chain is

$$E_6 \to SO(10) \to SU(5) \to SU(3)_C \times SU(2)_L \times U(1)_Y \qquad (4.12)$$

since the E_6, $SO(10)$ and $SU(5)$ scale can be sufficiently close. This is a necessary requirement because otherwise, the CKM phase is suppressed by a small mass ratio, as can be seen in Eq. (4.4).

Before we discuss explicit viable values for the various Yukawa couplings and VEVs, we analyze the structure of the various mass matrices in analytical terms.

4.2.1. Analysis of the Quark and Charged Lepton Sector

It is instructive to rewrite $\overline{f}_i$ and $\overline{F}_i$ in terms of light and heavy linear combinations, which we denote by $\overline{f}_{Li}$ and $\overline{F}_{Hi}$ respectively. To unclutter the following calculations, we neglect all Clebsch-Gordon coefficients and only include them in the final formulas.

We start with the ansatz

$$\overline{f} = a_f \cdot \overline{f}_L + A_f \cdot \overline{F}_H \,, \qquad \overline{F} = a_F \cdot \overline{f}_L + A_F \cdot \overline{F}_H \,, \tag{4.13}$$

where a_f, A_f, a_F, A_F denote 3×3 matrices that encode the mixing. By requiring canonically normalized kinetic terms, we find

$$a_f^\dagger a_f + a_F^\dagger a_F = 1_3 \,, \qquad A_f^\dagger A_f + A_F^\dagger A_F = 1_3 \,, \qquad a_f^\dagger A_f + a_F^\dagger A_F = 0 \,. \tag{4.14}$$

Moreover, if we demand that the there is no term which mixes $\overline{f}_L$ and F, we find

$$a_f^T M_{fF} + a_F^T M_{FF} = 0 \,. \tag{4.15}$$

Solving Eq. (4.14) and Eq. (4.15) yields

$$a_f = \left[1_3 + Z^\dagger Z\right]^{-1/2} \,, \qquad a_F = -Z \cdot a_f \,, \qquad Z = \left[M_{fF} (M_{FF})^{-1}\right]^T \,. \tag{4.16}$$

We can use this result to rewrite the quark sector of the Lagrangian in terms of the new linear combinations:

$$\mathcal{L} = t_i t_j (m_{10})_{ij} + t_i \overline{f}_{Lj} (m_5^{eff})_{ij} + \cdots \tag{4.17}$$

where

$$m_5^{eff} = m_5 \cdot a_f \,. \tag{4.18}$$

As mentioned above, all ordinary mass matrices like m_{10} and m_5 are real and complex numbers enter the effective mass matrix m_5^{eff} only through the mixing matrix a_f. It follows from Eq. (4.16) that the mixing matrix a_f is always hermitian. Therefore, while the effective mass matrix m_5^{eff}, in general, contains complex entries, its determinant is always real.

If we now include all Clebsch-Gordon coefficient, we find the following formulas for the quark and charged lepton mass matrices:

$$M_u = m_u \,, \qquad M_d = m_d \cdot a_d \,, \qquad M_e = a_e^T \cdot m_e \,, \tag{4.19}$$

where

$$m_u = H r_{\beta 1} + F r_{\beta 2} \,, \tag{4.20}$$
$$m_d = H + F \,, \tag{4.21}$$
$$m_e = H - 3F \tag{4.22}$$

and

$$a_d = \left[1 + Z_d^\dagger Z_d\right]^{-1/2} \,, \qquad Z_d = r_{10,6} \left(H + F r_{5,6}\right)^{-1} \left(H + F c_{5,10}\right) \,, \tag{4.23}$$

$$a_e = \left[1 + Z_e^\dagger Z_e\right]^{-1/2} \,, \qquad Z_e = r_{10,6} \left(H - \frac{3}{2} F r_{5,6}\right)^{-1} \left(H - \frac{3}{2} F c_{5,10}\right) \,. \tag{4.24}$$

In addition, we have introduced

$$H \equiv Y_{27} v_{d1} \,, \tag{4.25}$$
$$F \equiv Y_{35'} v_{d2} \,, \tag{4.26}$$

and five VEV ratios

$$r_{\beta 1} \equiv \frac{v_{u1}}{v_{d1}}\,, \qquad r_{\beta 2} \equiv \frac{v_{u2}}{v_{d2}}\,,$$
$$r_{10,6} \equiv \frac{|V_{10}^c|}{V_6}\,, \qquad r_{5,6} \equiv \frac{V_5}{V_6}\frac{v_{d1}}{v_{d2}}\,, \qquad c_{5,10} \equiv \frac{V_5^c}{V_{10}^c}\frac{v_{d1}}{v_{d2}}\,. \tag{4.27}$$

All parameters here, except for $c_{5,10}$ are real. Moreover, H and F are real symmetric matrices and, as mentioned above, we choose a basis where F is real. Therefore, there are in total $6 + 3 + 6 = 15$ model parameters relevant for the low-energy observables in the quark and lepton sectors.

In the following section, we carry out a similar analysis for the neutrino sector.

4.2.2. Analysis of the Neutrino Sector

The terms relevant for the masses of the superheavy singlets read

$$\mathcal{L}_{N,N'} = \frac{1}{2}\left(N_i, N_i'\right)\mathcal{M}_{N,ij}\begin{pmatrix} N_j \\ N_j' \end{pmatrix}\,, \tag{4.28}$$

where

$$\mathcal{M}_{N,ij} = \begin{pmatrix} M_{NN,ij} & M_{NN',ij} \\ M_{NN',ij} & M_{N'N',ij} \end{pmatrix}\,. \tag{4.29}$$

According to their definition in Eq. (4.11) all 3×3 matrices appearing as sub-matrices here are real and proportional to $Y_{351'}$. Since we work in a basis where $Y_{351'}$ is real and diagonal, $M_{NN,ij}$, $M_{NN',ij}$ and $M_{NN',ij}$ are real and diagonal too.

Therefore, to diagonalize $\mathcal{M}_{N,ij}$, we only need to diagonalize the 2×2 matrix

$$\mathcal{M} = \begin{pmatrix} V_{10} & V_{10}' \\ V_{10}' & \tilde{V}_6 \end{pmatrix}\,. \tag{4.30}$$

The eigenvalues of $\mathcal{M}$ correspond to the masses of the superheavy singlets.

Next, we rewrite the neutrino sector of the Lagrangian

$$\mathcal{L} = \nu_L^T a_e^T \left(H r_{\beta 1} - 3F r_{\beta 2}\right) N + \text{h.}c. \tag{4.31}$$

by integrating out the superheavy singlet N.

The resulting Majorana mass matrix of the light neutrino is then given by

$$m_\nu \approx r_\epsilon \left[a_e^T \cdot \left(H r_{\beta 1} - 3F r_{\beta 2}\right) \cdot F^{-1} \cdot \left(H r_{\beta 1} - 3F r_{\beta 2}\right) \cdot a_e\right]\,, \tag{4.32}$$

where

$$r_\epsilon \equiv \frac{v_{d2}}{V_{10}} \lll 1\,, \tag{4.33}$$

and the effective Lagrangian reads

$$\mathcal{L}_\nu = -1/2\, m_{\nu,ij}\nu_{L,i}\nu_{L,j} + \text{h.}c.\,. \tag{4.34}$$

We can neglect all contributions from N' since $V_{10} \sim V'_{10} \ll \tilde{V}_6$ and therefore, its contributions are suppressed by M_ν/M_{GUT}.

In the following section, we discuss how all fundamental low-energy observables in the Standard Model fermion sector can be reproduced using the 16 model parameters introduced above.

4.2.3. Fit to Fermion Masses and Mixing Angles

A crucial consistency check for any unified model is that all known low-energy data can be reproduced. We already discussed in Chapter 2 how this can be accomplished in general for the gauge couplings. In this section, we will therefore focus on a second type of low-energy data: fermion masses and mixing angles. The experimental values for the 18 fundamental low-energy Standard Model fermion observables that we use in the following are listed in Table 4.1.

Fermion observables at the electroweak scale $\mu = M_Z$			
m_d(MeV)	2.75 ± 0.29	$\Delta_{12}(\text{eV}^2)$	$(7.50 \pm 0.18) \times 10^{-5}$
m_s(MeV)	54.3 ± 2.9	$\Delta_{31}(\text{eV}^2)$	$(2.52 \pm 0.04) \times 10^{-3}$
m_b(GeV)	2.85 ± 0.03	$\sin\theta^q_{12}$	0.2254 ± 0.0007
m_u(MeV)	1.3 ± 0.4	$\sin\theta^q_{23}$	0.0421 ± 0.0006
m_c(GeV)	0.627 ± 0.019	$\sin\theta^q_{13}$	0.0036 ± 0.0001
m_t(GeV)	171.7 ± 1.5	$\sin^2\theta^l_{12}$	0.306 ± 0.012
m_e(MeV)	0.4866 ± 0.0005	$\sin^2\theta^l_{23}$	0.441 ± 0.024
m_μ(MeV)	102.7 ± 0.1	$\sin^2\theta^l_{13}$	0.0217 ± 0.0008
m_τ(GeV)	1.746 ± 0.002	δ_{CKM}	1.21 ± 0.05

Table 4.1.: *Experimental values of the Standard Model fermion observables at the electroweak scale. Quark masses, lepton masses and the quark mixing parameters are taken from Ref. [169]. Neutrino mixing parameters for a normal hierachy are taken from Ref. [170]. For all observables the arithmetic average of the errors is used.*

These 18 observables need to be reproduced using the parameters in H, F and the six VEV ratios $r_{\beta 1}, r_{\beta 2}, r_{10,6}, r_{5,6}, c_{5,10}, r_\epsilon$. Given concrete values of these 16 model parameters, the corresponding values of the fermion observables can be calculated by using Eq. (4.19) and Eq. (4.32).

We performed a numerical top-down fit of the model parameters using the Metropolis-Hastings algorithm [171, 172]. Since Eq. (4.19) and Eq. (4.32) are only valid at the GUT scale ($Q \simeq 10^{16}\,\text{GeV}$), we have solved the Yukawa RGEs numerically using REAP [173] for each given set of values of the model parameters. The numerical solutions were then used to calculate the corresponding values of the fermion observables at the electroweak scale M_Z. This way, the corresponding values $\mathcal{O}_i^{\text{fit}}$ of the observables $\mathcal{O}_i$ are calculated for each choice of the model parameters.

The goal of the fitting procedure is to minimize the function

$$\chi^2 \equiv \sum_{i=1}^{n} \left(\frac{\mathcal{O}_i^{exp} - \mathcal{O}_i^{\text{fit}}}{\sigma_i^{exp}} \right)^2 , \tag{4.35}$$

where $\mathcal{O}_i^{exp}$ denotes the measured value of the observable $\mathcal{O}_i$ and σ_i^{exp} the corresponding experimental error. During the fit, we assumed a 0.1% uncertainty of the charged lepton masses, since the fitting procedure would otherwise focus solely on these observables [174, 175].

The fit is non-trivial since there are only 16 model parameters and 18 observables.[5]

No viable fit point was found for an inverted neutrino hierarchy. Assuming normal ordering in the neutrino sector, however, we find a best-fit point with $\chi^2 \approx 15.55$. Specifically, our best-fit point reads,

$$H(\text{GeV}) = \begin{pmatrix} -0.00814 & 0.0292 & -0.0894 \\ 0.0292 & -0.217 & 2.49 \\ -0.0894 & 2.49 & -12.8 \end{pmatrix}, \qquad F(\text{GeV}) = \begin{pmatrix} -0.00248 & 0. & 0. \\ 0. & 0.0489 & 0. \\ 0. & 0. & 30.7 \end{pmatrix}$$

$$r_{\beta 1} = -1.28\,, \quad r_{\beta 2} = 2.26\,, \quad r_{10,6} = 2.21\,, \quad r_{5,6} = -0.433\,,$$
$$c_{5,10} = 2.20 \cdot e^{1.60\,i}\,, \quad r_\epsilon = 1.73 \cdot 10^{-10}\,. \tag{4.36}$$

This corresponding values of the fermion observables are listed in Table 4.2 and the corresponding pulls are plotted in Figure 4.1.

Fermion observables at the electroweak scale $\mu = M_Z$					
	fit	pull		fit	pull
m_d(MeV)	3.44	−2.4	$\Delta_{12}(\text{eV}^2)$	7.39×10^{-5}	0.63
m_s(MeV)	50.4	1.4	$\Delta_{13}(\text{eV}^2)$	-0.76×10^{-3}	−0.19
m_b(GeV)	2.85	0.27	$\sin\theta^q_{12}$	0.225	0.56
m_u(MeV)	1.32	−0.08	$\sin\theta^q_{23}$	0.0414	0.1
m_c(GeV)	0.63	−0.07	$\sin\theta^q_{13}$	0.0035	1.1
m_t(GeV)	171.58	0.08	$\sin^2\theta^l_{12}$	0.302	0.37
m_e(MeV)	0.486	0.15	$\sin^2\theta^l_{23}$	0.405	1.5
m_μ(MeV)	102.76	−0.61	$\sin^2\theta^l_{13}$	0.022	−0.26
m_τ(GeV)	1.746	−0.04	δ_{CKM}	1.13	1.5

Table 4.2.: *The fermion observables at the electroweak scale M_Z as calculated using the best-fit point in Eq. (4.36). The pull of is defined as pull$(\mathcal{O}_i^{fit}) = \left(\mathcal{O}_i^{exp} - \mathcal{O}_i^{fit}\right)/\sigma_i^{exp}$, where σ_i^{exp} is the corresponding experimental error and $\mathcal{O}_i^{exp}$ the experimental value as given in Table 4.1.*

In addition to being a consistency check, the fit of the model parameters in the Yukawa sector can also be used to make predictions for not yet measured observables. In particular, we can use our best-fit point in Eq. (4.36) to predict the effective mass

$$m_\beta = \sqrt{\sum |U_{ei}|^2\, m_i^2}\,, \tag{4.37}$$

which is probed by experiments like KATRIN [176], MARE [177] , Project 8 [178], or ECHo [179].

In addition, we can calculate the sum of neutrino masses

$$\Sigma = \sum m_i,$$

[5] Take note that this implies that there must be two relations between Standard Model observables. Unfortunately, due to complexity of the formulas we were not able to find analytical formulas for these relations.

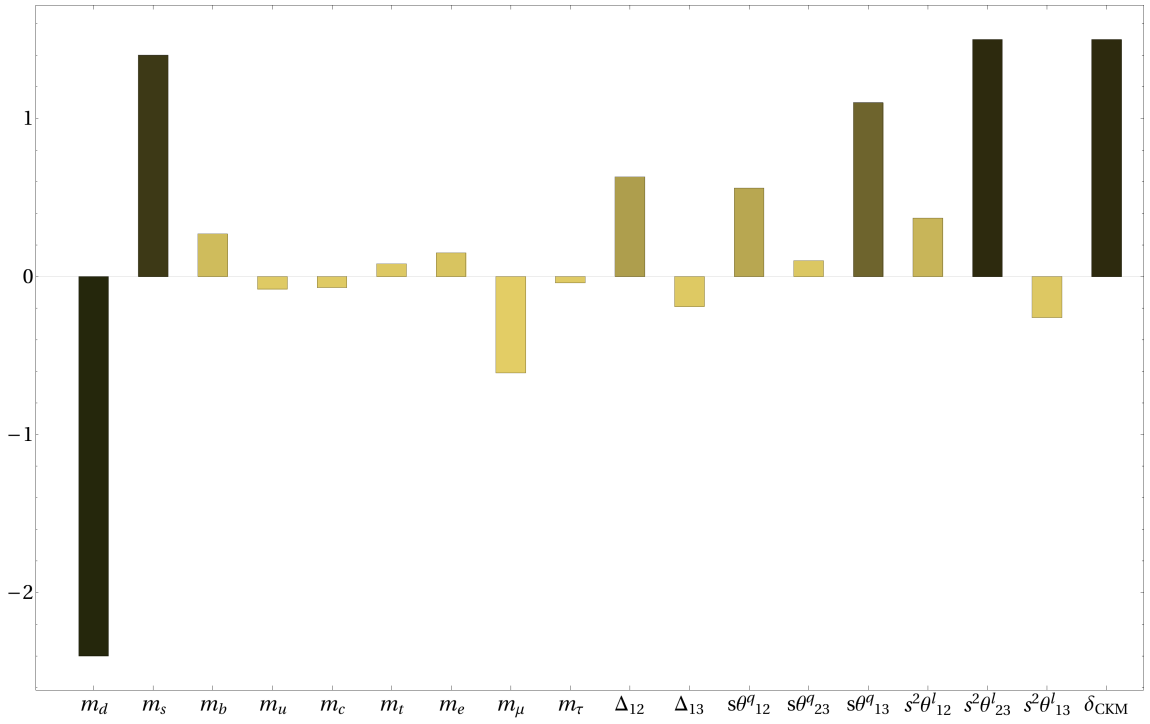

Figure 4.1.: *Pulls for the observables corresponding to the best-fit point in Eq.* (4.36).

which is tested by cosmological observations, and the "effective Majorana mass"

$$m_{\beta\beta} = \left| \sum U_{ei}^2 \, m_i \right| , \tag{4.38}$$

which is probed by neutrinoless double beta decay experiments, like, for example, GERDA [180], EXO-200 [181] or KamLAND-Zen [182]. The predicted values for these observables and for the Dirac and Majorana phases are summarized in Table 4.3.

	m_β [meV]	Σ [meV]	$m_{\beta\beta}$ [meV]	δ [°]	φ_1 [°]	φ_2 [°]
Prediction	8.8 ± 0.5	59 ± 3	1.8 ± 0.1	157 ± 3	187 ± 4	159 ± 5
Current bound	$\lesssim 2000$ [60]	$\lesssim 230$ [60, 183]	200 [184, 185]	-	-	-

Table 4.3.: *Predictions for the neutrino observables using the best-fit point in Eq.* (4.36). *All current bounds were taken from Ref. [186]. The uncertainty on the predicted values correspond to perturbations of the best fit point with* $\chi^2 \lesssim 150$.

The main result here is a quite narrow prediction for the Dirac phase $\delta \in [154, 157]^\circ$. This prediction can be probed in future experiments like Hyper-Kamiokande [187] or DUNE [100]. Moreover, the values for all mass observables are far below the ranges that can be probed by experiment in the near future.

Conclusions and Outlook 5

In this thesis, we have discussed an intrinsic GUT solution to the strong CP problem and how gauge coupling unification can be achieved in the absence of low energy supersymmetry.

To analyze the running of the gauge couplings, we introduced in Eq. 2.12 the quantities $\Delta\lambda_{12}(\mu)$ and $\Delta\lambda_{23}(\mu)$ that quantify the mismatch in the gauge couplings at a given scale μ. We then analyzed the running of the gauge couplings in a class of $SU(5)$, $SO(10)$ and E_6 models ("conservative models") that mimic the Standard Model group structure as much as possible.

In scenarios with a grand desert between the electroweak and the unification scale, the failure of the three Standard Model gauge couplings to meet at a common point at all scales can only be explained through threshold corrections. We therefore estimated the magnitude the of threshold corrections by calculating $\Delta\lambda_{12}$ and $\Delta\lambda_{23}$ in conservative grand desert scenarios using randomized mass spectra for the superheavy particles.

In conservative $SU(5)$ models, the threshold corrections are generically too small to explain the mismatch in the gauge couplings. This is shown explicitly in Figure 2.5. In $SO(10)$ models, the threshold corrections can be much larger since there are not just contributions from additional scalar contributions but from superheavy gauge bosons too. But, as shown in Figure 2.6, while the threshold corrections can, in principle, be large enough to explain the mismatch, this is only true for scales that are already ruled out by proton decay experiments. In conservative E_6 models, however, there can be significant contributions from superheavy scalars, gauge bosons *and* fermions. We find that the corresponding threshold corrections can be large enough to explain the mismatch in the gauge couplings up to a unification scale of $M_{\mathrm{E}_6}^{\mathrm{max}} \simeq 10^{16.3}$ GeV.

In addition, we analyzed the impact of particles at intermediate scales on the running of the gauge couplings. We quantified explicitly which scalar, fermion and gauge boson representations improve the running of the gauge couplings and used this information to discuss the viability of scenarios with just one intermediate scale.

In conservative $SU(5)$ scenarios, the running is only improved by scalars in the $(1, 3, 0)$, $(3, 3, -2)$ and $(\overline{6}, 3, -2)$ representation. But while it is possible to achieve gauge coupling unification with any of these representations, only for $(\overline{6}, 3, -2)$ scalars at an intermediate scale the unification scale can be sufficiently high to be in agreement with bounds from proton decay experiments (Figures 2.8-2.10). In conservative $SO(10)$ scenarios, the running can additionally be improved through gauge bosons at an intermediate scale, i.e. an

intermediate symmetry. We argued that even if we take threshold corrections into account, the only viable scenario with just one intermediate scale can be described by an

$$SU(3)_C \times SU(2)_L \times SU(2)_R \times U(1)_X$$

intermediate symmetry. By estimating possible threshold corrections as before using randomized mass spectra, we found that the proton lifetime can be as high as $\tau_{\max} \simeq 5.24 \times 10^{44}$ yrs (Figure 2.12). We also argued that scenarios with breaking chain

$$SO(10) \to SU(4) \times SU(2)_L \times U(1)_R \to G_{\rm SM}$$

are already ruled out by proton decay experiments, even if we take possibly large threshold corrections into account (Figure 2.11). Finally, we analyzed the impact of additional light E_6 fermions on the running of the gauge couplings. The main observation in this context was that vector-like E_6 leptons improve the running, while the vector-like E_6 quarks make it worse. Therefore, a large mass splitting between these leptons and quarks is necessary to achieve unification. With all vector-like quarks at the GUT scale, the unification scale can be as high as $M_{E_6}^{\max} \simeq 10^{16}$ GeV if the heaviest lepton generation lives around $m_{3L} \simeq 10^{14}$ GeV and we have a Standard Model like mass splitting between the generations, i.e. $m_{2L}/m_{3L} \simeq 10^{-2}$, $m_{1L}/m_{3L} \simeq 10^{-4}$ (Figure 2.13).

As mentioned above, we restricted our analyses to conservative scenarios with just one intermediate scales. These are arguably the simplest models that are not yet ruled out by proton decay bounds. There are, of course, several additional models with two or more intermediate scales that could be analyzed systematically in the future using the methods discussed in this thesis.

After this general discussion of the gauge unification problem, we shifted our focus to the strong CP problem. In Chapter 3, we reviewed the problem itself and motivated why the idea of spontaneous CP violation is an interesting first step towards a full solution.

We then argued in Chapter 4 that this idea can be naturally realized in the context of a unified model. To keep $\bar{\theta}$ small after CP has been broken spontaneously, we implemented the Nelson-Barr mechanism in the context of an E_6 model. In particular, we argued that by doing this, several generic problems of the Nelson-Barr mechanism can be avoided. For example, a high CP breaking scale is by no means mysterious in the context of a GUT model. Moreover, the vector-like quarks that are necessary to mediate the high-scale CP violation into the low-energy sector are automatically included in the fundamental representation of E_6. In addition, the required coincidence of the CP breaking scale and the scale of the vector-like quarks can be understood as a consequence of the breaking chain.

Most importantly, by implementing the Nelson-Barr mechanism in a grand unified context, we end up with a predictive model. This is possible since the idea of spontaneous CP violation, the requirements of the Nelson-Barr mechanism and the structure imposed by the unified gauge symmetry taken together leave us with an extremely restricted Yukawa sector. One consequence of the restricted form of the Yukawa sector is that there is a correlation between the CP phase in the quark sector and the CP phase in the lepton sector.

In total, there are only 16 real parameters in the Yukawa sector. To test the viability of the proposed model, we performed a fit of these model parameters and found a best fit point with $\chi^2 \approx 15.55$. Since there are less model parameters than fermion observables in the Standard Model, we were able to use this best fit point to calculate, among others, the prediction $\delta_{\mathrm{CP}} = 157 \pm 3^\circ$ for the leptonic CP phase. This prediction will be probed by experiments like Hyper-Kamiokande [187] or DUNE [100].

One interesting aspects of the model that is not yet fully understood and therefore could be analyzed further in the future is the exact analytic relationship between the CP phases in the quark and lepton sector. A second aspect that deserves further attention is why the fit was successful although there are less model parameters than observables. This result in particular implies that there are hidden relationships between Standard Model fermion observables that could provide new hints for the longstanding flavor puzzle.

Scalar Decompositions and and Threshold Formulas A

A.1. $SU(5)$

$SU(5)$	$3_C 2_L 1_Y$	A_{23}/r_I	A_{12}/r_I	Label
5	$(1,2,3)$	$\frac{1}{6}$	$-\frac{1}{15}$	φ_1
	$(3,1,-2)$	$-\frac{1}{6}$	$\frac{1}{15}$	φ_2
$\overline{5}$	$(1,2,-3)$	$\frac{1}{6}$	$-\frac{1}{15}$	H
	$(\overline{3},1,2)$	$-\frac{1}{6}$	$\frac{1}{15}$	φ_3
10	$(1,1,6)$	0	$\frac{1}{5}$	φ_4
	$(\overline{3},1,-4)$	$-\frac{1}{6}$	$\frac{4}{15}$	φ_5
	$(3,2,1)$	$\frac{1}{6}$	$-\frac{7}{15}$	φ_6
15	$(1,3,6)$	$\frac{2}{3}$	$-\frac{1}{15}$	φ_7
	$(3,2,1)$	$\frac{1}{6}$	$-\frac{7}{15}$	φ_8
	$(6,1,-4)$	$-\frac{5}{6}$	$\frac{8}{15}$	φ_9
24	$(1,1,0)$	0	0	s_1
	$(1,3,0)$	$\frac{1}{3}$	$-\frac{1}{3}$	φ_{10}
	$(3,2,-5)$	$\frac{1}{12}$	$\frac{1}{6}$	ξ_1
	$(\overline{3},2,5)$	$\frac{1}{12}$	$\frac{1}{6}$	ξ_2
	$(8,1,0)$	$-\frac{1}{2}$	0	φ_{11}
45	$(1,2,3)$	$\frac{1}{6}$	$-\frac{1}{15}$	φ_{12}
	$(3,1,-2)$	$-\frac{1}{6}$	$\frac{1}{15}$	φ_{13}
	$(3,3,-2)$	$\frac{3}{2}$	$-\frac{9}{5}$	φ_{14}
	$(\overline{3},1,8)$	$-\frac{1}{6}$	$\frac{16}{15}$	φ_{15}
	$(\overline{3},2,-7)$	$\frac{1}{6}$	$\frac{17}{15}$	φ_{16}
	$(\overline{6},1,-2)$	$-\frac{5}{6}$	$\frac{2}{15}$	φ_{17}
	$(8,2,3)$	$-\frac{2}{3}$	$-\frac{8}{15}$	φ_{18}
$\overline{45}$	$(1,2,-3)$	$\frac{1}{6}$	$-\frac{1}{15}$	φ_{19}
	$(\overline{3},1,2)$	$-\frac{1}{6}$	$\frac{1}{15}$	φ_{20}
	$(\overline{3},3,2)$	$\frac{3}{2}$	$-\frac{9}{5}$	φ_{21}
	$(3,1,-8)$	$-\frac{1}{6}$	$\frac{16}{15}$	φ_{22}
	$(3,2,7)$	$\frac{1}{6}$	$\frac{17}{15}$	φ_{23}
	$(6,1,2)$	$\frac{5}{6}$	$\frac{2}{15}$	φ_{24}
	$(8,2,-3)$	$-\frac{2}{3}$	$-\frac{8}{15}$	φ_{25}
$\overline{50}$	$(1,1,-12)$	0	$\frac{4}{5}$	φ_{26}
	$(3,1,-2)$	$-\frac{1}{6}$	$\frac{1}{15}$	φ_{27}
	$(\overline{3},2,-7)$	$\frac{1}{6}$	$\frac{17}{15}$	φ_{28}
	$(\overline{6},3,-2)$	$\frac{3}{2}$	$-\frac{18}{5}$	φ_{29}
	$(6,1,8)$	$-\frac{5}{6}$	$\frac{32}{15}$	φ_{30}
	$(8,2,3)$	$-\frac{2}{3}$	$-\frac{8}{15}$	φ_{31}

Table A.1.: *Decomposition of the scalar representations in conservative $SU(5)$ GUTs with respect to $SU(3)_C \times SU(2)_L \times U(1)_Y$. Goldstone bosons are labelled by ξ_i, SM singlets by s_i and all other fields by φ_i. The hypercharges are given in the normalization of Ref. [71]. The numbers in the A_{23} and A_{12} columns indicate whether or not the fields can help to achieve gauge unification.*

A.2. $SO(10)$

The threshold corrections in conservative $SO(10)$ GUTs can be calculated using Eq. (2.9) and read

$$\begin{aligned}
\lambda_{3C} = 5 &- 21\eta_{PSV} + \frac{1}{2}\eta_{\Phi_2} + \frac{1}{2}\eta_{\Phi_3} + \frac{1}{2}\eta_{\Phi_5} + \frac{1}{2}\eta_{\Phi_7} + \frac{1}{2}\eta_{\Phi_9} + \eta_{\Phi_{10}} + \frac{1}{2}\eta_{\Phi_{12}} + \eta_{\Phi_{13}} + \frac{1}{2}\eta_{\Phi_{15}} \\
&+ \frac{3}{2}\eta_{\Phi_{16}} + \frac{1}{2}\eta_{\Phi_{17}} + \eta_{\Phi_{18}} + \frac{5}{2}\eta_{\Phi_{19}} + 6\eta_{\Phi_{20}} + \frac{1}{2}\eta_{\Phi_{22}} + \frac{3}{2}\eta_{\Phi_{23}} + \frac{1}{2}\eta_{\Phi_{24}} + \eta_{\Phi_{25}} + \frac{5}{2}\eta_{\Phi_{26}} \\
&+ 6\eta_{\Phi_{27}} + \eta_{\Phi_{29}} + 2\eta_{\Phi_{31}} + 5\eta_{\Phi_{32}} + \eta_{\Phi_{34}} + 3\eta_{\Phi_{35}} + \eta_{\Phi_{36}} + 2\eta_{\Phi_{37}} + 5\eta_{\Phi_{38}} + 12\eta_{\Phi_{39}} \\
&+ \eta_{\Phi_{41}} + 2\eta_{\Phi_{42}} + 15\eta_{\Phi_{43}} + 5\eta_{\Phi_{44}} + 12\eta_{\Phi_{45}} + \frac{1}{2}\eta_{\Phi_{47}} + \eta_{\Phi_{48}} + \frac{1}{2}\eta_{\Phi_{50}} + \eta_{\Phi_{51}} + 3\eta_{\Phi_{53}} ,
\end{aligned}$$

$$\begin{aligned}
\lambda_{2L} = 6 &+ \frac{1}{2}\eta_{\Phi_1} + \frac{1}{2}\eta_{\Phi_4} + \frac{1}{2}\eta_{\Phi_6} + \frac{3}{2}\eta_{\Phi_{10}} + \frac{3}{2}\eta_{\Phi_{13}} + \frac{1}{2}\eta_{\Phi_{14}} + 6\eta_{\Phi_{16}} + \frac{3}{2}\eta_{\Phi_{18}} + 4\eta_{\Phi_{20}} \\
&+ \frac{1}{2}\eta_{\Phi_{21}} + 6\eta_{\Phi_{23}} + \frac{3}{2}\eta_{\Phi_{25}} + 4\eta_{\Phi_{27}} + \eta_{\Phi_{28}} + 4\eta_{\Phi_{30}} + 3\eta_{\Phi_{31}} + \eta_{\Phi_{33}} + 12\eta_{\Phi_{35}} \\
&+ 3\eta_{\Phi_{37}} + 8\eta_{\Phi_{39}} + 3\eta_{\Phi_{42}} + 24\eta_{\Phi_{43}} + 8\eta_{\Phi_{45}} + \frac{3}{2}\eta_{\Phi_{48}} + \frac{3}{2}\eta_{\Phi_{51}} + 2\eta_{\Phi_{52}} ,
\end{aligned}$$

$$\begin{aligned}
\lambda_{1Y} = 8 &- 21\left(\frac{8}{5}\eta_{PSV} + \frac{6}{5}\eta_{W_R}\right) + \frac{3}{10}\eta_{\Phi_1} + \frac{1}{5}\eta_{\Phi_2} + \frac{1}{5}\eta_{\Phi_3} + \frac{3}{10}\eta_{\Phi_4} + \frac{1}{5}\eta_{\Phi_5} + \frac{3}{10}\eta_{\Phi_6} \\
&+ \frac{1}{5}\eta_{\Phi_7} + \frac{3}{5}\eta_{\Phi_8} + \frac{4}{5}\eta_{\Phi_9} + \frac{1}{10}\eta_{\Phi_{10}} + \frac{3}{5}\eta_{\Phi_{11}} + \frac{4}{5}\eta_{\Phi_{12}} + \frac{1}{10}\eta_{\Phi_{13}} + \frac{3}{10}\eta_{\Phi_{14}} + \frac{1}{5}\eta_{\Phi_{15}} \\
&+ \frac{3}{5}\eta_{\Phi_{16}} + \frac{16}{5}\eta_{\Phi_{17}} + \frac{49}{10}\eta_{\Phi_{18}} + \frac{2}{5}\eta_{\Phi_{19}} + \frac{12}{5}\eta_{\Phi_{20}} + \frac{3}{10}\eta_{\Phi_{21}} + \frac{1}{5}\eta_{\Phi_{22}} + \frac{3}{5}\eta_{\Phi_{23}} + \frac{16}{5}\eta_{\Phi_{24}} \\
&+ \frac{49}{10}\eta_{\Phi_{25}} + \frac{2}{5}\eta_{\Phi_{26}} + \frac{12}{5}\eta_{\Phi_{27}} + \frac{3}{5}\eta_{\Phi_{28}} + \frac{2}{5}\eta_{\Phi_{29}} + \frac{18}{5}\eta_{\Phi_{30}} + \frac{1}{5}\eta_{\Phi_{31}} + \frac{16}{5}\eta_{\Phi_{32}} + \frac{3}{5}\eta_{\Phi_{33}} \\
&+ \frac{2}{5}\eta_{\Phi_{34}} + \frac{6}{5}\eta_{\Phi_{35}} + \frac{32}{5}\eta_{\Phi_{36}} + \frac{49}{5}\eta_{\Phi_{37}} + \frac{4}{5}\eta_{\Phi_{38}} + \frac{24}{5}\eta_{\Phi_{39}} + \frac{24}{5}\eta_{\Phi_{40}} + \frac{2}{5}\eta_{\Phi_{41}} + \frac{49}{5}\eta_{\Phi_{42}} \\
&+ \frac{12}{5}\eta_{\Phi_{43}} + \frac{64}{5}\eta_{\Phi_{44}} + \frac{24}{5}\eta_{\Phi_{45}} + \frac{3}{5}\eta_{\Phi_{46}} + \frac{4}{5}\eta_{\Phi_{47}} + \frac{1}{10}\eta_{\Phi_{48}} + \frac{3}{5}\eta_{\Phi_{49}} + \frac{4}{5}\eta_{\Phi_{50}} + \frac{1}{10}\eta_{\Phi_{51}} .
\end{aligned}$$

Here, PSV denotes the Pati-Salam gauge bosons in the $(\overline{3}, 1, -4)$ and W_R the right-handed $W_R^{\pm}$ in the $(1, 1, -6)$.

$SO(10)$	$SU(5)$	${}_C\mathbf{2}_L\mathbf{1}_Y$	Label
10	5	$(1, 2, 3)$	Φ_1
		$(3, 1, -2)$	Φ_2
	$\overline{5}$	$(1, 2, -3)$	H
		$(\overline{3}, 1, 2)$	Φ_3

Table A.2.: *Decomposition of the scalar* 10 *representation of* $SO(10)$ *with respect to the subgroups* $SU(5)$ *and* $SU(3)_C \times SU(2)_L \times U(1)_Y$. *For further details, see Table A.1.*

$SO(10)$	$SU(5)$	$3_C 2_L 1_Y$	Label
45	1	$(1,1,0)$	s_1
	10	$(1,1,6)$	Φ_4
		$(\overline{3},1,-4)$	Φ_5
		$(3,2,1)$	Φ_6
	$\overline{10}$	$(1,1,-6)$	Φ_7
		$(3,1,4)$	Φ_8
		$(\overline{3},2,-1)$	Φ_9
	24	$(1,1,0)$	s_2
		$(1,3,0)$	Φ_{10}
		$(3,2,-5)$	ξ_1
		$(\overline{3},2,5)$	ξ_2
		$(8,1,0)$	Φ_{11}

Table A.3.: *Decomposition of the scalar* 45 *representation of* $SO(10)$ *with respect to the subgroups* $SU(5)$ *and* $SU(3)_C \times SU(2)_L \times U(1)_Y$. *For further details, see Table A.1.*

$SO(10)$	$SU(5)$	$3_C 2_L 1_Y$	Label
120	5	$(1,2,3)$	Φ_{12}
		$(3,1,-2)$	Φ_{13}
	$\overline{5}$	$(1,2,-3)$	Φ_{14}
		$(\overline{3},1,2)$	Φ_{15}
	10	$(1,1,6)$	Φ_{16}
		$(\overline{3},1,-4)$	Φ_{17}
		$(3,2,1)$	Φ_{18}
	$\overline{10}$	$(1,1,-6)$	Φ_{19}
		$(3,1,4)$	Φ_{20}
		$(\overline{3},2,-1)$	Φ_{21}
	45	$(1,2,3)$	Φ_{22}
		$(3,1,-2)$	Φ_{23}
		$(3,3,-2)$	Φ_{24}
		$(\overline{3},1,8)$	Φ_{25}
		$(\overline{3},2,-7)$	Φ_{26}
		$(\overline{6},1,-2)$	Φ_{27}
		$(8,2,3)$	Φ_{28}
	$\overline{45}$	$(1,2,-3)$	Φ_{29}
		$(\overline{3},1,2)$	Φ_{30}
		$(\overline{3},3,2)$	Φ_{31}
		$(3,1,-8)$	Φ_{32}
		$(3,2,7)$	Φ_{33}
		$(6,1,2)$	Φ_{34}
		$(8,2,-3)$	Φ_{35}

Table A.4.: *Decomposition of the scalar* 120 *representation of* $SO(10)$ *with respect to the subgroups* $SU(5)$ *and* $SU(3)_C \times SU(2)_L \times U(1)_Y$. *For further details, see Table A.1.*

$SO(10)$	$SU(5)$	$3_C 2_L 1_Y$	Label
$\overline{126}$	1	$(1,1,0)$	s_3
	5	$(1,2,3)$	Φ_{36}
		$(3,1,-2)$	Φ_{37}
	$\overline{10}$	$(1,1,-6)$	ξ_3
		$(3,1,4)$	ξ_4
		$(\overline{3},2,-1)$	ξ_5
	15	$(1,3,6)$	Φ_{38}
		$(3,2,1)$	Φ_{39}
		$(6,1,-4)$	Φ_{40}
	$\overline{45}$	$(1,2,-3)$	Φ_{41}
		$(\overline{3},1,2)$	Φ_{42}
		$(\overline{3},3,2)$	Φ_{43}
		$(3,1,-8)$	Φ_{44}
		$(3,2,7)$	Φ_{45}
		$(6,1,2)$	Φ_{46}
		$(8,2,-3)$	Φ_{47}
	50	$(1,1,-12)$	Φ_{48}
		$(3,1,-2)$	Φ_{49}
		$(\overline{3},2,-7)$	Φ_{50}
		$(\overline{6},3,-2)$	Φ_{51}
		$(6,1,8)$	Φ_{52}
		$(8,2,3)$	Φ_{53}

Table A.5.: *Decomposition of the scalar $\overline{126}$ representation of $SO(10)$ with respect to the subgroups $SU(5)$ and $SU(3)_C \times SU(2)_L \times U(1)_Y$. For further details, see Table A.1.*

A.3. E_6

The threshold corrections in conservative E_6 GUTs can be calculated using Eq. (2.9) and read

$$\begin{aligned}
\lambda_{3C} = 9 &- 21\left(\eta_{PSV} + \eta_{E_2} + \eta_{E_4}\right) + \eta_{\Sigma_2} + \eta_{\Sigma_3} + \eta_{\Sigma_5} + \eta_{\Sigma_7} + 2\eta_{\Sigma_8} + \eta_{\Sigma_{10}} + \eta_{\Sigma_{12}} + \eta_{\Sigma_{14}} \\
&+ \eta_{\Sigma_{16}} + 2\eta_{\Sigma_{17}} + \eta_{\Sigma_{19}} + \eta_{\Sigma_{21}} + 2\eta_{\Sigma_{22}} + \eta_{\Sigma_{24}} + 2\eta_{\Sigma_{25}} + \eta_{\Sigma_{27}} + 2\eta_{\Sigma_{28}} + 6\eta_{\Sigma_{30}} + \eta_{\Sigma_{32}} \\
&+ \eta_{\Sigma_{34}} + \eta_{\Sigma_{36}} + 2\eta_{\Sigma_{37}} + \eta_{\Sigma_{39}} + 2\eta_{\Sigma_{40}} + \eta_{\Sigma_{42}} + 3\eta_{\Sigma_{43}} + \eta_{\Sigma_{44}} + 2\eta_{\Sigma_{45}} + 5\eta_{\Sigma_{46}} + 12\eta_{\Sigma_{47}} \\
&+ \eta_{\Sigma_{49}} + 3\eta_{\Sigma_{50}} + \eta_{\Sigma_{51}} + 2\eta_{\Sigma_{52}} + 5\eta_{\Sigma_{53}} + 12\eta_{\Sigma_{54}} + \eta_{\Sigma_{56}} + \eta_{\Sigma_{58}} + \eta_{\Sigma_{60}} + 2\eta_{\Sigma_{61}} + 2\eta_{\Sigma_{63}} \\
&+ 5\eta_{\Sigma_{64}} + 2\eta_{\Sigma_{66}} + 2\eta_{\Sigma_{67}} + 6\eta_{\Sigma_{68}} + 2\eta_{\Sigma_{70}} + \eta_{\Sigma_{71}} + 3\eta_{\Sigma_{72}} + 6\eta_{\Sigma_{73}} + 10\eta_{\Sigma_{74}} + \eta_{\Sigma_{76}} \\
&+ 3\eta_{\Sigma_{77}} + \eta_{\Sigma_{78}} + 2\eta_{\Sigma_{79}} + 5\eta_{\Sigma_{80}} + 12\eta_{\Sigma_{81}} + \eta_{\Sigma_{83}} + \eta_{\Sigma_{85}} + 2\eta_{\Sigma_{87}} + 5\eta_{\Sigma_{88}} + 2\eta_{\Sigma_{90}} + 5\eta_{\Sigma_{91}} \\
&+ 2\eta_{\Sigma_{93}} + 2\eta_{\Sigma_{94}} + 6\eta_{\Sigma_{95}} + \eta_{\Sigma_{97}} + 2\eta_{\Sigma_{99}} + 5\eta_{\Sigma_{100}} + \eta_{\Sigma_{102}} + 3\eta_{\Sigma_{103}} + \eta_{\Sigma_{104}} + 2\eta_{\Sigma_{105}} \\
&+ 5\eta_{\Sigma_{106}} + 12\eta_{\Sigma_{107}} + \eta_{\Sigma_{109}} + 2\eta_{\Sigma_{110}} + 15\eta_{\Sigma_{111}} + 5\eta_{\Sigma_{112}} + 12\eta_{\Sigma_{113}} + \eta_{\Sigma_{115}} + \eta_{\Sigma_{117}} + \eta_{\Sigma_{119}} \\
&+ 2\eta_{\Sigma_{120}} + 2\eta_{\Sigma_{122}} + 5\eta_{\Sigma_{123}} + 2\eta_{\Sigma_{125}} + 2\eta_{\Sigma_{126}} + 6\eta_{\Sigma_{127}} + 2\eta_{\Sigma_{129}} + \eta_{\Sigma_{130}} + 3\eta_{\Sigma_{131}} + 6\eta_{\Sigma_{132}} \\
&+ 10\eta_{\Sigma_{133}} + \eta_{\Sigma_{135}} + 3\eta_{\Sigma_{136}} + \eta_{\Sigma_{137}} + 2\eta_{\Sigma_{138}} + 5\eta_{\Sigma_{139}} + 12\eta_{\Sigma_{140}} + 8\left(\eta_{D_1} + \eta_{D_2} + \eta_{D_3}\right) ,
\end{aligned}$$

$$\begin{aligned}
\lambda_{2L} = 10 &- 21\eta_{E_1} + \eta_{\Sigma_1} + \eta_{\Sigma_4} + 3\eta_{\Sigma_8} + \eta_{\Sigma_9} + \eta_{\Sigma_{11}} + \eta_{\Sigma_{13}} + 3\eta_{\Sigma_{17}} + \eta_{\Sigma_{18}} + 3\eta_{\Sigma_{22}} + 3\eta_{\Sigma_{25}} \\
&+ 3\eta_{\Sigma_{28}} + 4\eta_{\Sigma_{29}} + \eta_{\Sigma_{31}} + \eta_{\Sigma_{33}} + 3\eta_{\Sigma_{37}} + 3\eta_{\Sigma_{40}} + \eta_{\Sigma_{41}} + 12\eta_{\Sigma_{43}} + 3\eta_{\Sigma_{45}} + 8\eta_{\Sigma_{47}} + \eta_{\Sigma_{48}} \\
&+ 12\eta_{\Sigma_{50}} + 3\eta_{\Sigma_{52}} + 8\eta_{\Sigma_{54}} + \eta_{\Sigma_{55}} + \eta_{\Sigma_{57}} + 3\eta_{\Sigma_{61}} + 4\eta_{\Sigma_{62}} + 3\eta_{\Sigma_{63}} + 4\eta_{\Sigma_{65}} + 3\eta_{\Sigma_{66}} \\
&+ 3\eta_{\Sigma_{67}} + \eta_{\Sigma_{69}} + 3\eta_{\Sigma_{70}} + 12\eta_{\Sigma_{72}} + 6\eta_{\Sigma_{74}} + \eta_{\Sigma_{75}} + 12\eta_{\Sigma_{77}} + 3\eta_{\Sigma_{79}} + 8\eta_{\Sigma_{81}} + \eta_{\Sigma_{82}} \\
&+ \eta_{\Sigma_{84}} + 4\eta_{\Sigma_{86}} + 3\eta_{\Sigma_{87}} + 4\eta_{\Sigma_{89}} + 3\eta_{\Sigma_{90}} + 4\eta_{\Sigma_{92}} + 3\eta_{\Sigma_{93}} + 3\eta_{\Sigma_{94}} + \eta_{\Sigma_{96}} + 4\eta_{\Sigma_{98}} \\
&+ 3\eta_{\Sigma_{99}} + \eta_{\Sigma_{101}} + 12\eta_{\Sigma_{103}} + 3\eta_{\Sigma_{105}} + 8\eta_{\Sigma_{107}} + 3\eta_{\Sigma_{110}} + 24\eta_{\Sigma_{111}} + 8\eta_{\Sigma_{113}} + \eta_{\Sigma_{114}} \\
&+ \eta_{\Sigma_{116}} + 3\eta_{\Sigma_{120}} + 4\eta_{\Sigma_{121}} + 3\eta_{\Sigma_{122}} + 4\eta_{\Sigma_{124}} + 3\eta_{\Sigma_{125}} + 3\eta_{\Sigma_{126}} + \eta_{\Sigma_{128}} + 3\eta_{\Sigma_{129}} \\
&+ 12\eta_{\Sigma_{131}} + 6\eta_{\Sigma_{133}} + \eta_{\Sigma_{134}} + 12\eta_{\Sigma_{136}} + 3\eta_{\Sigma_{138}} + 8\eta_{\Sigma_{140}} + 8\left(\eta_{L_1} + \eta_{L_2} + \eta_{L_3}\right) ,
\end{aligned}$$

$$
\begin{aligned}
\lambda_{1Y} = 12 - 21(&\frac{6}{5}\eta_{W_R} + \frac{8}{5}\eta_{PSV} + \frac{3}{5}\eta_{E_1} + \frac{2}{5}\eta_{E_2} + \frac{6}{5}\eta_{E_3} + \frac{8}{5}\eta_{E_4}) + \frac{3}{5}\eta_{\Sigma_1} + \frac{2}{5}\eta_{\Sigma_2} + \frac{2}{5}\eta_{\Sigma_3} \\
&+ \frac{3}{5}\eta_{\Sigma_4} + \frac{2}{5}\eta_{\Sigma_5} + \frac{6}{5}\eta_{\Sigma_6} + \frac{8}{5}\eta_{\Sigma_7} + \frac{1}{5}\eta_{\Sigma_8} + \frac{3}{5}\eta_{\Sigma_9} + \frac{2}{5}\eta_{\Sigma_{10}} + \frac{3}{5}\eta_{\Sigma_{11}} + \frac{2}{5}\eta_{\Sigma_{12}} + \frac{3}{5}\eta_{\Sigma_{13}} \\
&+ \frac{2}{5}\eta_{\Sigma_{14}} + \frac{6}{5}\eta_{\Sigma_{15}} + \frac{8}{5}\eta_{\Sigma_{16}} + \frac{1}{5}\eta_{\Sigma_{17}} + \frac{3}{5}\eta_{\Sigma_{18}} + \frac{2}{5}\eta_{\Sigma_{19}} + \frac{6}{5}\eta_{\Sigma_{20}} + \frac{8}{5}\eta_{\Sigma_{21}} + \frac{1}{5}\eta_{\Sigma_{22}} + \frac{6}{5}\eta_{\Sigma_{23}} \\
&+ \frac{8}{5}\eta_{\Sigma_{24}} + \frac{1}{5}\eta_{\Sigma_{25}} + \frac{6}{5}\eta_{\Sigma_{26}} + \frac{8}{5}\eta_{\Sigma_{27}} + \frac{1}{5}\eta_{\Sigma_{28}} + \frac{3}{5}\eta_{\Sigma_{31}} + \frac{2}{5}\eta_{\Sigma_{32}} + \frac{3}{5}\eta_{\Sigma_{33}} + \frac{2}{5}\eta_{\Sigma_{34}} + \frac{6}{5}\eta_{\Sigma_{35}} \\
&+ \frac{8}{5}\eta_{\Sigma_{36}} + \frac{1}{5}\eta_{\Sigma_{37}} + \frac{6}{5}\eta_{\Sigma_{38}} + \frac{8}{5}\eta_{\Sigma_{39}} + \frac{1}{5}\eta_{\Sigma_{40}} + \frac{3}{5}\eta_{\Sigma_{41}} + \frac{2}{5}\eta_{\Sigma_{42}} + \frac{6}{5}\eta_{\Sigma_{43}} + \frac{32}{5}\eta_{\Sigma_{44}} \\
&+ \frac{49}{5}\eta_{\Sigma_{45}} + \frac{4}{5}\eta_{\Sigma_{46}} + \frac{24}{5}\eta_{\Sigma_{47}} + \frac{3}{5}\eta_{\Sigma_{48}} + \frac{2}{5}\eta_{\Sigma_{49}} + \frac{6}{5}\eta_{\Sigma_{50}} + \frac{32}{5}\eta_{\Sigma_{51}} + \frac{49}{5}\eta_{\Sigma_{52}} + \frac{4}{5}\eta_{\Sigma_{53}} \\
&+ \frac{24}{5}\eta_{\Sigma_{54}} + \frac{3}{5}\eta_{\Sigma_{55}} + \frac{2}{5}\eta_{\Sigma_{56}} + \frac{3}{5}\eta_{\Sigma_{57}} + \frac{2}{5}\eta_{\Sigma_{58}} + \frac{6}{5}\eta_{\Sigma_{59}} + \frac{8}{5}\eta_{\Sigma_{60}} + \frac{1}{5}\eta_{\Sigma_{61}} + \frac{18}{5}\eta_{\Sigma_{62}} \\
&+ \frac{1}{5}\eta_{\Sigma_{63}} + \frac{16}{5}\eta_{\Sigma_{64}} + 5\eta_{\Sigma_{66}} + 5\eta_{\Sigma_{67}} + \frac{27}{5}\eta_{\Sigma_{69}} + \frac{1}{5}\eta_{\Sigma_{70}} + \frac{8}{5}\eta_{\Sigma_{71}} + \frac{24}{5}\eta_{\Sigma_{72}} + \frac{48}{5}\eta_{\Sigma_{73}} \\
&+ \frac{2}{5}\eta_{\Sigma_{74}} + \frac{3}{5}\eta_{\Sigma_{75}} + \frac{2}{5}\eta_{\Sigma_{76}} + \frac{6}{5}\eta_{\Sigma_{77}} + \frac{32}{5}\eta_{\Sigma_{78}} + \frac{49}{5}\eta_{\Sigma_{79}} + \frac{4}{5}\eta_{\Sigma_{80}} + \frac{24}{5}\eta_{\Sigma_{81}} + \frac{3}{5}\eta_{\Sigma_{82}} \\
&+ \frac{2}{5}\eta_{\Sigma_{83}} + \frac{3}{5}\eta_{\Sigma_{84}} + \frac{2}{5}\eta_{\Sigma_{85}} + \frac{18}{5}\eta_{\Sigma_{86}} + \frac{1}{5}\eta_{\Sigma_{87}} + \frac{16}{5}\eta_{\Sigma_{88}} + \frac{18}{5}\eta_{\Sigma_{89}} + \frac{1}{5}\eta_{\Sigma_{90}} + \frac{16}{5}\eta_{\Sigma_{91}} \\
&+ 5\eta_{\Sigma_{93}} + 5\eta_{\Sigma_{94}} + \frac{3}{5}\eta_{\Sigma_{96}} + \frac{2}{5}\eta_{\Sigma_{97}} + \frac{18}{5}\eta_{\Sigma_{98}} + \frac{1}{5}\eta_{\Sigma_{99}} + \frac{16}{5}\eta_{\Sigma_{100}} + \frac{3}{5}\eta_{\Sigma_{101}} + \frac{2}{5}\eta_{\Sigma_{102}} \\
&+ \frac{6}{5}\eta_{\Sigma_{103}} + \frac{32}{5}\eta_{\Sigma_{104}} + \frac{49}{5}\eta_{\Sigma_{105}} + \frac{4}{5}\eta_{\Sigma_{106}} + \frac{24}{5}\eta_{\Sigma_{107}} + \frac{24}{5}\eta_{\Sigma_{108}} + \frac{2}{5}\eta_{\Sigma_{109}} + \frac{49}{5}\eta_{\Sigma_{110}} \\
&+ \frac{12}{5}\eta_{\Sigma_{111}} + \frac{64}{5}\eta_{\Sigma_{112}} + \frac{24}{5}\eta_{\Sigma_{113}} + \frac{3}{5}\eta_{\Sigma_{114}} + \frac{2}{5}\eta_{\Sigma_{115}} + \frac{3}{5}\eta_{\Sigma_{116}} + \frac{2}{5}\eta_{\Sigma_{117}} + \frac{6}{5}\eta_{\Sigma_{118}} \\
&+ \frac{8}{5}\eta_{\Sigma_{119}} + \frac{1}{5}\eta_{\Sigma_{120}} + \frac{18}{5}\eta_{\Sigma_{121}} + \frac{1}{5}\eta_{\Sigma_{122}} + \frac{16}{5}\eta_{\Sigma_{123}} + 5\eta_{\Sigma_{125}} + 5\eta_{\Sigma_{126}} + \frac{27}{5}\eta_{\Sigma_{128}} + \frac{1}{5}\eta_{\Sigma_{129}} \\
&+ \frac{8}{5}\eta_{\Sigma_{130}} + \frac{24}{5}\eta_{\Sigma_{131}} + \frac{48}{5}\eta_{\Sigma_{132}} + \frac{2}{5}\eta_{\Sigma_{133}} + \frac{3}{5}\eta_{\Sigma_{134}} + \frac{2}{5}\eta_{\Sigma_{135}} + \frac{6}{5}\eta_{\Sigma_{136}} + \frac{32}{5}\eta_{\Sigma_{137}} \\
&+ \frac{49}{5}\eta_{\Sigma_{138}} + \frac{4}{5}\eta_{\Sigma_{139}} + \frac{24}{5}\eta_{\Sigma_{140}} + 8\left(\frac{2}{5}\eta_{D_1} + \frac{3}{5}\eta_{L_1} + \frac{2}{5}\eta_{D_2} + \frac{3}{5}\eta_{L_2} + \frac{2}{5}\eta_{D_3} + \frac{3}{5}\eta_{L_3}\right) .
\end{aligned}
$$

The subscript PSV denotes the Pati-Salam gauge bosons in the $(\overline{3}, 1, -4)$ and W_R denotes the right-handed $W_R^{\pm}$ in the $(1, 1, -6)$. Moreover, E_i denotes additional E_6 gauge bosons in the $(1, 2, -3)$, $(\overline{3}, 1, 2)$, $(1, 1, 6)$, $(\overline{3}, 1, -4)$ respectively. The subscripts D_i and L_i possible corrections from vector-like quarks and leptons.

E_6	$SO(10)$	$SU(5)$	${}^3{}_C 2_L 1_Y$	Label
27	1	1	$(1, 1, 0)$	s_1
	10	5	$(1, 2, 3)$	Σ_1
			$(3, 1, -2)$	Σ_2
		$\overline{5}$	$(1, 2, -3)$	H
			$(\overline{3}, 1, 2)$	Σ_3
	16	1	$(1, 1, 0)$	s_2
		$\overline{5}$	$(1, 2, -3)$	Σ_4
			$(\overline{3}, 1, 2)$	Σ_5
		10	$(1, 1, 6)$	Σ_6
			$(\overline{3}, 1, -4)$	Σ_7
			$(3, 2, 1)$	Σ_8

Table A.6.: *Decomposition of the scalar 27-dimensional representation of E_6 with respect to the subgroups $SO(10)$, $SU(5)$ and $SU(3)_C \times SU(2)_L \times U(1)_Y$. For further details, see Table A.1.*

E_6	$SO(10)$	$SU(5)$	$3_C 2_L 1_Y$	A_{23}/r_I	A_{12}/r_I
27	1	1	$(1,1,0)$	0	0
	10	5	$(1,2,3)$	$1/3$	$-2/15$
			$(3,1,-2)$	$-1/3$	$2/15$
		$\overline{5}$	$(1,2,-3)$	$1/3$	$-2/15$
			$(\overline{3},1,2)$	$-1/3$	$2/15$

Table A.7.: *Contributions of the exotic fermions in the fundamental 27-dimensional representation of E_6 to the ratio A_{23}/A_{12}.*

E_6	$SO(10)$	$SU(5)$	${}^3{}_C 2_L 1_Y$	Label
351	10	5	$(1,2,3)$	Σ_9
			$(3,1,-2)$	Σ_{10}
		$\overline{5}$	$(1,2,-3)$	Σ_{11}
			$(\overline{3},1,2)$	Σ_{12}
	16	1	$(1,1,0)$	s_3
		$\overline{5}$	$(1,2,-3)$	Σ_{13}
			$(\overline{3},1,2)$	Σ_{14}
		10	$(1,1,6)$	Σ_{15}
			$(\overline{3},1,-4)$	Σ_{16}
			$(3,2,1)$	Σ_{17}
	$\overline{16}$	1	$(1,1,0)$	s_4
		5	$(1,2,3)$	Σ_{18}
			$(3,1,-2)$	Σ_{19}
		$\overline{10}$	$(1,1,-6)$	Σ_{20}
			$(3,1,4)$	Σ_{21}
			$(\overline{3},2,-1)$	Σ_{22}
	45	1	$(1,1,0)$	s_5
		10	$(1,1,6)$	Σ_{23}
			$(\overline{3},1,-4)$	Σ_{24}
			$(3,2,1)$	Σ_{25}
		$\overline{10}$	$(1,1,-6)$	Σ_{26}
			$(3,1,4)$	Σ_{27}
			$(\overline{3},2,-1)$	Σ_{28}
		24	$(1,1,0)$	s_6
			$(1,3,0)$	Σ_{29}
			$(3,2,-5)$	ξ_1
			$(\overline{3},2,5)$	ξ_2
			$(8,1,0)$	Σ_{30}
	120	5	$(1,2,3)$	Σ_{31}
			$(3,1,-2)$	Σ_{32}
		$\overline{5}$	$(1,2,-3)$	Σ_{33}
			$(\overline{3},1,2)$	Σ_{34}
		10	$(1,1,6)$	Σ_{35}
			$(\overline{3},1,-4)$	Σ_{36}
			$(3,2,1)$	Σ_{37}
		$\overline{10}$	$(1,1,-6)$	Σ_{38}
			$(3,1,4)$	Σ_{39}
			$(\overline{3},2,-1)$	Σ_{40}
		45	$(1,2,3)$	Σ_{41}
			$(3,1,-2)$	Σ_{42}
			$(3,3,-2)$	Σ_{43}
			$(\overline{3},1,8)$	Σ_{44}
			$(\overline{3},2,-7)$	Σ_{45}
			$(\overline{6},1,-2)$	Σ_{46}
			$(8,2,3)$	Σ_{47}
		$\overline{45}$	$(1,2,-3)$	Σ_{48}
			$(\overline{3},1,2)$	Σ_{49}
			$(\overline{3},3,2)$	Σ_{50}
			$(3,1,-8)$	Σ_{51}
			$(3,2,7)$	Σ_{52}
			$(6,1,2)$	Σ_{53}
			$(8,2,-3)$	Σ_{54}
	144	5	$(1,2,3)$	Σ_{55}
			$(3,1,-2)$	Σ_{56}
		$\overline{5}$	$(1,2,-3)$	Σ_{57}
			$(\overline{3},1,2)$	Σ_{58}
		10	$(1,1,6)$	Σ_{59}
			$(\overline{3},1,-4)$	Σ_{60}
			$(3,2,1)$	Σ_{61}
		15	$(1,3,6)$	Σ_{62}
			$(3,2,1)$	Σ_{63}
			$(6,1,-4)$	Σ_{64}
		24	$(1,1,0)$	s_7
			$(1,3,0)$	Σ_{65}
			$(3,2,-5)$	Σ_{66}
			$(\overline{3},2,5)$	Σ_{67}
			$(8,1,0)$	Σ_{68}
		40	$(1,2,-9)$	Σ_{69}
			$(3,2,1)$	Σ_{70}
			$(\overline{3},1,-4)$	Σ_{71}
			$(\overline{3},3,-4)$	Σ_{72}
			$(8,1,6)$	Σ_{73}
			$(\overline{6},2,1)$	Σ_{74}
		$\overline{45}$	$(1,2,-3)$	Σ_{75}
			$(\overline{3},1,2)$	Σ_{76}
			$(\overline{3},3,2)$	Σ_{77}
			$(3,1,-8)$	Σ_{78}
			$(3,2,7)$	Σ_{79}
			$(6,1,2)$	Σ_{80}
			$(8,2,-3)$	Σ_{81}

Table A.8.: *Decomposition of the* 351 *representation of* E_6 *with respect to the subgroups* $SO(10)$, $SU(5)$ *and* $SU(3)_C \times SU(2)_L \times U(1)_Y$. *For further details, see Table A.1.*

E_6	$SO(10)$	$SU(5)$	$^3{}_C{}^2{}_L{}^1{}_Y$	Label
$351'$	1	1	$(1,1,0)$	s_8
	10	5	$(1,2,3)$	Σ_{82}
			$(3,1,-2)$	Σ_{83}
		$\overline{5}$	$(1,2,-3)$	Σ_{84}
			$(\overline{3},1,2)$	Σ_{85}
	$\overline{16}$	1	$(1,1,0)$	s_9
		5	$(1,2,3)$	ξ_3
			$(3,1,-2)$	ξ_4
		$\overline{10}$	$(1,1,-6)$	ξ_5
			$(3,1,4)$	ξ_6
			$(\overline{3},2,-1)$	ξ_7
	54	15	$(1,3,6)$	Σ_{86}
			$(3,2,1)$	Σ_{87}
			$(6,1,-4)$	Σ_{88}
		$\overline{15}$	$(1,3,-6)$	Σ_{89}
			$(\overline{3},2,-1)$	Σ_{90}
			$(\overline{6},1,4)$	Σ_{91}
		$\overline{24}$	$(1,1,0)$	s_{10}
			$(1,3,0)$	Σ_{92}
			$(3,2,-5)$	Σ_{93}
			$(\overline{3},2,5)$	Σ_{94}
			$(8,1,0)$	Σ_{95}
	$\overline{126}$	1	$(1,1,0)$	s_{11}
		5	$(1,2,3)$	Σ_{96}
			$(3,1,-2)$	Σ_{97}
		$\overline{10}$	$(1,1,-6)$	ξ_8
			$(3,1,4)$	ξ_9
			$(\overline{3},2,-1)$	ξ_{10}
		15	$(1,3,6)$	Σ_{98}
			$(3,2,1)$	Σ_{99}
			$(6,1,-4)$	Σ_{100}
		45	$(1,2,-3)$	Σ_{101}
			$(\overline{3},1,2)$	Σ_{102}
			$(\overline{3},3,2)$	Σ_{103}
			$(3,1,-8)$	Σ_{104}
			$(3,2,7)$	Σ_{105}
			$(6,1,2)$	Σ_{106}
			$(8,2,-3)$	Σ_{107}
		50	$(1,1,-12)$	Σ_{108}
			$(3,1,-2)$	Σ_{109}
			$(\overline{3},2,-7)$	Σ_{110}
			$(\overline{6},3,-2)$	Σ_{111}
			$(6,1,8)$	Σ_{112}
			$(8,2,3)$	Σ_{113}
	144	5	$(1,2,3)$	Σ_{114}
			$(3,1,-2)$	Σ_{115}
		$\overline{5}$	$(1,2,-3)$	Σ_{116}
			$(\overline{3},1,2)$	Σ_{117}
		10	$(1,1,6)$	Σ_{118}
			$(\overline{3},1,-4)$	Σ_{119}
			$(3,2,1)$	Σ_{120}
		15	$(1,3,6)$	Σ_{121}
			$(3,2,1)$	Σ_{122}
			$(6,1,-4)$	Σ_{123}
		24	$(1,1,0)$	s_{12}
			$(1,3,0)$	Σ_{124}
			$(3,2,-5)$	Σ_{125}
			$(\overline{3},2,5)$	Σ_{126}
			$(8,1,0)$	Σ_{127}
		40	$(1,2,-9)$	Σ_{128}
			$(3,2,1)$	Σ_{129}
			$(\overline{3},1,-4)$	Σ_{130}
			$(\overline{3},3,-4)$	Σ_{131}
			$(8,1,6)$	Σ_{132}
			$(\overline{6},2,1)$	Σ_{133}
		$\overline{45}$	$(1,2,-3)$	Σ_{134}
			$(\overline{3},1,2)$	Σ_{135}
			$(\overline{3},3,2)$	Σ_{136}
			$(3,1,-8)$	Σ_{137}
			$(3,2,7)$	Σ_{138}
			$(6,1,2)$	Σ_{139}
			$(8,2,-3)$	Σ_{140}

Table A.9.: *Decomposition of the $351'$ representation of E_6 with respect to the subgroups $SO(10)$, $SU(5)$ and $SU(3)_C \times SU(2)_L \times U(1)_Y$. For further details, see Table A.1.*

A.4. $SO(10) \to SU(4)_C \times SU(2)_L \times U(1)_R$

The threshold corrections at the $SO(10)$ scale can be calculated using Eq. (2.9) and read

$$\begin{aligned}\lambda_{4C} = 4 &+ 2\eta_{\zeta_1} + 8\eta_{\zeta_4} + 6\eta_{\zeta_7} + 6\eta_{\zeta_8} + 2\eta_{\zeta_9} + 2\eta_{\zeta_{10}} + 2\eta_{\zeta_{11}} + 6\eta_{\zeta_{12}} \\ &+ 16\eta_{\zeta_{13}} + 16\eta_{\zeta_{14}} + 2\eta_{\zeta_{15}} + 18\eta_{\zeta_{16}} + 6\eta_{\zeta_{17}} + 6\eta_{\zeta_{18}} + 16\eta_{\zeta_{19}} ,\end{aligned}$$

$$\lambda_{2L} = 6 + \eta_{\zeta_2} + 4\eta_{\zeta_3} + \eta_{\zeta_5} + \eta_{\zeta_6} + 24\eta_{\zeta_{12}} + 15\eta_{\zeta_{13}} + 15\eta_{\zeta_{14}} + 40\eta_{\zeta_{16}} + 15\eta_{\zeta_{19}} ,$$

$$\lambda_{1R} = 8 + \eta_{\zeta_2} + \eta_{\zeta_5} + \eta_{\zeta_6} + 12\eta_{\zeta_9} + 12\eta_{\zeta_{11}} + 36\eta_{\zeta_{12}} + 15\eta_{\zeta_{13}} + 15\eta_{\zeta_{14}} + 20\eta_{\zeta_{17}} + 15\eta_{\zeta_{19}} .$$

For the corrections at the $SU(4)_C \times SU(2)_L \times U(1)_R$ scale, we find

$$\lambda_{3C} = 1 - 21\,(\eta_{PSV}) + 2\eta_{\zeta_1} + 2\eta_{\zeta_2} + 12\eta_{\zeta_3} + 5\eta_{\zeta_5} ,$$

$$\lambda_{2L} = 3\eta_{\zeta_1} + 3\eta_{\zeta_2} + 8\eta_{\zeta_3} + \eta_{\zeta_4} ,$$

$$\lambda_{1Y} = \frac{8}{5} + \frac{49}{5}\eta_{\zeta_1} + \frac{49}{5}\eta_{\zeta_2} + \frac{24}{5}\eta_{\zeta_3} + \frac{3}{5}\eta_{\zeta_4} + \frac{64}{5}\eta_{\zeta_5} - 21\left(\frac{8}{5}\eta_{PSV} + \frac{6}{5}\eta_{W_R}\right) .$$

As before, PSV denotes the Pati-Salam gauge bosons in the $(\overline{3}, 1, -4)$ and W_R the right-handed $W_R^{\pm}$ in the $(1, 1, -6)$.

A.5. $SO(10) \to SU(3)_C \times SU(2)_L \times SU(2)_R \times U(1)_X$

The threshold corrections at the $SO(10)$ scale can be calculated using Eq. (2.9) and read

$$\begin{aligned}\lambda_{3C} = 5 &- 21\,(4\eta_{LR} + \eta_{PSV}) + \frac{1}{2}\eta_{\zeta_1} + \frac{1}{2}\eta_{\zeta_2} + 3\eta_{\zeta_5} + \frac{1}{2}\eta_{\zeta_8} + \frac{5}{2}\eta_{\zeta_9} + \frac{1}{2}\eta_{\zeta_{11}} \\ &+ \frac{5}{2}\eta_{\zeta_{12}} + \frac{3}{2}\eta_{\zeta_{13}} + \frac{3}{2}\eta_{\zeta_{14}} + \frac{3}{2}\eta_{\zeta_{15}} + \frac{3}{2}\eta_{\zeta_{16}} + 2\eta_{\zeta_{18}} + 2\eta_{\zeta_{19}} + 12\eta_{\zeta_{20}} + \frac{1}{2}\eta_{\zeta_{21}} \\ &+ \frac{1}{2}\eta_{\zeta_{22}} + \frac{3}{2}\eta_{\zeta_{24}} + \frac{15}{2}\eta_{\zeta_{25}} + \frac{3}{2}\eta_{\zeta_{26}} + \frac{15}{2}\eta_{\zeta_{27}} + 2\eta_{\zeta_{28}} + 2\eta_{\zeta_{29}} + 12\eta_{\zeta_{30}} ,\end{aligned}$$

$$\begin{aligned}\lambda_{2L} = 6 &- 21(3\eta_{V_1} + 3\eta_{V_2}) + 2\eta_{\zeta_4} + \eta_{\zeta_6} + 6\eta_{\zeta_{13}} + 6\eta_{\zeta_{14}} + \eta_{\zeta_{17}} + 3\eta_{\zeta_{18}} \\ &+ 3\eta_{\zeta_{19}} + 8\eta_{\zeta_{20}} + 2\eta_{\zeta_{23}} + 6\eta_{\zeta_{24}} + 12\eta_{\zeta_{25}} + 3\eta_{\zeta_{28}} + 3\eta_{\zeta_{29}} + 8\eta_{\zeta_{30}} ,\end{aligned}$$

$$\begin{aligned}\lambda_{2R} = 6 &- 21(3\eta_{V_1} + 3\eta_{V_2}) + 2\eta_{\zeta_3} + \eta_{\zeta_6} + 6\eta_{\zeta_{15}} + 6\eta_{\zeta_{16}} + \eta_{\zeta_{17}} + 3\eta_{\zeta_{18}} \\ &+ 3\eta_{\zeta_{19}} + 8\eta_{\zeta_{20}} + 6\eta_{\zeta_{26}} + 12\eta_{\zeta_{27}} + 3\eta_{\zeta_{28}} + 3\eta_{\zeta_{29}} + 8\eta_{\zeta_{30}} ,\end{aligned}$$

$$\begin{aligned}\lambda_{1X} = 8 - 21(4\eta_{LR} + 4\eta_{PSV}) + \frac{1}{2}\eta_{\zeta_1} + \frac{1}{2}\eta_{\zeta_2} + \frac{3}{2}\eta_{\zeta_7} + \frac{1}{2}\eta_{\zeta_8} + \eta_{\zeta_9} + \frac{3}{2}\eta_{\zeta_{10}} \\ + \frac{1}{2}\eta_{\zeta_{11}} + \eta_{\zeta_{12}} + \frac{3}{2}\eta_{\zeta_{13}} + \frac{3}{2}\eta_{\zeta_{14}} + \frac{3}{2}\eta_{\zeta_{15}} + \frac{3}{2}\eta_{\zeta_{16}} + 8\eta_{\zeta_{18}} + 8\eta_{\zeta_{19}} + \frac{1}{2}\eta_{\zeta_{21}} \\ + \frac{1}{2}\eta_{\zeta_{22}} + \frac{9}{2}\eta_{\zeta_{23}} + \frac{3}{2}\eta_{\zeta_{24}} + 3\eta_{\zeta_{25}} + \frac{3}{2}\eta_{\zeta_{26}} + 3\eta_{\zeta_{27}} + 8\eta_{\zeta_{28}} + 8\eta_{\zeta_{29}} \,.\end{aligned}$$

For the corrections at the $SU(3)_C \times SU(2)_L \times SU(2)_R \times U(1)_X$ scale, we find

$$\begin{aligned}\lambda_{3C} &= 5 \,, \\ \lambda_{2L} &= 6 + \eta_{\zeta_1} + \eta_{\zeta_2} + \eta_{\zeta_3} \,, \\ \lambda_{1Y} &= 8 + \frac{3}{5}\eta_{\zeta_1} + \frac{3}{5}\eta_{\zeta_2} + \frac{3}{5}\eta_{\zeta_3} \,.\end{aligned}$$

The subscript PSV denotes the Pati-Salam gauge bosons in the $(\overline{3}, 1, 1, -4/3)$ representation and LR additional bosons in the $(3, 2, 2, -2/3)$.

$SO(10)$	${}^4C\,{}^2L\,{}^1R$	${}^3C\,{}^2L\,{}^1Y$	Label	Scale
10	$(6,1,0)$		ζ_1	M_{GUT}
	$(1,2,1/2)$		ζ_2	M_{GUT}
	$(1,2,-1/2)$	$(1,2,-3)$	H	M_Z
45	$(1,1,1)$		ξ_1	M_{GUT}
	$(1,1,0)$		s_1	M_{GUT}
	$(1,1,-1)$		ξ_2	M_{GUT}
	$(1,3,0)$		ζ_3	M_{GUT}
	$(6,2,1/2)$		ξ_3	M_{GUT}
	$(6,2,-1/2)$		ξ_4	M_{GUT}
	$(15,1,0)$		ζ_4	M_{GUT}
120	$(1,2,1/2)$		ζ_5	M_{GUT}
	$(1,2,-1/2)$		ζ_6	M_{GUT}
	$(10,1,0)$		ζ_7	M_{GUT}
	$(\overline{10},1,0)$		ζ_8	M_{GUT}
	$(6,3,1)$		ζ_9	M_{GUT}
	$(6,1,1)$		ζ_{10}	M_{GUT}
	$(6,1,0)$		ζ_{11}	M_{GUT}
	$(6,1,-1)$		ζ_{12}	M_{GUT}
	$(15,2,1/2)$		ζ_{13}	M_{GUT}
	$(15,2,-1/2)$		ζ_{14}	M_{GUT}
$\overline{126}$	$(\overline{6},1,0)$		ζ_{15}	M_{GUT}
	$(\overline{10},3,0)$		ζ_{16}	M_{GUT}
	$(10,1,1)$	$(1,1,0)$	s_2	M_I
		$(3,1,4)$	ζ_{17}	M_I
		$(6,1,8)$	ξ_5	M_I
	$(10,1,0)$		ζ_{18}	M_{GUT}
	$(10,1,-1)$		ζ_{19}	M_{GUT}
	$(15,2,1/2)$		ζ_{20}	M_{GUT}
	$(15,2,-1/2)$	$(1,2,-3)$	ζ_{21}	M_I
		$(\overline{3},2,-7)$	ζ_{22}	M_I
		$(3,2,7)$	ζ_{23}	M_I
		$(8,2,-3)$	ζ_{24}	M_I

Table A.10.: *Decomposition of the scalar representations in an $SO(10)$ model with $SU(4)_C \times SU(2)_L \times U(1)_R$ intermediate symmetry. Only relevant decompositions are shown. For further details, see Table A.1.*

$SO(10)$	$^3C\,^2L\,^2R\,^1X$	$^3C\,^2L\,^1Y$	Label	Scale
10	$(3,1,1,-2/3)$		Ω_1	M_U
	$(\overline{3},1,1,2/3)$		Ω_2	M_U
	$(1,2,2,0)$	$(1,2,3)$	Ω_3	M_I
		$(1,2,-3)$	H	M_Z
45	$(1,1,3,0)$		Ω_4	M_U
	$(1,3,1,0)$		Ω_5	M_U
	$(3,2,2,-2/3)$		ξ_1	M_U
	$(\overline{3},2,2,2/3)$		ξ_2	M_U
	$(1,1,1,0)$		s_1	M_U
	$(3,1,1,4/3)$		ξ_3	M_U
	$(\overline{3},1,1,-4/3)$		ξ_4	M_U
	$(8,1,1,0)$		Ω_6	M_U
120	$(1,2,2,0)$		Ω_7	M_U
	$(1,1,1,2)$		Ω_8	M_U
	$(3,1,1,2/3)$		Ω_9	M_U
	$(6,1,1,-2/3)$		Ω_{10}	M_U
	$(1,1,1,-2)$		Ω_{11}	M_U
	$(\overline{3},1,1,-2/3)$		Ω_{12}	M_U
	$(\overline{6},1,1,2/3)$		Ω_{13}	M_U
	$(3,3,1,2/3)$		Ω_{14}	M_U
	$(\overline{3},3,1,-2/3)$		Ω_{15}	M_U
	$(3,1,3,2/3)$		Ω_{16}	M_U
	$(\overline{3},1,3,-2/3)$		Ω_{17}	M_U
	$(1,2,2,0)$		Ω_{18}	M_U
	$(\overline{3},2,2,-4/3)$		Ω_{19}	M_U
	$(3,2,2,4/3)$		Ω_{20}	M_U
	$(8,2,2,0)$		Ω_{21}	M_U
$\overline{126}$	$(3,1,1,-2/3)$		Ω_{22}	M_U
	$(\overline{3},1,1,2/3)$		Ω_{23}	M_U
	$(1,3,1,2)$		Ω_{24}	M_U
	$(\overline{3},3,1,2/3)$		Ω_{25}	M_U
	$(\overline{6},3,1,-2/3)$		Ω_{26}	M_U
	$(1,1,3,-2)$		s_2	M_I
	$(3,1,3,-2/3)$		Ω_{27}	M_U
	$(6,1,3,2/3)$		Ω_{28}	M_U
	$(1,2,2,0)$	$(1,2,3)$	Ω_{29}	M_I
		$(1,2,-3)$	Ω_{30}	M_I
	$(3,2,2,4/3)$		Ω_{31}	M_U
	$(\overline{3},2,2,-4/3)$		Ω_{32}	M_U
	$(8,2,2,0)$		Ω_{33}	M_U

Table A.11.: *Decomposition of the scalar representations in an $SO(10)$ model with $SU(3)_C \times SU(2)_L \times SU(2)_R \times U(1)_X$ intermediate symmetry. Only relevant decompositions are shown. For further details, see Table A.1.*

E_6 Decompositions in the Unified Nelson-Barr Model

B

E_6	$SO(10) \times U(1)_Z$	$SU(5) \times U(1)_X$	$SU(3)_C \times SU(2)_L \times U(1)_Y$
27	16_1	$10_{-1} \equiv t$	$(\overline{3},1)_{-2/3} \oplus (1,1)_1 \oplus (3,2)_{1/6} \equiv u_R^c + e_R^c + Q_L$
27	16_1	$\overline{5}_3 \equiv \overline{f}$	$(1,2)_{-1/2} \oplus (\overline{3},1)_{1/3} \equiv l_L + d_R^c$
27	16_1	$1_{-5} \equiv N$	$(1,1)_0 \equiv \nu_R^c$
27	10_{-2}	$5_2 \equiv F$	$(1,2)_{1/2} \oplus (3,1)_{-1/3} \equiv L_R^c + D_L$
27	10_{-2}	$\overline{5}_{-2} \equiv \overline{F}$	$(1,2)_{-1/2} \oplus (\overline{3},1)_{1/3} \equiv L_L + D_R^c$
27	1_4	$1_0 \equiv N'$	$(1,1)_0 \equiv s$

Table B.1.: *Decomposition of the fermionic* 27 *with respect to all relevant subgroups. The subscripts denote the corresponding* $U(1)$ *charges.*

E_6	$SO(10) \times U(1)_{10}$	$SU(5) \times U(1)_5 \times U(1)_{10}$	$SU(3)_C \times SU(2)_L \times U(1)_Y$
27_F	16_1	$10_{1,1} = t$	q, u, e
		$\overline{5}_{-3,1} = \overline{f}$	d, l
		$1_{5,1}$	N
	10_{-2}	$\overline{5}_{2,-2} = \overline{F}$	D, L
		$5_{-2,-2} = F$	$\overline{D}, \overline{L}$
	1_4	$1_{0,4}$	N'
27_S	16_1	$10_{1,1}$	
		$\overline{5}_{-3,1}$	$h^c_{27,16,\overline{5}}$
		$1_{5,1}$	$s_{27,16,1}$
	10_{-2}	$\overline{5}_{2,-2}$	$h^c_{27,10,\overline{5}}$
		$5_{-2,-2}$	$h_{27,10,5}$
	1_4	$1_{0,4}$	$s_{27,1,1}$
78_S	45_0	$24_{0,0}$	$s_{78,45,24}$
		$\overline{10}_{4,0}$	
		$10_{-4,0}$	
		$1_{0,0}$	$s_{78,45,1}$
	16_{-3}	$10_{1,-3}$	
		$\overline{5}_{-3,-3}$	$h^c_{78,16,\overline{5}}$
		$1_{5,-3}$	$s_{78,16,1}$
	$\overline{16}_3$	$\overline{10}_{-1,3}$	
		$5_{3,3}$	$h_{78,\overline{16},5}$
		$1_{-5,3}$	$s_{78,\overline{16},1}$
	1_0	$1_{0,0}$	$s_{78,1,1}$
$351'_S$	144_1	$\overline{45}_{-3,1}$	$h^c_{351,144,\overline{45}}$
		$40_{1,1}$	
		$24_{5,1}$	$s_{351,144,24}$
		$15_{1,1}$	
		$10_{1,1}$	
		$5_{-7,1}$	$h_{351,144,5}$
		$\overline{5}_{-3,1}$	$h^c_{351,144,\overline{5}}$
	$\overline{126}_{-2}$	$50_{-2,-2}$	
		$\overline{45}_{2,-2}$	$h^c_{351,\overline{126},\overline{45}}$
		$15_{6,-2}$	
		$\overline{10}_{-6,-2}$	
		$5_{-2,-2}$	$h_{351,\overline{126},5}$
		$1_{-10,-2}$	$s_{351,\overline{126},1}$
	54_4	$24_{0,4}$	$s_{351,54,24}$
		$\overline{15}_{4,4}$	
		$15_{-4,4}$	
	$\overline{16}_{-5}$	$\overline{10}_{-1,-5}$	
		$5_{3,-5}$	$h_{351,\overline{16},5}$
		$1_{-5,-5}$	$s_{351,\overline{16},1}$
	10_{-2}	$\overline{5}_{2,-2}$	$h^c_{351,10,\overline{5}}$
		$5_{-2,-2}$	$h_{351,10,5}$
	1_{-8}	$1_{0,-8}$	$s_{351,1,1}$

Table B.2.: *Decomposition of the scalar E_6 representations with respect to all relevant subgroups.*

Acknowledgements

First of all, I want to thank Prof. Ulrich Nierste for supervising my PhD thesis, for his support and invaluable guidance. I'm extremely grateful for the freedom he gave me to explore my own ideas. I'm also thankful to Prof. Thomas Schwetz-Mangold for being the second supervisor of this dissertation.

Special thanks a due to Paul Tremper for countless inspiring discussions and many enjoyable coffee breaks. Moreover, I am very grateful to Robert Ziegler for his patient explanations of many subtle model building aspects and our enjoyable collaboration.

I also want to thank Andreas Pargner and Marcel Köpke for many insightful discussions and lots of fun at various workshops and conferences. Furthermore, I thank all my TTP colleagues. I always appreciated the friendly atmosphere.

Last but not least, I would like to thank my family for their never-ending support.

Bibliography C

[1] M. Gell-Mann. The interpretation of the new particles as displaced charge multiplets. *Il Nuovo Cimento (1955-1965)*, 4(2):848–866, Apr 1956.

[2] Jakob Schwichtenberg. *Physics from Symmetry*. Springer, Cham, Switzerland, 2018.

[3] P. A. M. Dirac. *The principles of quantum mechanics*. Clarendon Press, Oxford England, 1981.

[4] H. Georgi and S. L. Glashow. Unity of All Elementary Particle Forces. *Phys. Rev. Lett.*, 32:438–441, 1974.

[5] Harald Fritzsch and Peter Minkowski. Unified Interactions of Leptons and Hadrons. *Annals Phys.*, 93:193–266, 1975.

[6] F. Gursey, Pierre Ramond, and P. Sikivie. A Universal Gauge Theory Model Based on E6. *Phys. Lett.*, B60:177, 1976.

[7] S. Dimopoulos, S. A. Raby, and Frank Wilczek. Unification of couplings. *Phys. Today*, 44N10:25–33, 1991.

[8] Peter Minkowski. $\mu \to e\gamma$ at a Rate of One Out of 10^9 Muon Decays? *Phys. Lett.*, B67:421–428, 1977.

[9] Rabindra N. Mohapatra and Goran Senjanovic. Neutrino Mass and Spontaneous Parity Violation. *Phys. Rev. Lett.*, 44:912, 1980.

[10] P. Ramond M. Gell-Mann and R. Slansky. Complex spinors and unified theories. *Supergravity, D. Freedman and P. Van Nieuwenhuizen (eds.)*, pages 315–321, 1979.

[11] Tsutomu Yanagida. Horizontal Symmetry and Masses of Neutrinos. *Prog. Theor. Phys.*, 64:1103, 1980.

[12] Dimitri V. Nanopoulos and Steven Weinberg. Mechanisms for Cosmological Baryon Production. *Phys. Rev.*, D20:2484, 1979.

[13] A. D. Sakharov. Violation of CP Invariance, c Asymmetry, and Baryon Asymmetry of the Universe. *Pisma Zh. Eksp. Teor. Fiz.*, 5:32–35, 1967. [Usp. Fiz. Nauk161,61(1991)].

[14] Dimitri V. Nanopoulos. Grand Unified Models. In *In *Les Arcs 1980, Proceedings, Electroweak Interactions and Unified Theories, Vol. 2*, 427-468 and CERN Geneva - TH. 2896 (80,REC.SEP.) 41p*, 1980.

[15] Natalie Wolchover. Grand Unification Dream Kept at Bay. *Quanta Magazine*, 2016.

[16] Paul Langacker. Grand unification and the standard model. In *Proceedings, Tennessee International Symposium on Radiative Corrections*, pages 415–437, 1994.

[17] Luca Di Luzio, Andreas Ringwald, and Carlos Tamarit. Axion mass prediction from minimal grand unification. *Phys. Rev.*, D98(9):095011, 2018.

[18] Paul Langacker. Grand Unified Theories and Proton Decay. *Phys. Rept.*, 72:185, 1981.

[19] K. Abe et al. Search for proton decay via $p \to e^+\pi^0$ and $p \to \mu^+\pi^0$ in 0.31 megaton years exposure of the Super-Kamiokande water Cherenkov detector. *Phys. Rev.*, D95(1):012004, 2017.

[20] J Preskill. Magnetic monopoles. *Annual Review of Nuclear and Particle Science*, 34(1):461–530, 1984.

[21] Gerard 't Hooft. Magnetic Monopoles in Unified Gauge Theories. *Nucl. Phys.*, B79:276–284, 1974. [,291(1974)].

[22] Alexander M. Polyakov. Particle Spectrum in the Quantum Field Theory. *JETP Lett.*, 20:194–195, 1974. [,300(1974)].

[23] Ya. B. Zeldovich and M. Yu. Khlopov. On the Concentration of Relic Magnetic Monopoles in the Universe. *Phys. Lett.*, 79B:239–241, 1978.

[24] John Preskill. Cosmological Production of Superheavy Magnetic Monopoles. *Phys. Rev. Lett.*, 43:1365, 1979.

[25] L. Patrizii and M. Spurio. Status of Searches for Magnetic Monopoles. *Ann. Rev. Nucl. Part. Sci.*, 65:279–302, 2015.

[26] P. Goddard. Magnetic Monopoles in Grand Unified Theories. In *Meeting on Gauge Theories of the Fundamental Interactions London, England, April 29-30, 1981*, pages 87–95, 1981.

[27] Alan H. Guth and S. H. H. Tye. Phase transitions and magnetic monopole production in the very early universe. *Phys. Rev. Lett.*, 44:631–635, Mar 1980.

[28] Paul Langacker and So-Young Pi. Magnetic Monopoles in Grand Unified Theories. *Phys. Rev. Lett.*, 45:1, 1980.

[29] G. Lazarides, M. Magg, and Q. Shafi. Phase transitions and magnetic monopoles in so(10). *Physics Letters B*, 97(1):87 – 92, 1980.

[30] N. G. Deshpande, E. Keith, and Palash B. Pal. Implications of LEP results for

SO(10) grand unification with two intermediate stages. *Phys. Rev.*, D47:2892–2896, 1993.

[31] Stefano Bertolini, Thomas Schwetz, and Michal Malinsky. Fermion masses and mixings in SO(10) models and the neutrino challenge to SUSY GUTs. *Phys. Rev.*, D73:115012, 2006.

[32] R. N. Mohapatra. *Unification and supersymmetry : the frontiers of quark-lepton physics*. Springer, New York, 2003.

[33] Yann Mambrini, Natsumi Nagata, Keith A. Olive, Jeremie Quevillon, and Jiaming Zheng. Dark matter and gauge coupling unification in nonsupersymmetric SO(10) grand unified models. *Phys. Rev.*, D91(9):095010, 2015.

[34] Guido Altarelli and Davide Meloni. A non supersymmetric SO(10) grand unified model for all the physics below M_{GUT}. *JHEP*, 08:021, 2013.

[35] K. S. Babu and S. Khan. Minimal nonsupersymmetric $SO(10)$ model: Gauge coupling unification, proton decay, and fermion masses. *Phys. Rev.*, D92(7):075018, 2015.

[36] Pierre Ramond. The Family Group in Grand Unified Theories. In *International Symposium on Fundamentals of Quantum Theory and Quantum Field Theory Palm Coast, Florida, February 25-March 2, 1979*, pages 265–280, 1979.

[37] Ugo Amaldi, Wim de Boer, and Hermann Furstenau. Comparison of grand unified theories with electroweak and strong coupling constants measured at LEP. *Phys. Lett.*, B260:447–455, 1991.

[38] P. H. Frampton and T. W. Kephart. Exceptionally Simple E_6 Theory. *Phys. Rev.*, D25:1459, 1982.

[39] Jihn E. Kim. Invisible Axion and Neutrino Oscillation in SU(11). *Phys. Rev.*, D24:3007, 1981.

[40] Kyungsik Kang, In-Gyu Koh, and Stephane Ouvry. The Strong CP Problem and Axion Invisibility. *Phys. Lett.*, 119B:361, 1982.

[41] Paul H. Frampton. Simultaneous Solution of Strong CP and Flavor Problems. *Phys. Rev.*, D25:294, 1982.

[42] Anne Ernst. *Axions in the Presence of Gauge Theories Beyond the Standard Model*. PhD thesis, DESY, Hamburg, 2018.

[43] Hai-Yang Cheng. The Strong CP Problem Revisited. *Phys. Rept.*, 158:1, 1988.

[44] Jakob Schwichtenberg. Dark matter in E_6 Grand unification. *JHEP*, 02:016, 2018.

[45] C. S. Lam. Built-in horizontal symmetry of SO(10). *Phys. Rev.*, D89(9):095017, 2014.

[46] Borut Bajc and Alexei Yu. Smirnov. Hidden flavor symmetries of SO(10) GUT. *Nucl. Phys.*, B909:954–979, 2016.

[47] Jakob Schwichtenberg, Paul Tremper, and Robert Ziegler. A grand-unified Nelson–Barr model. *Eur. Phys. J.*, C78(11):910, 2018.

[48] Jakob Schwichtenberg. Gauge Coupling Unification without Supersymmetry. *Eur. Phys. J.*, C79(4):351, 2019.

[49] M. Holder et al. Measurement of the Neutral to Charged Current Cross-Section Ratio in Neutrino and anti-neutrino Interactions. *Phys. Lett.*, B71:222, 1977. [,6.37(1977)].

[50] A. J. Buras, John R. Ellis, M. K. Gaillard, and Dimitri V. Nanopoulos. Aspects of the Grand Unification of Strong, Weak and Electromagnetic Interactions. *Nucl. Phys.*, B135:66–92, 1978.

[51] P. Abreu et al. A Comparison of jet production rates on the Z^0 resonance to perturbative QCD. *Phys. Lett.*, B247:167–176, 1990.

[52] Paul Frampton. *Last Workshop on Grand Unification : University of North Carolina at Chapel Hill, April 20-22, 1989*. World Scientific, Singapore Teaneck, NJ, 1989.

[53] Guido Altarelli. The Higgs: so simple yet so unnatural. *Phys. Scripta*, T158:014011, 2013.

[54] Borut Bajc, Alejandra Melfo, Goran Senjanovic, and Francesco Vissani. Yukawa sector in non-supersymmetric renormalizable SO(10). *Phys. Rev.*, D73:055001, 2006.

[55] Stefano Bertolini, Luca Di Luzio, and Michal Malinsky. On the vacuum of the minimal nonsupersymmetric SO(10) unification. *Phys. Rev.*, D81:035015, 2010.

[56] Anjan S. Joshipura and Ketan M. Patel. Fermion Masses in SO(10) Models. *Phys. Rev.*, D83:095002, 2011.

[57] Franco Buccella, Domenico Falcone, Chee Sheng Fong, Enrico Nardi, and Giulia Ricciardi. Squeezing out predictions with leptogenesis from SO(10). *Phys. Rev.*, D86:035012, 2012.

[58] D. R. T. Jones. The Two Loop beta Function for a G(1) x G(2) Gauge Theory. *Phys. Rev.*, D25:581, 1982.

[59] Florian Lyonnet and Ingo Schienbein. PyR@TE 2: A Python tool for computing RGEs at two-loop. *Comput. Phys. Commun.*, 213:181–196, 2017.

[60] C. Patrignani et al. Review of Particle Physics. *Chin. Phys.*, C40(10):100001, 2016. See the review by K. Nakamura and S.T. Petcov on "Neutrino mass, mixing, and oscillations" therein.

[61] Abdel Perez-Lorenzana and William A. Ponce. GUTs and string GUTs. *Europhys. Lett.*, 49:296–301, 2000.

[62] Renato M. Fonseca. On the chirality of the SM and the fermion content of GUTs. *Nucl. Phys.*, B897:757–780, 2015.

[63] Keith R. Dienes. String theory and the path to unification: A Review of recent developments. *Phys. Rept.*, 287:447–525, 1997.

[64] Frans R. Klinkhamer and G. E. Volovik. Merging gauge coupling constants without grand unification. *Pisma Zh. Eksp. Teor. Fiz.*, 81:683–687, 2005. [JETP Lett.81,551(2005)].

[65] John F. Donoghue and Preema Pais. Gauge federation as an alternative to unification. *Phys. Rev.*, D79:095020, 2009.

[66] H. Georgi. Effective field theory. *Ann. Rev. Nucl. Part. Sci.*, 43:209–252, 1993.

[67] Vijai V. Dixit and Marc Sher. The Futility of High Precision SO(10) Calculations. *Phys. Rev.*, D40:3765, 1989.

[68] R. N. Mohapatra and M. K. Parida. Threshold effects on the mass scale predictions in SO(10) models and solar neutrino puzzle. *Phys. Rev.*, D47:264–272, 1993.

[69] L. Lavoura and L. Wolfenstein. Resuscitation of minimal SO(10) grand unification. *Phys. Rev.*, D48:264–269, 1993.

[70] Lawrence J. Hall. Grand Unification of Effective Gauge Theories. *Nucl. Phys.*, B178:75, 1981.

[71] R. Slansky. Group Theory for Unified Model Building. *Phys. Rept.*, 79:1–128, 1981.

[72] M. K. Parida. Heavy Particle Effects in Grand Unified Theories With Fine Structure Constant Matching. *Phys. Lett.*, B196:163–169, 1987.

[73] C. S. Aulakh and R. N. Mohapatra. Implications of supersymmetric so(10) grand unification. *Phys. Rev. D*, 28:217–227, Jul 1983.

[74] Luca Di Luzio. *Aspects of symmetry breaking in Grand Unified Theories*. PhD thesis, SISSA, Trieste, 2011.

[75] Sebastian A. R. Ellis and James D. Wells. Visualizing gauge unification with high-scale thresholds. *Phys. Rev.*, D91(7):075016, 2015.

[76] Goran Senjanovic. See-saw and grand unification. In *Seesaw mechanism. Proceedings, International Conference, SEESAW25, Paris, France, June 10-11, 2004*, pages 45–64, 2005.

[77] D. Chang, R. N. Mohapatra, J. M. Gipson, R. E. Marshak, and M. K. Parida. Experimental tests of new so(10) grand unification. *Phys. Rev. D*, 31:1718–1732, Apr 1985.

[78] Amit Giveon, Lawrence J. Hall, and Uri Sarid. SU(5) unification revisited. *Phys. Lett.*, B271:138–144, 1991.

[79] Ernest Ma. Efficacious additions to the standard model. *Phys. Lett.*, B625:76–78, 2005.

[80] Natsumi Nagata, Keith A. Olive, and Jiaming Zheng. Weakly-Interacting Massive Particles in Non-supersymmetric SO(10) Grand Unified Models. *JHEP*, 10:193, 2015.

[81] Ilja Dorsner and Pavel Fileviez Perez. Unification versus proton decay in SU(5). *Phys. Lett.*, B642:248–252, 2006.

[82] Rabindra N. Mohapatra and Goran Senjanovic. Higgs Boson Effects in Grand Unified Theories. *Phys. Rev.*, D27:1601, 1983.

[83] L. Michel. Minima of Higgs-Landau Polynomials. In *Marseille Collog.1979:157*, page 157, 1979.

[84] L. O'Raifeartaigh. *Group Structure of Gauge Theories (Cambridge Monographs on Mathematical Physics)*. Cambridge University Press, 1988.

[85] M. Abud, G. Anastaze, P. Eckert, and H. Ruegg. Counter example to Michel's conjecture. *Phys. Lett.*, B142:371–374, 1984.

[86] Stefano Bertolini, Luca Di Luzio, and Michal Malinsky. Intermediate mass scales in the non-supersymmetric SO(10) grand unification: A Reappraisal. *Phys. Rev.*, D80:015013, 2009.

[87] John M. Gipson and R. E. Marshak. Intermediate Mass Scales in the New SO(10) Grand Unification in the One Loop Approximation. *Phys. Rev.*, D31:1705, 1985.

[88] D. Chang, R. N. Mohapatra, J. Gipson, R. E. Marshak, and M. K. Parida. Experimental Tests of New SO(10) Grand Unification. *Phys. Rev.*, D31:1718, 1985.

[89] N. G. Deshpande, E. Keith, and Palash B. Pal. Implications of LEP results for SO(10) grand unification. *Phys. Rev.*, D46:2261–2264, 1993.

[90] Berthold Stech and Zurab Tavartkiladze. Generation symmetry and E6 unification. *Phys. Rev.*, D77:076009, 2008.

[91] Stefano Bertolini, Luca Di Luzio, and Michal Malinsky. Seesaw Scale in the Minimal Renormalizable SO(10) Grand Unification. *Phys. Rev.*, D85:095014, 2012.

[92] A. De Rujula, H. Georgi, and S. L. Glashow. Flavor goniometry by proton decay. *Phys. Rev. Lett.*, 45:413, 1980.

[93] Stephen M. Barr. A New Symmetry Breaking Pattern for SO(10) and Proton Decay. *Phys. Lett.*, 112B:219–222, 1982.

[94] K. S. Babu, Ilia Gogoladze, Pran Nath, and Raza M. Syed. A Unified framework for symmetry breaking in SO(10). *Phys. Rev.*, D72:095011, 2005.

[95] T. W. B. Kibble, George Lazarides, and Q. Shafi. Walls Bounded by Strings. *Phys. Rev.*, D26:435, 1982.

[96] D. Chang, R. N. Mohapatra, and M. K. Parida. Decoupling Parity and SU(2)-R Breaking Scales: A New Approach to Left-Right Symmetric Models. *Phys. Rev. Lett.*, 52:1072, 1984.

[97] Joydeep Chakrabortty, Rinku Maji, Sunando Kumar Patra, Tripurari Srivastava, and Subhendra Mohanty. Roadmap of left-right models based on GUTs. *Phys. Rev.*, D97(9):095010, 2018.

[98] F. del Aguila and Luis E. Ibanez. Higgs Bosons in SO(10) and Partial Unification. *Nucl. Phys.*, B177:60, 1981.

[99] K. S. Babu and R. N. Mohapatra. Predictive neutrino spectrum in minimal SO(10) grand unification. *Phys. Rev. Lett.*, 70:2845–2848, 1993.

[100] R. Acciarri et al. Long-Baseline Neutrino Facility (LBNF) and Deep Underground Neutrino Experiment (DUNE). 2015. arXiv:1512.06148 (physics.ins-det).

[101] K. Abe et al. Hyper-Kamiokande Design Report, 2018. arXiv:1805.04163 (physics.ins-det).

[102] S. Dimopoulos and Frank Wilczek. *Supersymmetric Unified Models*, pages 237–249. Springer US, Boston, MA, 1983.

[103] Mark Srednicki. Supersymmetric Grand Unified Theories and the Early Universe. *Nucl. Phys.*, B202:327–335, 1982.

[104] Adam Falkowski, David M. Straub, and Avelino Vicente. Vector-like leptons: Higgs decays and collider phenomenology. *JHEP*, 05:092, 2014.

[105] R. D. Peccei. The Strong CP Problem. *Adv. Ser. Direct. High Energy Phys.*, 3:503–551, 1989.

[106] Jihn E. Kim and Gianpaolo Carosi. Axions and the Strong CP Problem. *Rev. Mod. Phys.*, 82:557–602, 2010.

[107] Michael Dine. TASI lectures on the strong CP problem. In *Flavor physics for the millennium. Proceedings, Theoretical Advanced Study Institute in elementary particle physics, TASI 2000, Boulder, USA, June 4-30, 2000*, pages 349–369, 2000.

[108] J. M. Pendlebury et al. Revised experimental upper limit on the electric dipole moment of the neutron. *Phys. Rev.*, D92(9):092003, 2015.

[109] Ettore Vicari and Haralambos Panagopoulos. Theta dependence of SU(N) gauge theories in the presence of a topological term. *Phys. Rept.*, 470:93–150, 2009.

[110] A. Altland and B. D. Simons. *Condensed matter field theory.* Cambridge University Press, Leiden, 2010.

[111] V. A. Rubakov. *Classical theory of gauge fields.* Princeton University Press, Princeton, N.J. Oxford, 2002.

[112] Alexander G. Abanov. Topology, geometry and quantum interference in condensed matter physics. 2017.

[113] N. S. Manton. Topology in the Weinberg-Salam Theory. *Phys. Rev.*, D28:2019, 1983.

[114] Monika Leibscher and Burkhard Schmidt. Quantum dynamics of a plane pendulum. *Phys. Rev. A*, 80:012510, Jul 2009.

[115] Kerson Huang. *Quarks, leptons and gauge fields*. World Scientific, Singapore New Jersey, 1992.

[116] Mark Srednicki. *Quantum field theory*. Cambridge University Press, Cambridge, 2007.

[117] R. Jackiw and C. Rebbi. Vacuum Periodicity in a Yang-Mills Quantum Theory. *Phys. Rev. Lett.*, 37:172–175, 1976. [,353(1976)].

[118] Curtis G. Callan, Jr., R. F. Dashen, and David J. Gross. The Structure of the Gauge Theory Vacuum. *Phys. Lett.*, B63:334–340, 1976. [,357(1976)].

[119] Curtis G. Callan, Jr., Roger F. Dashen, and David J. Gross. Toward a Theory of the Strong Interactions. *Phys. Rev.*, D17:2717, 1978. [,36(1977)].

[120] A. Anderson. Nontrivial homotopy and tunneling by instantons. *Phys. Rev.*, D37:1030–1035, 1988.

[121] R. Jackiw. Introduction to the Yang-Mills Quantum Theory. *Rev. Mod. Phys.*, 52:661–673, 1980.

[122] R. Rajaraman. *Solitons and Instantons, Volume 15: An Introduction to Solitons and Instantons in Quantum Field Theory (North-Holland Personal Library)*. North Holland, 1987.

[123] A. A. Belavin, Alexander M. Polyakov, A. S. Schwartz, and Yu. S. Tyupkin. Pseudoparticle Solutions of the Yang-Mills Equations. *Phys. Lett.*, B59:85–87, 1975. [,350(1975)].

[124] Gregory Gabadadze and M. Shifman. QCD vacuum and axions: What's happening? *Int. J. Mod. Phys.*, A17:3689–3728, 2002. [,521(2002)].

[125] Claude W. Bernard and Erick J. Weinberg. The Interpretation of Pseudoparticles in Physical Gauges. *Phys. Rev.*, D15:3656, 1977.

[126] Erick J. Weinberg. *Classical Solutions in Quantum Field Theory - Solitons and Instantons in High Energy Physics*. Cambridge University Press, Cambridge, 2012.

[127] R.J. Crewther, P. Di Vecchia, G. Veneziano, and E. Witten. Chiral estimate of the electric dipole moment of the neutron in quantum chromodynamics. *Physics Letters B*, 88(1):123 – 127, 1979.

[128] Varouzhan Baluni. CP Violating Effects in QCD. *Phys. Rev.*, D19:2227–2230, 1979.

[129] T. D. Lee. CP Nonconservation and Spontaneous Symmetry Breaking. *Phys. Rept.*, 9:143–177, 1974. [,124(1974)].

[130] R. Jackiw. Effects of Dirac's negative energy sea on quantum numbers. 1999. arXiv:9903255 (hep-th).

[131] Luis Alvarez-Gaumé and Miguel Vázquez-Mozo. *An invitation to quantum field theory.* Springer, Heidelberg New York, 2012.

[132] M. F. Atiyah and I. M. Singer. The index of elliptic operators: I. *Annals of Mathematics*, 87(3):484–530, 1968.

[133] N.K. Nielsen and Bert Schroer. Axial anomaly and atiyah-singer theorem. *Nuclear Physics B*, 127(3):493 – 508, 1977.

[134] Philip C. Nelson and Luis Alvarez-Gaume. Hamiltonian Interpretation of Anomalies. *Commun. Math. Phys.*, 99:103, 1985.

[135] J. S. Bell and R. Jackiw. A PCAC puzzle: $\pi^0 \to \gamma\gamma$ in the σ model. *Nuovo Cim.*, A60:47–61, 1969.

[136] Stephen L. Adler. Axial-vector vertex in spinor electrodynamics. *Phys. Rev.*, 177:2426–2438, Jan 1969.

[137] N. S. Manton. The Schwinger Model and Its Axial Anomaly. *Annals Phys.*, 159:220–251, 1985.

[138] Sidney R. Coleman. The Uses of Instantons. *Subnucl. Ser.*, 15:805, 1979. [,382(1978)].

[139] Kazuo Fujikawa. Path Integral for Gauge Theories with Fermions. *Phys. Rev.*, D21:2848, 1980. [Erratum: Phys. Rev.D22,1499(1980)].

[140] Kazuo Fujikawa. Evaluation of the chiral anomaly in gauge theories with γ_5 couplings. *Phys. Rev. D*, 29:285–292, Jan 1984.

[141] Robert Marshak. *Conceptual foundations of modern particle physics.* World Scientific, Singapore River Edge, NJ, 1993.

[142] F. Wilczek. Problem of strong p and t invariance in the presence of instantons. *Phys. Rev. Lett.*, 40:279–282, Jan 1978.

[143] Steven Weinberg. A new light boson? *Phys. Rev. Lett.*, 40:223–226, Jan 1978.

[144] R. D. Peccei and Helen R. Quinn. CP conservation in the presence of pseudoparticles. *Phys. Rev. Lett.*, 38:1440–1443, Jun 1977.

[145] Cumrun Vafa and Edward Witten. Parity Conservation in QCD. *Phys. Rev. Lett.*, 53:535, 1984.

[146] Mark Srednicki. Axions: Past, present, and future. In *Continuous advances in QCD. Proceedings, Conference, Minneapolis, USA, May 17-23, 2002*, pages 509–520, 2002.

[147] R. D. Peccei and Helen R. Quinn. CP Conservation in the Presence of Instantons. *Phys. Rev. Lett.*, 38:1440–1443, 1977.

[148] R. D. Peccei. The Strong CP problem and axions. *Lect. Notes Phys.*, 741:3–17, 2008. [,3(2006)].

[149] Frank Wilczek. *The U(1) Problem: Instantons, Axions, and Familons*, pages 157–229. Springer US, Boston, MA, 1985.

[150] Peter Svrcek and Edward Witten. Axions In String Theory. *JHEP*, 06:051, 2006.

[151] P. Sikivie. Axions, domain walls, and the early universe. *Phys. Rev. Lett.*, 48:1156–1159, Apr 1982.

[152] Pierre Sikivie. Axion Cosmology. *Lect. Notes Phys.*, 741:19–50, 2008. [,19(2006)].

[153] Ann E. Nelson. Naturally Weak CP Violation. *Phys. Lett.*, 136B:387–391, 1984.

[154] Ann E. Nelson. Calculation of θ Barr. *Phys. Lett.*, 143B:165–170, 1984.

[155] Stephen M. Barr. Solving the Strong CP Problem Without the Peccei-Quinn Symmetry. *Phys. Rev. Lett.*, 53:329, 1984.

[156] Stephen M. Barr. A Natural Class of Nonpeccei-quinn Models. *Phys. Rev.*, D30:1805, 1984.

[157] Anson Hook. TASI Lectures on the Strong CP Problem and Axions. 2018.

[158] Michael Dine and Patrick Draper. Challenges for the Nelson-Barr Mechanism. *JHEP*, 08:132, 2015.

[159] Luis Bento, Gustavo C. Branco, and Paulo A. Parada. A Minimal model with natural suppression of strong CP violation. *Phys. Lett.*, B267:95–99, 1991.

[160] G. C. Branco, P. A. Parada, and M. N. Rebelo. A Common origin for all CP violations. 2003. arXiv:0307119 (hep-ph).

[161] Q. Shafi. E(6) as a Unifying Gauge Symmetry. *Phys. Lett.*, B79:301, 1978.

[162] Berthold Stech. Exceptional Groups for Grand Unification. In *Workshop on Nuclear Dynamics Granlibakken, Tahoe City, California, March 17 - 21, 1980*, 1980.

[163] R. Barbieri and D.V. Nanopoulos. An exceptional model for grand unification. *Physics Letters B*, 91(3-4):369 – 375, 1980.

[164] Edward Witten. Quest for unification. In *Supersymmetry and unification of fundamental interactions. Proceedings, 10th International Conference, SUSY'02, Hamburg, Germany, June 17-23, 2002*, pages 604–610, 2002.

[165] Luca Vecchi. Spontaneous CP violation and the strong CP problem. *JHEP*, 04:149, 2017.

[166] Paul Tremper. *Aspects of CP Violation*. PhD thesis, Karlsruhe Institute of Technology, 2018.

[167] W. Grimus and H. Kuhbock. A renormalizable SO(10) GUT scenario with spontaneous CP violation. *Eur. Phys. J.*, C51:721–729, 2007.

[168] Aharon Davidson and Kameshwar C. Wali. Symmetric Versus Antisymmetric Mass Matrices in Grand Unified Theories. *Phys. Lett.*, B94:359, 1980.

[169] Stefan Antusch and Vinzenz Maurer. Running quark and lepton parameters at various scales. *JHEP*, 11:115, 2013.

[170] Ivan Esteban, M. C. Gonzalez-Garcia, Michele Maltoni, Ivan Martinez-Soler, and Thomas Schwetz. Updated fit to three neutrino mixing: exploring the accelerator-reactor complementarity. *JHEP*, 01:087, 2017.

[171] Nicholas Metropolis, Arianna W. Rosenbluth, Marshall N. Rosenbluth, Augusta H. Teller, and Edward Teller. Equation of state calculations by fast computing machines. *Journal of Chemical Physics*, 21:1087–1092, 1953.

[172] W.K. Hastings. Monte carlo samping methods using markov chains and their applications. *Biometrika*, 57:97–109, 1970.

[173] Stefan Antusch, Jörn Kersten, Manfred Lindner, Michael Ratz, and Michael Andreas Schmidt. Running neutrino mass parameters in see-saw scenarios. *JHEP*, 03:024, 2005.

[174] Alexander Dueck and Werner Rodejohann. Fits to SO(10) Grand Unified Models. *JHEP*, 09:024, 2013.

[175] Davide Meloni, Tommy Ohlsson, and Stella Riad. Effects of intermediate scales on renormalization group running of fermion observables in an SO(10) model. *JHEP*, 12:052, 2014.

[176] A. Osipowicz et al. KATRIN: A Next generation tritium beta decay experiment with sub-eV sensitivity for the electron neutrino mass. Letter of intent. 2001.

[177] A. Monfardini et al. The Microcalorimeter arrays for a Rhenium experiment (MARE): A Next-generation calorimetric neutrino mass experiment. *Nucl. Instrum. Meth.*, A559:346–348, 2006.

[178] Benjamin Monreal and Joseph A. Formaggio. Relativistic Cyclotron Radiation Detection of Tritium Decay Electrons as a New Technique for Measuring the Neutrino Mass. *Phys. Rev.*, D80:051301, 2009.

[179] K. Blaum et al. The Electron Capture ^{163}Ho Experiment ECHo. In *The Future of Neutrino Mass Measurements: Terrestrial, Astrophysical, and Cosmological Measurements in the Next Decade (NUMASS2013) Milano, Italy, February 4-7, 2013*, 2013.

[180] M. Agostini et al. Results on Neutrinoless Double-β Decay of ^{76}Ge from Phase I of

the GERDA Experiment. *Phys. Rev. Lett.*, 111(12):122503, 2013.

[181] J. B. Albert et al. Search for Majorana neutrinos with the first two years of EXO-200 data. *Nature*, 510:229–234, 2014.

[182] A. Gando et al. Limit on Neutrinoless $\beta\beta$ Decay of ^{136}Xe from the First Phase of KamLAND-Zen and Comparison with the Positive Claim in ^{76}Ge. *Phys. Rev. Lett.*, 110(6):062502, 2013.

[183] P. A. R. Ade et al. Planck 2015 results. XIII. Cosmological parameters. *Astron. Astrophys.*, 594:A13, 2016.

[184] Francesco Capozzi, Eleonora Di Valentino, Eligio Lisi, Antonio Marrone, Alessandro Melchiorri, and Antonio Palazzo. Global constraints on absolute neutrino masses and their ordering. *Phys. Rev.*, D95(9):096014, 2017.

[185] A. Gando et al. Search for Majorana Neutrinos near the Inverted Mass Hierarchy Region with KamLAND-Zen. *Phys. Rev. Lett.*, 117(8):082503, 2016. [Addendum: Phys. Rev. Lett.117,no.10,109903(2016)].

[186] Heinrich Päs and Werner Rodejohann. Neutrinoless Double Beta Decay. *New J. Phys.*, 17(11):115010, 2015.

[187] K. Abe et al. A Long Baseline Neutrino Oscillation Experiment Using J-PARC Neutrino Beam and Hyper-Kamiokande. 2014.